SHORT CIRCUIT

How brain connectivity and disconnectivity relate to brain function

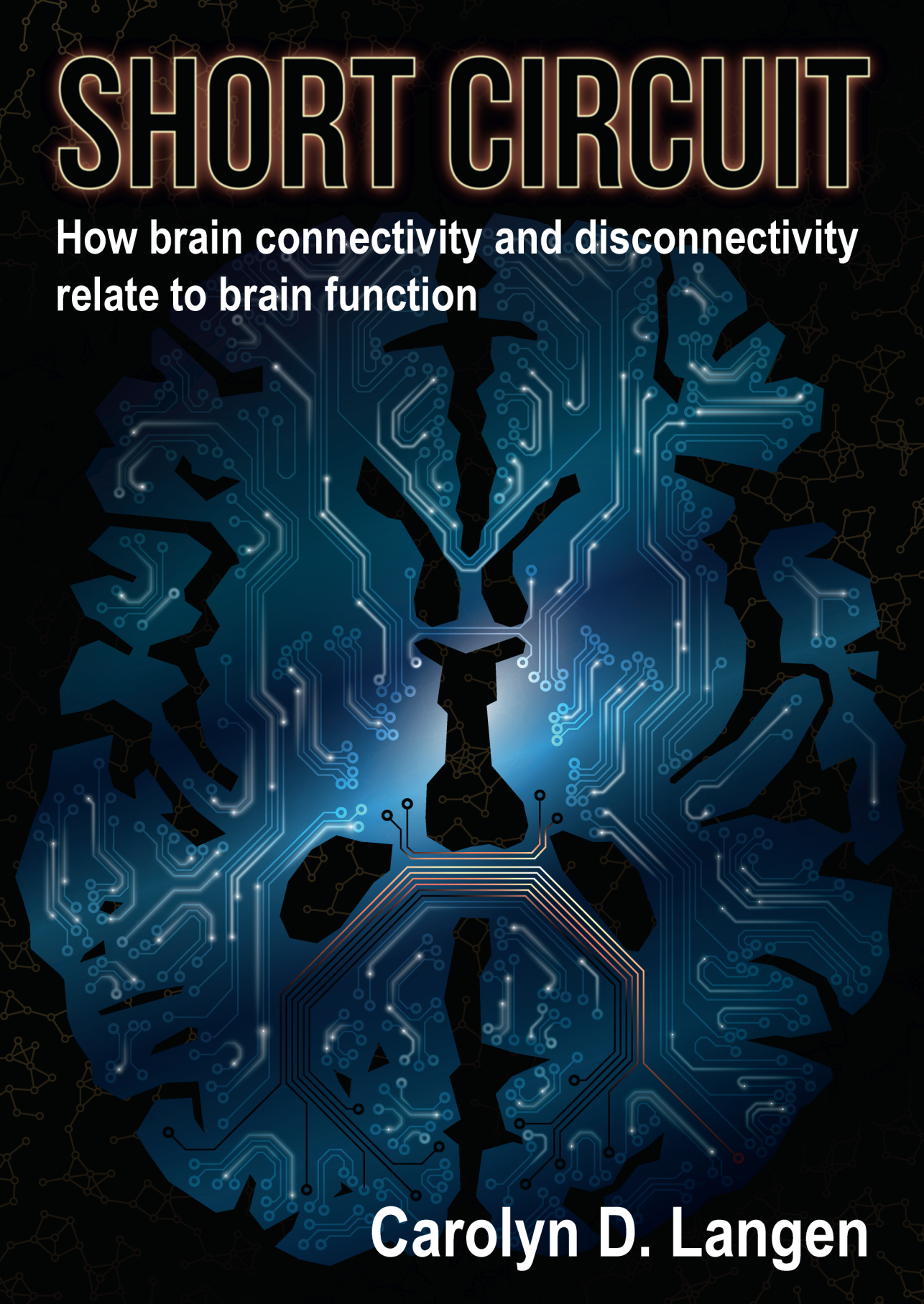

Carolyn D. Langen

SHORT CIRCUIT

How brain connectivity and disconnectivity relate to brain function

Carolyn D. Langen

Cover design and thesis layout by Carolyn Langen

Image in part dividers (pages 8, 9, 74, 75):
Cortical Circuitboard
22K reflective microetching
2013-4
Greg Dunn and Brian Edwards

Printed by GVO drukkers & vormgevers B.V.

Financial support for the publication of this thesis was generously provided by the Department of Radiology and Nuclear Medicine (Erasmus MC), Erasmus University, and Almende B.V.

ISBN 978-94-6332-320-8

Short Circuit:

How brain connectivity and disconnectivity relate to brain function

Kortsluiting:
Hoe hersenconnectiviteit en -disconnectiviteit samen hangen met hersenfunctie

Thesis

to obtain the degree of Doctor from the
Erasmus University Rotterdam
by command of the
rector magnificus

Prof.dr. H.A.P. Pols

and in accordance with the decision of the Doctorate Board.
The public defense shall be held on

Wednesday 18 April 2018 at 11:30 hours

by

Carolyn Diana Langen
born in Calgary, Canada

Erasmus University Rotterdam

DOCTORAL COMMITTEE

Promotor	Prof.dr. W.J. Niessen
Other members	Prof.dr. V.D. Calhoun Dr. M. Smits Dr. M.P. van den Heuvel
Copromotor	Dr. T.J.H. White

Contents

1

General introduction

The brain is the supercomputer of the body. It is a massively parallel and distributed network of computational units, all working together to control our organs, interpret our senses and to provide us with thoughts and emotions. Its function is at the core of who we are, while loss of function stands in the way of who we want to be. But the mysteries of brain function and dysfunction are elusive. The human race has been observing it for millennia [212], and yet it is as though we have only just begun to understand how it functions.

The ancient Greeks and Egyptians were the first to attribute behavior to the brain as early as 540 BC [99]. These ideas were expanded by the Romans. In the middle ages, Albertus Magnus hypothesized that several brain structures, including the cortex, midbrain and cerebellum were responsible for behavior. During the renaissance through to the 18th centuries, several scholars developed theories about the location of brain function, including Leonardo da Vinci, Thomas Willis, Emmanuel Swedenborg, Franz Joseph Gall and Pierre Flourens. In the 19th century, Paul Broca and Carl Wernicke separately localized two regions related to speech and language, coined *Broca's* and *Wernicke's areas*. Later neuropsychological research by Alexander Luria, Ward Halstead and Ralph Reitan, among others, focused on the development of batteries of tests designed to evaluate brain function. The field of clinical neuropsychology has since flourished, and we have made great strides in developing our knowledge about brain function.

The pioneers of modern neuroscience were limited to what they could observe in the clinic and laboratory. While these experiments form the basis of our understanding of brain function, the resulting observations were on a much coarser scale than what we can observe today. In the last few decades our knowledge base has grown by leaps and bounds with the help of modern technology. The invention of magnetic resonance imaging (MRI) provided a technique to non-invasively visualize the brain. Brain anatomy can be observed using structural MRI, whereas functional and structural connectivity can be studied using functional and diffusion MRI.

Structural MRI can be used to non-invasively peer into the head and examine brain anatomy. The brain is composed of grey matter and white matter and is protected by the skull and cerebral spinal fluid (Figure 1.1). Grey matter is found both on the surface of the brain, which is referred to as the cortex, and deep in the brain, which is referred to as the subcortex. Grey matter is where brain function originates. It can be

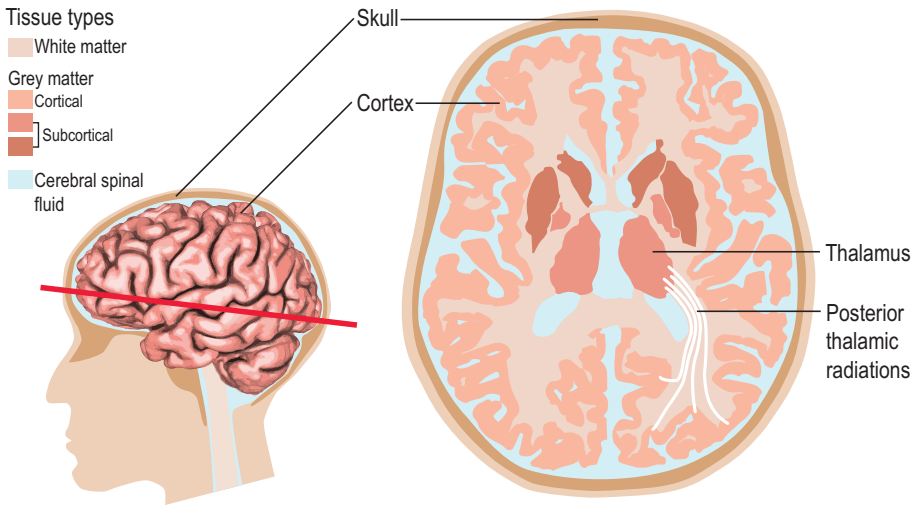

Figure 1.1: ***Brain anatomy.*** *The brain is protected by the skull and cerebral spinal fluid. It is composed of white matter and grey matter, where grey matter is found both on the surface of the brain (i.e. cortical) and deep within the brain (subcortical). White matter tracts connect grey matter regions to each other. For example, the thalamus is connected to the occipital lobe (i.e. the visual cortex) via the posterior thalamic radiations.*

subdivided into regions of interest based on the assumed or estimated functional role of each region in the brain. For example, the thalamus is a subcortical grey matter region that is associated with memory, sleep, emotion and executive function [148].

Grey matter regions are connected to each other by tracts in the white matter, much like components of a computer are connected to each other by circuits. Signals are passed between regions, thus allowing communication and consequently higher brain functions. For example, the thalamus is connected to the occipital lobe by the posterior thalamic radiations.

Diffusion-based imaging, including diffusion weighted-imaging (DWI) is used to estimate the topology and microstructural properties of white matter pathways, whereas functional MRI (fMRI) is used to estimate the activity of grey matter regions. The resulting data can be used to reconstruct the network of connections which give rise to higher brain functions. The networks are high-dimensional data structures requiring advanced analysis techniques in order to uncover the underlying knowledge and insights.

Brain connectivity

The *connectome* is a data structure which represents brain connectivity as a network of connections between brain regions [87, 176]. It is a *graph*-based data structure in which grey matter regions are represented as *nodes*, and relationships between regions are represented as *edges* (Figure 1.2). For example, the thalamus is connected to the precuneus via the posterior thalamic radiations, and to the lateral orbitofrontal cortex via the anterior thalamic radiations. In this case, there are three nodes, one for each region (i.e. thalamus, precuneus and lateral orbitofrontal cortex). If we define edges where there is *direct connectivity* via white matter tracts, then there would be two edges: one between the thalamus and precuneus, and the other between the thalamus and lateral orbitofrontal cortex. Note that connectivity can also be defined indirectly, where it is assumed that communication between regions occurs via an intermediate region. In this example, one could define an indirect connection between the precuneus and lateral obitofrontal cortex, where communication occurs via the thalamus.

There are a variety of ways in which both regions and connections can be defined, all of which have benefits and drawbacks [88]. For example, brain regions are often delineated, or *parcellated*, based on anatomical features [25, 37, 60, 120, 183]. Regions may also be defined using functional [21, 163] or diffusion data, or even random parcellations [217]. While choosing from the multitude of parcellation schemes may be daunting, deciding on edge definitions only adds to the complexity of building a connectome. Generally speaking, there are three main classes of edge definitions: structural, functional and anatomical.

Structural connectome edges reflect the white matter connections between regions, and are derived from DWIs or more advanced diffusion imaging protocols. Data derived from DWI is used to trace streamlines in the white matter, which is an estimation of the pathways between grey matter regions. Edges can be defined based on the number of streamlines between regions, based on aggregated measures of diffusion, or based on more complex metrics.

Functional connectome edges reflect the communication of brain regions, and are often defined using correlations of the temporal signals obtained from fMRI. The general idea behind functional connectivity is that regions which are physically connected, whether that be directly or indirectly, will communicate with each other, and thus will have a similar activity patterns. Previous studies have shown that there is a

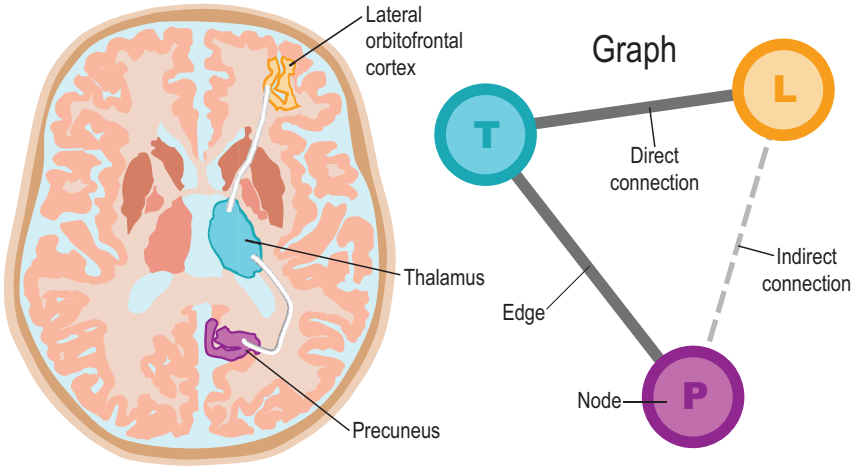

Figure 1.2: ***The connectome.*** *The connectome is a graph, which is a collection of nodes (i.e. grey matter regions) and edges (i.e. connections between them). In the structural connectome, edges often represent direct physical connections between nodes. However, regions that are not directly connected can communicate via intermediate regions, and may thus be indirectly connected. Indirect connections are frequently encountered in the functional connectome, in which edges often represent correlations of activity between regions. For example, this simple network has three nodes representing the* ***(L)****ateral orbitofrontal cortex,* ***(T)****halamus and* ***(P)****recuneus. The edges between the thalamus and the other two regions are direct, due to the presence of white matter tracts. The lateral orbitofrontal cortex and precuneus are not directly connected, but may communicate indirectly via the thalamus.*

link between activity of regions and the degree to which they are structurally connected [79, 93, 100, 189].

The third method of defining edges is based on correlations of cortical region thickness or volume measures and is often defined using T1-weighted images [90]. It has been used to gain new insights into neuro-degenerative disease, brain development, behavior and cognitive abilities [6]. This type of connectome is not included in the works presented in this thesis.

No matter which parcellation method or connectivity definition is chosen, the connectome has proven to be a useful tool for studying brain connectivity. It has been used to gain new insights into normal processes such as aging [120, 131] and development [17, 48], as well as disorders [31, 61, 152, 178] such as schizophrenia [62, 153] and dementia [34, 128].

Pathology of the brain

While brain connectivity studies have yielded enlightening results, they are not designed to observe pathology directly. White matter pathologies are hypothesized to result in deficits in brain function, according to the *disconnection hypothesis* [66]. This link has been shown in several previous studies of white matter lesions (WMLs). WMLs are associated with cognitive decline, stroke and dementia [45], as well as impairment in gait [179] and depression [35].

A link between WMLs and functional connectivity has been established in animal studies. In rats, induced WMLs initially resulted in decreased functional connectivity and decreased sensorimotor function, however connectivity and function both partially recovered several weeks later [197]. In monkeys, after the corpus callosum was sectioned, interhemispheric functional connectivity was largely maintained when the anterior commissural tract was left intact, but was completely lost when all interhemispheric tracts were severed [142]. These studies suggest that the brain is vulnerable to white matter damage, but that in some cases it is capable of compensating for damage.

Studies of individuals with brain tumours and stroke-related WMLs have shed light on the relationship between white matter pathology and functional connectivity in humans. A study of a subject with a brain tumor used fMRI to better define ROIs for seeding tractography of white matter tracts which were deformed due to the presence of the tumor [159]. fMRI and DTI were also used together in a study of an infant with perinatal stroke to localize the reductions in connectivity to the visual cortex due to the pathology [161]. In adults with stroke, it was found that increased structural integrity of lesioned white matter tracts corresponded to greater recovery of motor function and lesser activation of the motor cortex [172]. These studies show that pathology is associated with changes in functional connectivity and brain function. However, the sample sizes of these studies were small and they focused on individual tracts or brain regions.

In humans, whole-brain connectivity studies of WML-related conditions often compare the connectomes of afflicted subjects with those of healthy controls in order to ascertain which connections and regions may be related to changes in brain function. For example, this approach has been used to study schizophrenia and autism [152]. Presumably, differences in traditional measures of connectivity reflect the underlying

pathology to some degree. However, since these measures do not directly measure pathology, they are incapable of determining whether the observed differences are due to pathologic, genetic, environmental, or any number of other factors.

A small number of previous studies have investigated pathology in the connectome directly. Studies of grey-matter lesioning in the connectome have included a meta-analysis of data from earlier studies of a variety of brain disorders [31] and a simulation of the effect of lesions on functional connectivity. Simulations have also been used to examine the effects of hypothetical WMLs on graph-theory-derived connectome measures [44]. Another study used connectivity derived from healthy controls and patient WML maps to estimate the connectomes of patients [117]. To date, there has not been a study which directly models the effect of WMLs on connectivity.

Thesis overview

The studies presented in this thesis provide new insight into brain structure and function using advanced neuroimage analysis techniques applied to DWI and functional MRI. The thesis is divided into two parts. Part I focuses on expressions of brain connectivity whereas Part II sheds light on disconnection in the brain due to pathology.

Part I begins by describing methods of comparing groups using the both the functional and structural connectome, including how to visualize the results of such analyses (Chapter 2). Chapter 3 uses some of the principles and visualizations defined in Chapter 2 in order to study functional connectivity in brain development.

Part II begins with an introduction of the *structural disconnectome*, which is an adaptation of the structural connectome that directly estimates the degree to which pathology affects brain connectivity (Chapter 4). The disconnectome is used in Chapter's 5 and 6 in order to study heritability and cognition, respectively. Part II concludes with a study that makes a direct relation between WMLs and functional connectivity, not using the disconnectome, but by using anatomically-defined white matter tracts, presented in Chapter 7.

The studies presented in this thesis are summarized and discussed in Chapter 8.

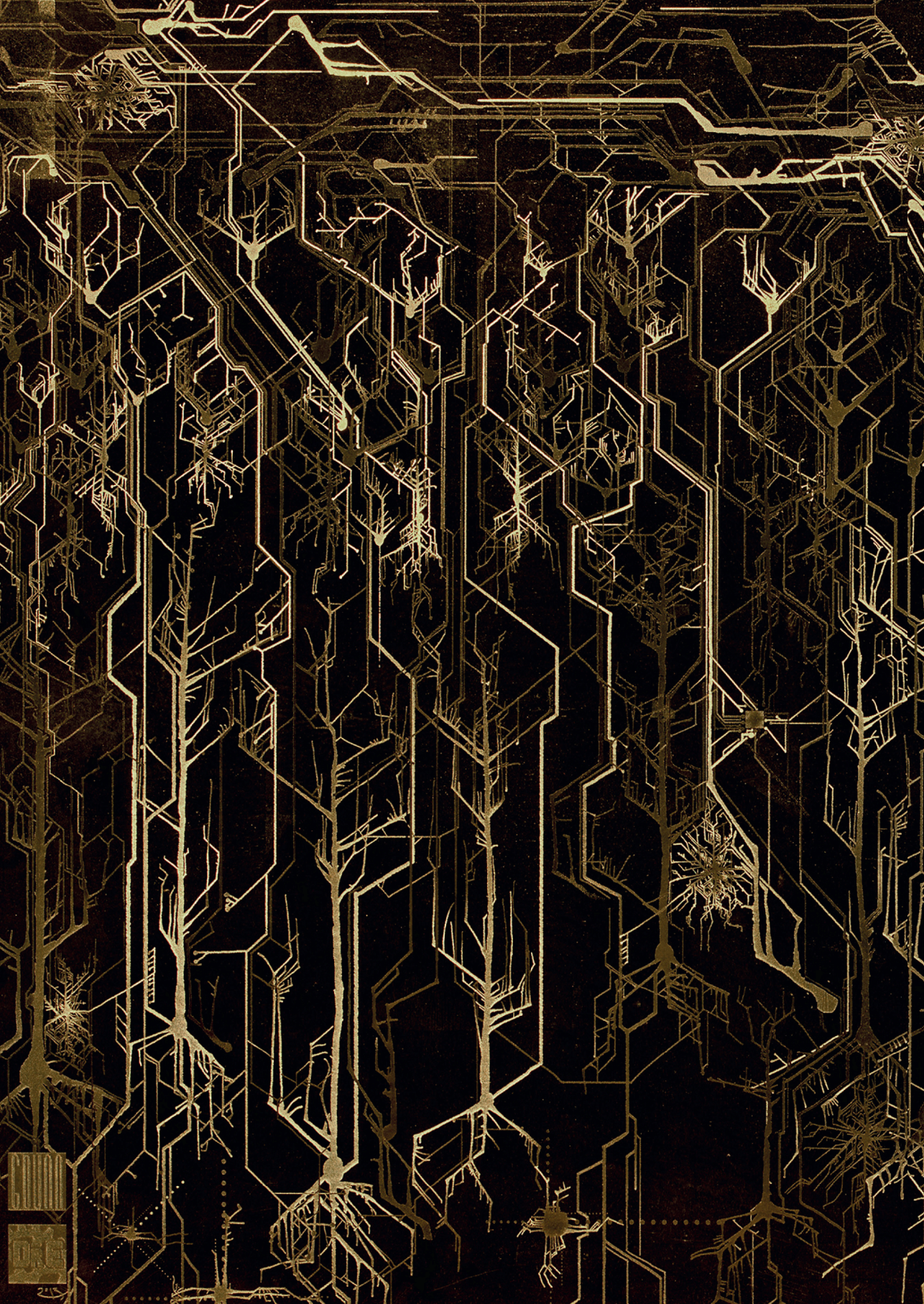


PART I
THE CONNECTOME

2

Integrated analysis and visualization of group differences in structural and functional brain connectivity: Applications in typical ageing and schizophrenia

Carolyn D Langen, Tonya White, M Arfan Ikram, Meike W Vernooij, Wiro J Niessen

PLOS One, 2015

Abstract

Structural and functional brain connectivity are increasingly used to identify and analyze group differences in studies of brain disease. This study presents methods to analyze uni- and bi-modal brain connectivity and evaluate their ability to identify differences. Novel visualizations of significantly different connections comparing multiple metrics are presented. On the global level, the “bi-modal comparison plot” shows the distribution of uni- and bi-modal group differences and the relationship between structure and function. Differences between brain lobes are visualized using “worm plots”. Group differences in connections are examined with an existing visualization, the “connectogram”. These visualizations were evaluated in two proof-of-concept studies: (1) middle-aged versus elderly subjects; and (2) patients with schizophrenia versus controls. Each included two measures derived from diffusion weighted images and two from functional magnetic resonance images. The structural measures were minimum cost path between two anatomical regions according to the “Statistical Analysis of Minimum cost path based Structural Connectivity” method and the average fractional anisotropy along the fiber. The functional measures were Pearson’s correlation and partial correlation of mean regional time series. The relationship between structure and function was similar in both studies. Uni-modal group differences varied greatly between connectivity types. Group differences were identified in both studies globally, within brain lobes and between regions. In the ageing study, minimum cost path was highly effective in identifying group differences on all levels; fractional anisotropy and mean correlation showed smaller differences on the brain lobe and regional levels. In the schizophrenia study, minimum cost path and fractional anisotropy showed differences on the global level and within brain lobes; mean correlation showed small differences on the lobe level. Only fractional anisotropy and mean correlation showed regional differences. The presented visualizations were helpful in comparing and evaluating connectivity measures on multiple levels in both studies.

Introduction

Brain connectivity is an area of research receiving increasing attention. In the brain, regions communicate through networks of structural and functional links, which is termed connectivity. Connectivity can be studied non-invasively using advanced imaging techniques such as magnetic resonance imaging (MRI). Relationships between regions of interest (ROIs) are extracted from MRI's and used to define a network. Variations in MRI acquisition and analysis have resulted in several types of connectivity. With ever increasing choices, comparing connectivity types becomes an important first step in addressing a given research question.

Structural connectivity refers to the anatomical connectivity of the brain. It can be extracted from diffusion weighted images (DWI). DWI is a type of MRI that estimates the movement of water in each voxel of the image. Water diffuses along white matter tracts. From DWI, pathways travelled by water molecules (and thus the orientation of nerve fibers) can be approximated. These pathways are referred to as streamlines [29]. Measures of microstructure along the length of streamlines, such as fractional anisotropy (FA), which is the degree of diffusion directedness, can be collected and used to define structural connectivity [150]. Structural connectivity measures have also been derived without using streamlines, such as in estimating minimum cost to travel between regions [37, 109].

It is believed that structural connections enable communication between regions, resulting in functional connectivity [101], characterized by regions having similar neural dynamics. Functional connectivity can be quantified using functional MRI (fMRI). Several methods of defining functional connectivity exist, such as using Pearson's correlation, partial correlation or mutual information of time patterns [29], which are typically calculated between the mean time series of brain regions.

In the last few years, DWI and fMRI data have been combined to study multimodal aspects of brain connectivity [220]. DWI is typically used to study white matter, whereas fMRI focuses on grey matter. The roles of grey and white matter in the brain have long been studied separately, but their interaction with each other is essential in the function of the brain. The study of functional and structural connectivity, and especially how they relate to each other, could help to better understand the roles and interaction of grey and white matter. Structural and functional connectivity have been combined both to model their relationship [100] and to derive new types of connectivity

[22]. Wee et al. (2012) [204] built a machine learning model using structural and functional connectivity to determine which subjects would develop mild cognitive impairment. With an increased interest in multimodal brain connectivity analysis, it is likely that many more publications on the subject will appear in the coming years.

As the study of multimodal group comparisons progresses and new types of connectivity are developed, researchers require methods to evaluate which connectivity metric is best suited to their research question, e.g. to make an informed decision about which network types to include in their study, or to study the relation between different network types and make inferences about potential biological explanations for the observed differences and similarities. There is a need for methods of comparing functional and structural connectivity with respect to their suitability for group analyses, both uni-modally, and bi-modally.

An integral component of such analyses is visualization of results. Margulies et al. (2013) [130] conducted an in-depth review of uni- and multi-modal visualizations used in brain connectivity research, including an explanation of the benefits and drawbacks of each. Networks of connections between ROIs are often depicted in a matrix representation [17, 23, 198], where each row and column correspond to an ROI, and each element in the matrix represents a connection between the two (see Supplementary Figure 1a). The same information can be displayed in a connectogram [130, 196], which is a circular representation in which nodes are aligned along the edge of a circle and connections are represented by lines between them (see Figure 2.1b). Both representations have benefits and drawbacks. For example, the matrix representation is able to show all possible connections simultaneously, however they are an abstract way of representing connectivity and the focus on connections may result in understating or not detecting important individual ROIs. Connectograms, on the other hand, are well-suited to draw attention to important nodes and they represent connections in an intuitive way, namely by connecting two ROIs by a line; however they are limited in the number of connections that they can effectively show at the same time. Connectivity is also frequently shown within a three-dimensional (3D) representation of the brain [1, 23, 62, 100, 198], where each ROI is represented as a point in 3D space and a connection is depicted as a line between two points (see Figure 2.1c). While these visualizations can be impressive, they are also limited by the number of connections that they can display without obscuring valuable connectivity

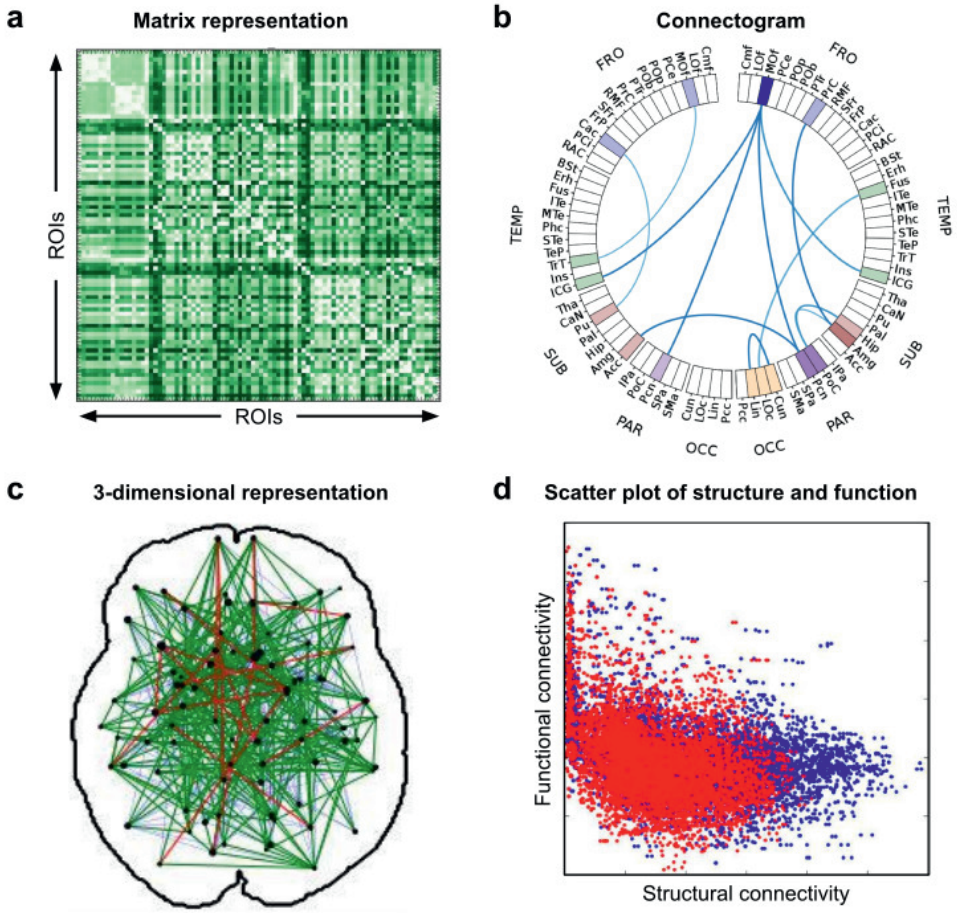

Figure 2.1: ***Illustration of figures previously used in connectivity studies.*** *Each sub-figure was generated from data used in this study. Matrix representation (a) can be used to show the contents of a network [17, 23, 198]. Each row and column represents an ROI, and each element in the matrix represents a connection between the ROIs in the corresponding row and column. Connectograms (b) show connectivity by arranging ROIs on the outer edge of a circle and representing connections as lines between them [130, 196]. 3-dimensional representations (c) represent ROIs as points positioned at their location within the brain, which are connected by lines [1, 23, 62, 100, 198]. This visualization requires projection of the 3-dimensional representation into 2-dimensional space. Scatter plots (d) show relationships between structural and functional connectivity [100], where each point represents a connection and in this case color is used to represent groups.*

information [130] and the depiction of these 3D objects in two-dimensional images results in ambiguity about the position of each node in the third dimension. Relationships between structural and functional connectivity have previously been presented using scatter plots [100] (see Figure 2.1d). However, a network often contains hundreds or thousands of connections. When displayed together in the same scatter plot, overlapping points make it difficult or impossible to know the density of points at given position in the plot. Additionally, when two groups are displayed within the same scatter plot, the points of one group may obscure the view of points from the other group, making it impossible to know where the groups overlap and where they do not.

The aim of this study is to enable multi-level comparison, integrated analysis and visualization of multiple functional and structural connectivity types, where connectivity is defined between pairs of ROIs. Our contribution is three-fold. First, we propose a method to enable both uni- and bi-modal analysis of structural and functional data. Second, we present two proof-of-concept studies by comparing groups of middle-aged to elderly subjects and patients with schizophrenia to controls. Third, we propose a set of visualizations that address some of the above-mentioned issues in the context of an analysis of group differences in structural and functional connectivity.

Material and methods

The proposed method to perform integrated analysis of functional and structural connectivity is illustrated in Figure 2.2. Each subject requires a DWI, fMRI and structural T1-weighted image. First the T1 image is segmented into a set of regions using FreeSurfer [55], after which structural and functional connectivity maps are extracted. The connectivity maps of each subject are compared uni- and bi-modally for their utility in group-wise analysis as well as identification of connections that contribute to group differences and similarities. The methods are applied to two proof-of-concept studies, one that compares groups of middle-age and elderly subjects, and the second that compares patients with schizophrenia to controls. More details of these steps are provided below.

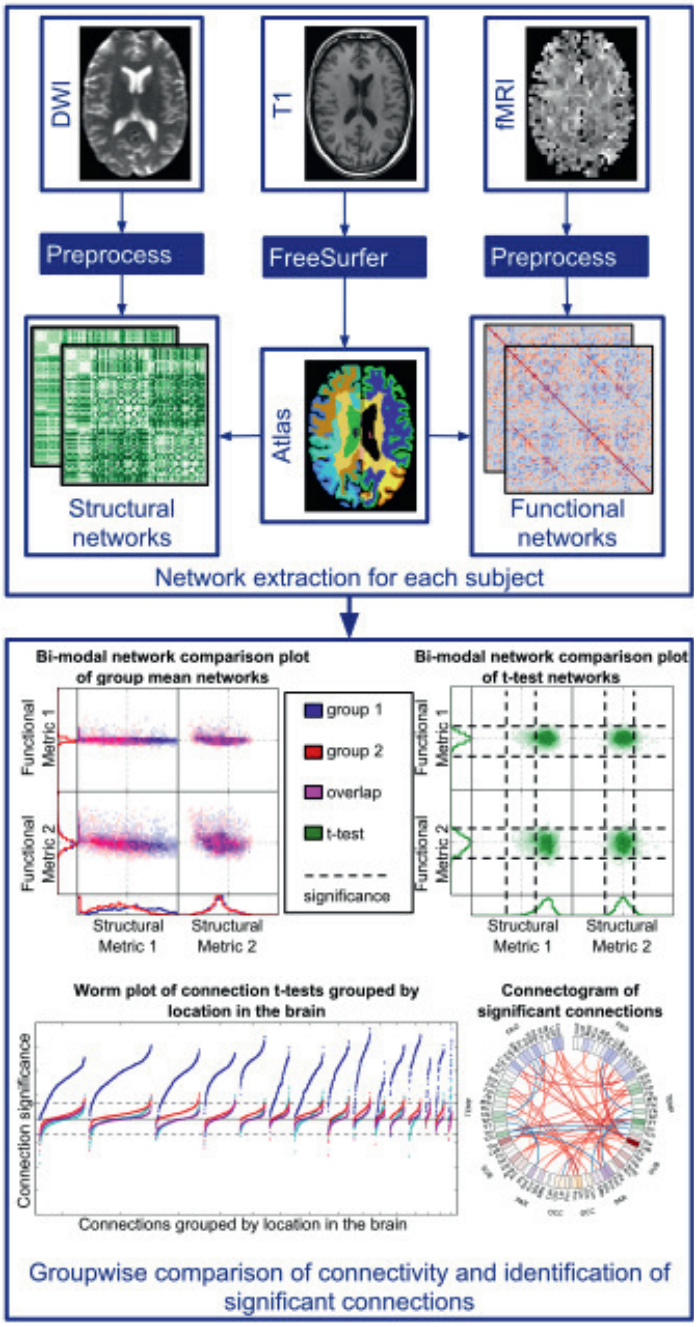

Figure 2.2: ***Schematic of method.*** *Networks are extracted for each individual (upper panel) by extracting brain regions from the T1 image using FreeSurfer, and extracting structural and functional connectivity between these regions from preprocessed DWI and fMRI, respectively. Subsequently, integrated analysis of group differences in structural and functional connectivity is performed (lower panel). Group differences are visualized on a global level using bi-modal distribution plots, on an individual connection level using connectograms and on a mid-level using worm plots, where connections are grouped by location in the brain.*

Segmentation of cortical ROIs

Cortical reconstruction and volumetric segmentation of each subject's T1 image to produce an ROI atlas was performed using the FreeSurfer image analysis suite [55], available online at http://surfer.nmr.mgh.harvard.edu. The atlas was registered with 12 degrees of freedom to both the DWI's b0 image and a mean fMRI, also using FSL's FLIRT algorithm.

Extraction of structural connectivity

The DWI's were preprocessed using AFNI and FSL tools [111]. First they were corrected for motion and Eddy currents and the brain extraction tool was used for skull stripping of the Eddy-corrected DWI. Duplicate b0 volumes were merged into a single volume by taking the median across duplicate images at each voxel. FA and mean diffusivity (MD) images were generated from the skull-stripped DWI using DTIFit. All three images (DWI, FA and MD) were masked using a mask generated from the registered FreeSurfer image, including cortex, white matter and subcortical regions.

The network extraction step of the "Statistical Analysis of Minimum cost path based Structural Connectivity" (SAMSCo) framework [37] was used to define structural connectivity because it minimizes the influence of directional uncertainty while finding globally optimal paths. A minimum cost path network (DMC) was extracted, with nodes defined by ROIs in the registered atlas and edges defined as minimum cumulative cost to travel between ROIs. A second metric of structural connectivity, the average fractional anisotropy (DFA) network, was produced by dividing the sum of fractional anisotropy along a minimum cost path by the Euclidean distance of the path. SAMSCo produces two values per connection, one from the seed to target region and the other from the target to seed region. Therefore, the SAMSCo networks were symmetrized by choosing the minimum of the two costs (and corresponding DFA values) to represent the edge between each pair of regions. It is important to note that SAMSCo is a less traditional choice of structural connectivity measure, an aspect which is discussed in more detail in the "Image preprocessing and network generation" subsection of the Discussion section.

Extraction of functional connectivity

Preprocessing of the fMRI's was accomplished using ANFI and FSL tools [28, 111]. The fMRI images were slice-timing and motion-corrected, both using AFNI tools. The first four TRs were removed to allow for equilibration and a temporal 0.01Hz high pass filter was applied to remove low frequency signals. Global mean, mean cerebral spinal fluid, and mean white matter time series as well as the six motion parameters resulting from motion correction were regressed out from the image. Finally, an 8mm full-width-half-maximum Gaussian spatial filter [210] was applied to increase the signal to noise ratio.

We defined two atlas-based metrics for defining functional connectivity. Typically, functional connectivity studies include a preprocessing step where fMRI images are spatially normalized to a common reference space and blurred to account for differences in structural and functional variability. However, anatomical and functional variation between subjects can be large [210], and thus the deformations involved in spatial normalization may stretch or contract parts of the brain for some subjects more than others. In this study, spatial normalization was not performed. Rather, the FreeSurfer ROIs were registered to the fMRI image for each subject separately, and then used to define connectivity. This reduced the effects of structural variability.

The average time series for each ROI was calculated. For the first network type, connectivity between two ROIs was defined as the Pearson correlation coefficient between each ROI's mean time series (fMT). For the other type of connectivity we used partial correlation (fPC), which was calculated for every ROI pair with the influence of all other ROI's removed according to the formula $r_{ij} = -p_{ij}/\sqrt{p_{ii}p_{jj}}$ [126], where p_{ij} is the (i,j)th element of the inverted covariance matrix from the mean time-series data of all ROIs.

Integrated analysis and visualization of structural and functional networks

An ordinary least squares linear regression model was estimated for each connection including group membership, modeled as a single variable containing zeros and ones, and covariates as variables, along with a constant term to model the mean of the data. The t-statistic and p-values associated with group membership were used to determine

whether a connection's weight differs significantly between groups. The group mean of each connection was also computed for each group of subjects. The t-statistic and group means were visualized using three types of visualizations, illustrated in the lower panel of Figure 2.2. These include bi-modal network comparison plots of group mean networks and t-statistic networks, worm plots and connectograms. This section provides an explanation of each. All of the visualizations presented in this manuscript can also be used to study continuous variables rather than group differences, which is discussed in more detail in the Discussion section.

Bi-modal network comparison plots enable simultaneous evaluation of multiple network types on a global level, both uni- and bi-modally. As seen in Figure 2.2, they can show distributions of group mean connection weights from two groups simultaneously, or distributions of t-statistics, which illustrates degree of group differences on a global level. Each type of connectivity is represented by a column or row, where rows represent the functional measures and columns represent structural measures. Each connectivity type is evaluated uni-modally in one-dimensional (1D) histograms. The relationship between structure and function is shown in two-dimensional (2D) histograms for each pair of structural/functional network types, which is displayed in the center of the plots. In the case of the group mean networks, colors are used to differentiate between groups, where blue represents one group and red represents the other. In the 2D histograms of group mean networks, magenta indicates group overlap. In the plot of the t-statistics, green is used to represent group differences.

Worm plots show the connection t-statistics grouped by the location of the associated ROIs. Even when very few connections are individually identified as significant, the worm plot may show clusters of connections that have significant group differences when considered together (regional shifts in connectivity between multiple ROIs). Significance is thus evaluated on two scales, namely on the level of individual connections and on the level of groups of connections. Worm plots are a derivative of Manhattan plots, which are scatter plots used to show significance of a large number of tests, most of which have very large p-values. They are frequently used in genetic studies [73], where genomic coordinates are on the x-axis and colors of points represent groupings of points. A few key changes to the Manhattan plot were made to make it more suitable to brain connectivity analysis. First of all, connections were

clustered by the parts of the brain to which its ROIs belong. Unlike in genetic studies where base-pairs are ordered based on their position within DNA, in the brain there is no intrinsic ordering of connections within each cluster, therefore each cluster was ordered according to t-statistic values. This reordering gives an indication of the distribution of points within each cluster, and enables simultaneous plotting and comparison of multiple network measures. Normally the y-axis of a Manhattan Plot is $-log_{10}(p)$, where p is the p-value corresponding to a statistical test. We instead used $-log_{10}(p) \cdot sign(t) \cdot s_{0.05,M_{eff,G}}$, where t is the t-statistic of a given connection, p is the corresponding p-value and $s_{0.05,M_{eff,G}} = log_{10}(\alpha_{M_{eff,G}})$ is a scaling factor used to ensure that the reference line corresponding to the adjusted significance threshold, $\alpha_{M_{eff,G}}$ (see below for details of its derivation), is the same for all networks G. $sign(t)$ adds information about whether an observed association is positive or negative. This, combined with ordering connections, resulted in clusters of points with a worm-shape, hence the name *Worm Plot*. The distance of the mean of each cluster from zero indicates the degree to which the associated parts of the brain play a role in the relationship being tested.

Significant connections for each network were also plotted in a connectogram, which was originally used to study brain connectivity by van Horn et al. (2012) [196]. The 2D circular representation in a connectogram provides a cleaner view of brain connectivity than 3D representations. While 3D representations can provide spatial information about ROIs [1, 23, 62, 100, 198], viewing them requires projections onto a 2D space. The loss of one dimension results in ROIs appearing spatially closer than they actually are. For example, when viewing a 3D representation axially, the frontal pole and lingual gyrus appear to be located beside each other, when in reality they are on opposite sides of the brain. This also presents difficulties in interpreting region groupings, since groups which are spatially separate will likely appear to overlap in the projected view. The connectogram removes these complications by disregarding 3D spatial information. In the circular representation, ROIs are arranged on the edge of the circle, grouped into the same clusters as in the worm plots. Each cluster is assigned a color, and the concentration of color is adjusted according to node degree. Significant connections are represented as lines between ROIs. The color of each significant connection is determined by the sign of the t-statistic and the opacity indicates the degree of significance.

Both worm plots and connectograms require a threshold of test significance. Given that a t-statistic is computed for each connection, some form of multiple testing correction must be used. In the case of a symmetric network G with r regions, the total number of tests is $M_G = r(r-1)/2$. Traditional methods, such as the Bonferroni and Šidák methods, assume independence of tests and calculate a new significance threshold from the total number of tests. However, the connected nature of brain networks implies dependence between connections. As such, traditional methods are overly conservative for connectivity analysis. To address this, we used a method proposed by Li et al (2012) [125], where an "effective number of independent tests" for network G, $M_{eff,G}$, is calculated. $M_{eff,G}$ replaces M_G in the traditional methods. $M_{eff,G}$ was applied to the Bonferroni correction to calculate an adjusted p-value threshold, $\alpha_{M_{eff,G}} = \alpha / M_{eff,G}$. We used $\alpha = 0.05$ as the uncorrected threshold.

Proof-of-concept

Two proof-of-concept studies were performed using the analysis described above. The first compared middle-age and elderly subjects from the Rotterdam Scan Study (RSS) [104, 105]. The second compared patients with schizophrenia to healthy controls from the Massachusetts General Hospital (MGH) in the MIND Clinical Imaging Consortium data collection [76], which is an open-access multi-site collaborative study of patients with schizophrenia. The original MGH imaging data and subject meta-data is available for download via http://coins.mrn.org/dataexchange. The networks calculated for each subject and the regression results calculated as part of this study are available at http://dx.doi.org/10.5061/dryad.88q04.

There were 84 and 82 cortical and subcortical regions chosen for network construction for the MGH and RSS studies, respectively. The cerebellum was excluded in the RSS sample because it was only partially scanned. After registration of the FreeSurfer segmentation to the diffusion image space, which required up-sampling of the data, two regions of one subject in the RSS study did not have any voxels remaining. Regional statistical tests involving these regions were computed by substituting group means for the missing values. See Table 2.1 for a list of regions used in these studies.

Table 2.1: *Regions involved in the proof-of-concept studies, grouped by location in the brain.*

Cluster	Region	Abbreviation
Cerebellum (Cb, RSS only)	Cerebellum	CeB
Frontal (Fro)	Caudal anterior cingulate cortex	Cac
	Caudal middle frontal gyrus	Cmf
	Frontal pole	FrP
	Lateral orbitofrontal cortex	LOf
	Medial orbitofrontal cortex	MOf
	Paracentral lobule	PCe
	Pars opercularis	POp
	Pars orbitalis	POb
	Pars triangularis	PTr
	Posterior cingulate gyrus	PCi
	Precentral gyrus	PrC
	Rostral anterior cingulate gyrus	RAC
	Rostral middle frontal gyrus	RMF
	Superior frontal gyrus	SFr
Occipital (Occ)	Cuneus	Cun
	Lateral occipital gyrus	LOc
	Lingual gyrus	Lin
	Pericalcarine cortex	Pcc
Parietal (Par)	Inferior parietal lobule	IPa
	Postcentral gyrus	PoC
	Precuneus	Pcn
	Superior parietal lobule	SPa
	Supramarginal gyrus	SMa
Subcortical (Sub)	Accumbens area	Acc
	Amygdala	Amg
	Caudate	CaN
	Hippocampus	Hip
	Pallidum	Pal

	Putamen	Pu
	Thalamus	Tha
Temporal (Temp)	Banks of superior temporal sulcus	BSt
	Entorhinal cortex	Erh
	Fusiform gyrus	Fus
	Inferior temporal gyrus	ITe
	Insula	Ins
	Isthmus of cingulate gyrus	ICG
	Middle temporal gyrus	MTe
	Parahippocampal gyrus	Phc
	Superior temporal gyrus	STe
	Temporal pole	TeP
	Transverse temporal gyrus	TrT

In the RSS data, after registration and down-sampling of the FreeSurfer atlas to the fMRI-space, in two regions of one subject no voxels survived the down-sampling (the left entorhinal cortex and the right temporal pole). All analyses did not include the missing values.

Participants

In the RSS study, non-demented subjects with T1, rs-fMRI and DWI scans were divided into two groups (middle-aged and elderly) based on age. Age ranges were 74 to 95 in the elderly group and 51 to 53 in the middle-aged group. They were selected such that the gender ratio in each group was the same. Subjects with mild cognitive impairment (as determined by the Mini-Mental State Examination [58], MMSE), large infarcts, and gliomas were excluded from the study. The MMSE score is a derived measure of a subject's global cognitive functioning with a total possible score of 30 [58].

In the MGH study, groups of patients with schizophrenia were compared to controls. Exclusion criteria included an intelligence quotient less than 70, a history of significant head injury and a contraindication for MRI scanning. Only subjects who had DWI, fMRI and pre-computed FreeSurfer segmentations were included. Parental socio-economic status (P-SES) was defined by the Hollingshead-Redlich scale [98], in which a score of

Table 2.2: *Subject demographics*

RSS	Middle-aged	Elderly	p-values
No. of subjects	37	37	n/a
Gender (M/F)	13 M / 24 F	13 M / 24 F	0^{χ}
Age	52.3 $\pm$ 0.6	81.1 $\pm$ 4.4	$< 0.0001^{t}$
MMSE	28.9 $\pm$ 1.1*	27.1 $\pm$ 1.7*	0.002^{t}
fMRI absolute head motion (mm)	1.0 $\pm$ 1.0	1.0 $\pm$ 0.9	0.9^{t}

MGH	Patient	Control	p-values
No. of subjects	23	21	n/a
Gender (M/F)	17 M / 6 F	12 M / 9 F	0.9^{χ}
Age	34.8 $\pm$ 9.8	38.7 $\pm$ 8.7	0.2^{t}
Years of education	11.5 $\pm$ 2.2	15.9 $\pm$ 2.0*	$< 0.0001^{*t}$
P-SES	3.3 $\pm$ 1.0	3.0 $\pm$ 1.0	0.9^{χ}
fMRI absolute head motion (mm)	0.4 $\pm$ 0.4	0.6 $\pm$ 0.6	0.4^{t}

Continuous variables are presented as mean $\pm$ SD

* One subject was missing this information, statistics computed over the remaining subjects

^{t} Calculated using Welch's t-test

$^{\chi}$ Calculated using χ^2 test

one defines the highest status and five defines the lowest. P-SES is often used as an estimate of what the socio-economic status of patients would have been if they did not have schizophrenia. Years of education is defined as the total number of years that a subject pursued elementary, secondary and post-secondary education.

In both studies, subjects with more than 4mm of head movement were excluded. All participants gave written informed consent and the original studies were approved by the medical ethics committee of the Erasmus MC, University Medical Center Rotterdam (for the RSS study) and the institutional review board of the Massachusetts General Hospital (for the MGH study). Table 2.2 describes the demographics of each group for the subjects that were included.

Image acquisition

All subjects from the RSS were scanned on the same 1.5 Tesla GE scanner with an 8-channel head coil. A research physician visually inspected each scan to ensure good quality. The T1-weighted protocol included a 3D fast RF spoiled gradient recalled acquisition in steady state with an inversion recovery prepulse sequence (TR $= 13.8$ms, TE $= 2.8$ms, TI $= 400$ms, FOV $= 21 \times 21$cm^2, matrix $= 416 \times 256$, zero-padded to 512×512, flip angle $= 20°$, NEX $= 1$, bandwidth $= 12.50$kHz) with 96 contiguous slices with slice thickness of 1.6mm zero-padded to 0.8mm. The final voxel size was $0.49 \times 0.49 \times 0.8$mm. The DWI protocol utilized a single shot, diffusion-weighted spin echo-planar sequence (TR $= 8000$ms, TE $= 68.7$ms, FOV $= 21 \times 21$cm^2, matrix $= 96 \times 64$, zero-padded to 256×256, NEX $= 1$) with 36 contiguous slices with 3.5mm slice thickness. The maximum b-value was 1000s/mm^2 in 25 non-collinear directions. Volumes were also acquired without diffusion weighting (b0). The final voxel size was $0.8 \times 0.8 \times 3.5$mm. The rs-fMRI protocol included a gradient-echo BOLD sequence, (TR $= 2900$ms, TE $= 60$ms, matrix $= 64 \times 64$, flip angle $= 90°$) with 35 contiguous 3.3mm slices and 160 volumes (total scan length = 464s). The voxel size was $3.3 \times 3.3 \times 3.3$mm.

The MGH subjects were scanned on a 3 Tesla Siemens Trio scanner with an 8-channel head coil. The imaging parameters of the T1-weighted sequence were TR $= 2530$ms, TE $= 3.79$ms, TI $= 1100$ms, FOV $= 16$mm, matrix $= 256 \times 256 \times 128$cm, flip angle $= 7°$, bandwidth $= 181$Hz/pixel, 0.625×0.625mm voxel size and slice thickness 1.5mm. The DWI scan parameters were TR $= 10500$ms, TE $= 98$ms, NEX $= 2$, bandwidth $= 1342$Hz/pixel, 64 slices, thickness $= 2$mm, 2×2mm voxel size. The maximum b-value was 1000s/mm^2 in 12 directions. The fMRI parameters were TR $= 2000$ms, TE $= 30$ms, flip angle $= 90°$, FOV $= 22$cm, bandwidth $= 3126$Hz/pixel, 27 slices, slice thickness $= 4$mm with 1mm skip, 3.4mm in plane resolution and 177 volumes (total scan length $= 354$s). Three runs of the Sternberg item recognition paradigm (SIRP) [180] were collected. SIRP is a task-based fMRI sequence with a block design that measures working memory. The run with the least amount of motion was selected for connectivity analysis.

Covariates

Covariates were included in the regression model to control for their influence. In the RSS study covariates included MMSE and gender. In the MGH study covariates included age and gender.

Results

The chosen connectivity metrics were evaluated both uni- and bi-modally described in the methods section. The resulting figures and tables are described below for both the MGH and RSS studies.

The bi-modal network comparison plots in Figure 2.3 show the structure-function relationship for the mean networks and t-statistic distributions for each study. 2D histogram opacity indicates number of connections, and in the mean network plots, color indicates the proportion of each group involved. Along the axes, distributions of connection weights for each individual connectivity type are plotted.

In the RSS study, group differences are easily visible in the mean network histograms of DMC, which is also reflected in the t-statistic distributions. Global group differences are not obvious in the mean network plots or the t-statistic plots for fPC and fMT in both groups and DFA in the RSS. In the MGH study, global group differences are not obvious in the mean network plots, but do show in the t-statistic plots for DMC and DFA.

Both studies show a large peak in mean DMC near zero. In order to determine whether this peak is fully explained by connections between adjacent regions we regenerated the histograms after omitting all connections between adjacent regions. In the MGH study, the peak disappeared. In the RSS study the peak did not fully disappear, but did become much smaller.

In the unimodal t-statistic histograms, all types of connectivity appear to be approximately normally distributed. The positive shift in t-statistic of DMC in the RSS study indicate a global increase in minimum cost in the elderly population. In the MGH study, there is a global decrease in DMC and DFA. It is interesting to note that both fMT and fPC mean network values were centered around zero and the standard deviation of fPC was much smaller than fMT in both studies, but the t-statistic indicated similar levels of group differences. The 2D t-statistic histograms show no significant correlation between structural and functional t-statistics.

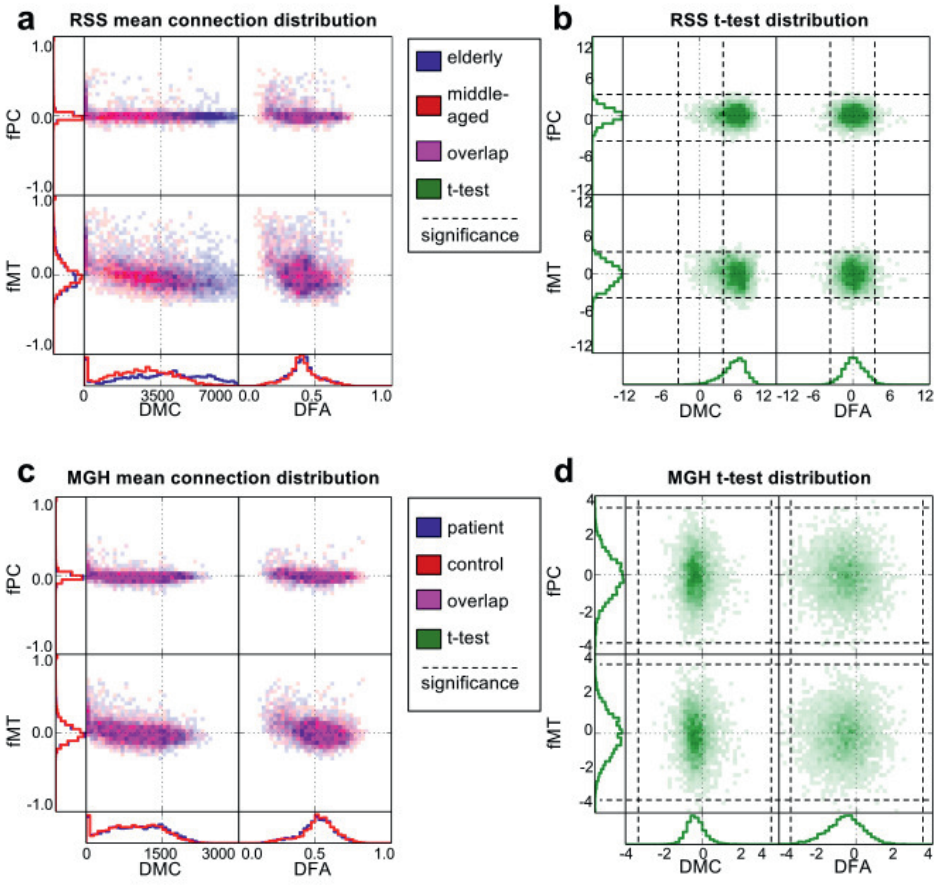

Figure 2.3: ***Bi-modal network comparison plots.*** *Structure-function relationships are shown for the mean connectivity network of each group in (a) and (c), and the distribution of t-statistics in (b) and (d). (a) and (b) correspond to RSS, where in (a) blue represents the elderly group and red indicates the middle-aged group. (c) and (d) correspond to MGH, where in (c) blue represents the patients with schizophrenia and red represents controls. In the 2D structure-function histograms, magenta indicates overlap of the two groups. In the t-statistic histograms, green shows group differences, where positive values indicate elderly > middle-aged in RSS and schizophrenia > control in MGH.*

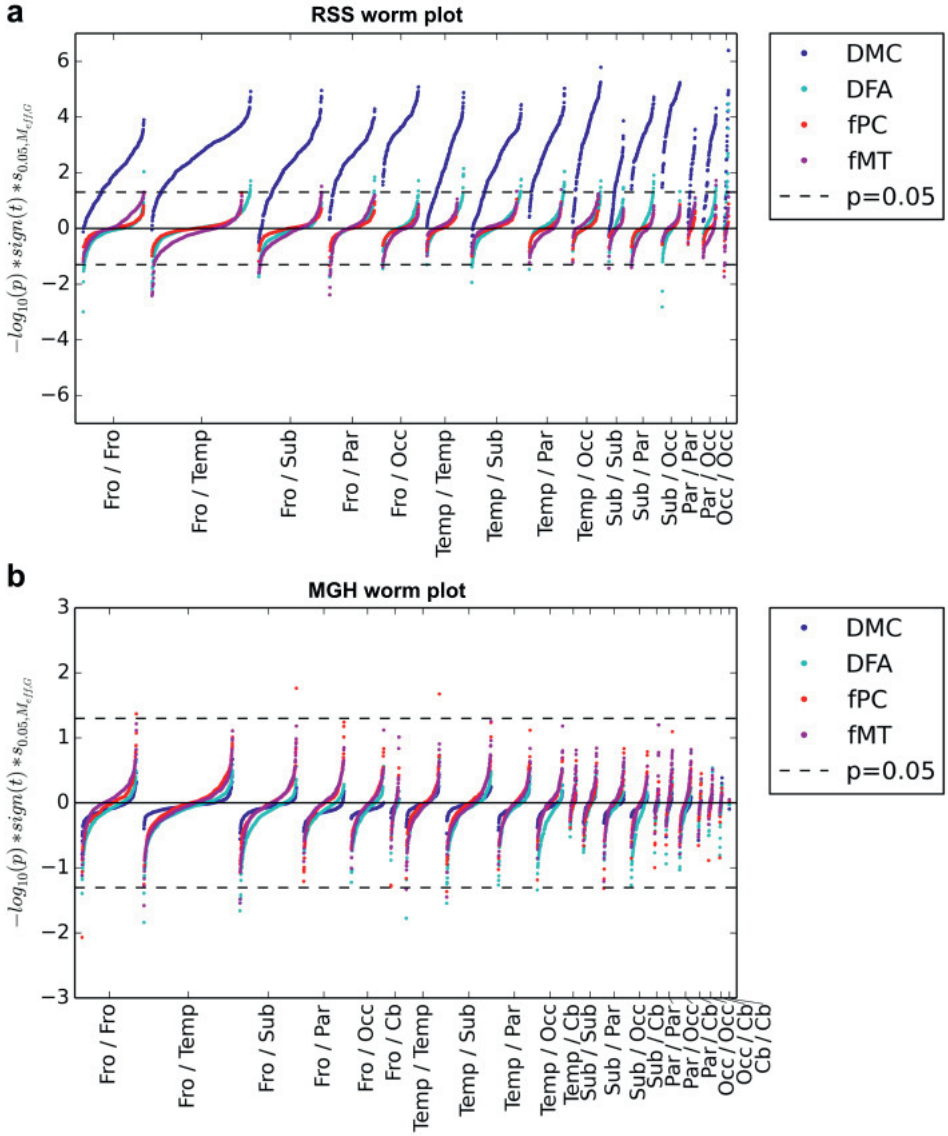

Figure 2.4: ***Worm plots.*** *Connections in the (a) RSS and (b) MGH studies are grouped by location of region pairs. Groupings include subcortical (Sub), occipital (Occ), parietal (Par), temporal (Temp), frontal (Fro) and the cerebellum (Cb). Cb was not included in the RSS study. On the y-axis is the negative log of the p-value, multiplied by the sign of the corresponding t-statistic and scaled such that the line indicating p=0.05 is at the same position for all plots.*

A worm plot of the p-values corresponding to the t-statistics of each connection is shown in Figure 2.4. The regions of the brain are divided anatomically into groups corresponding to different parts of the brain, including subcortical, occipital, parietal, temporal, frontal and the cerebellum. The cerebellum was not included in the RSS study because it was only partially scanned.

In the RSS study, DMC has many highly significant connections, with values well above the significance level for the majority of connections in all regions (Figure 2.4a). In the MGH study, very few connections show significant group differences. In both studies, some networks are shifted away from $-log_{10}(p) = 0$ for some clusters. T-tests were done on the t-statistic values of the connections in each worm in Figure 2.4 to determine the degree to which they were shifted away from $t = 0$, which is visualized in Figure 2.5.

In the RSS worm plot, it is obvious that all clusters except Fro/Temp have highly significant positive DMC associations with age. The shifts in DFA and fMT are weaker than those of DMC and are mixed between positive and negative connections. Several significant cluster shifts appear in both. There were no significant fPC cluster shifts.

In the MGH study, DMC and DFA had the most significant associations with schizophrenia, all of which were exclusively negative. fMT and fPC had a mixture of positive and negative associations which were much weaker than the structural connectivity associations. fPC had particularly weak associations.

The connectograms in Figure 2.6 show the significant connections of some of the networks for each study. Red indicates significant connections with positive association (in the MGH this implies schizophrenia > control, in the RSS old > young), and blue indicates negative association. The opacity of the lines indicates the level of significance and the saturation of each region indicates the number of significant connections involving that region. In the RSS study, DMC is not shown because it had too many connections to extract meaningful conclusions. In the MGH study DMC is not shown because it had no connections with $p < \alpha_{M_{eff,G}}$.

In the RSS study, the DFA network had several significant connections with both positive and negative associations with age. The positive associations were concentrated in the temporal and occipital lobes. The left temporal pole had many more significant connections than the other regions. The right temporal pole also had several significant connections. Inter-hemispheric significant DFA connections were

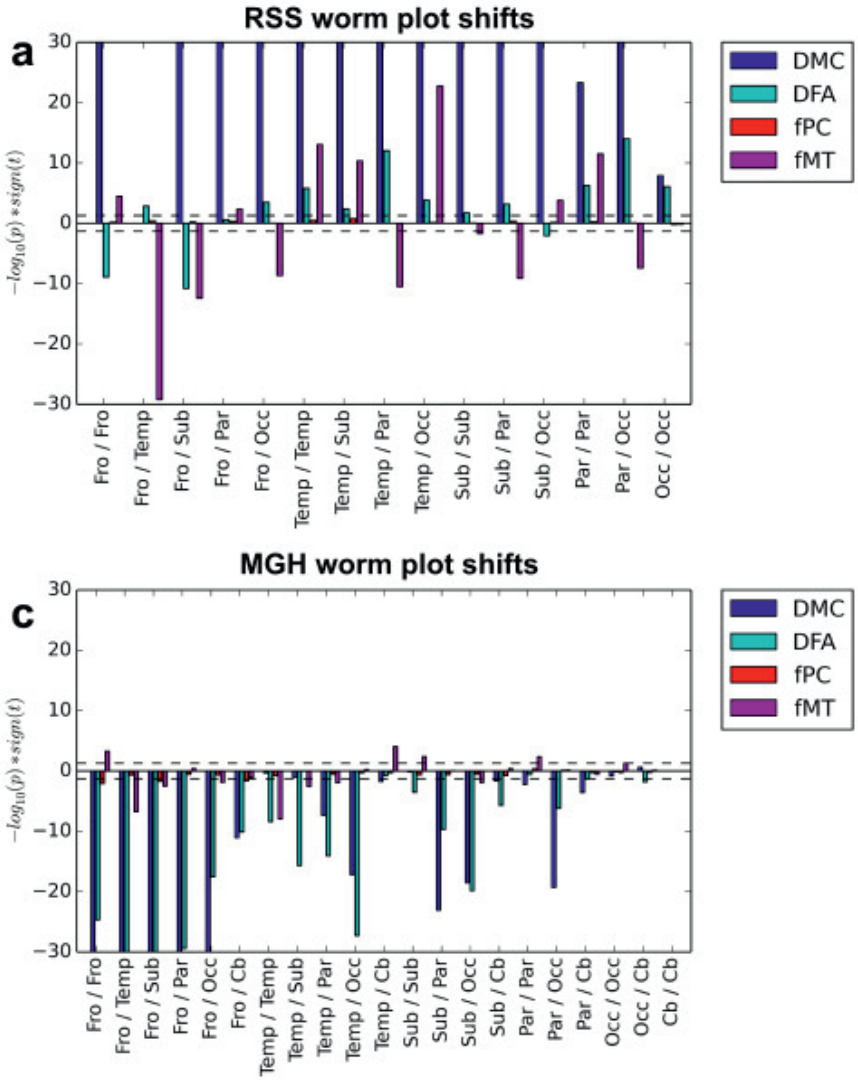

Figure 2.5: ***Bar plot of worm plot shifts.*** *One-sample, two-sided t-tests were used to determine the degree to which each worm in the worm plot is shifted away from zero in the (a) RSS and (b) MGH studies for all pairs of region clusters. Groupings include subcortical (Sub), occipital (Occ), parietal (Par), temporal (Temp), frontal (Fro) and the cerebellum (Cb). Cb was not included in the RSS study. On the y-axis is the negative log of the p-value, multiplied by the sign of the corresponding t-test and scaled such that the line indicating p=0.05 is at the same position for all plots.*

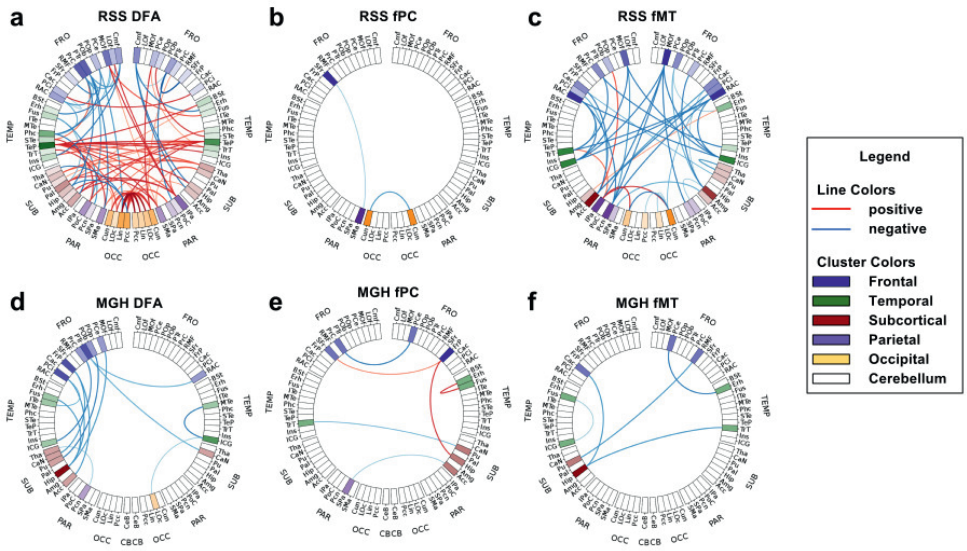

Figure 2.6: ***Connectograms of significant connections.*** *Red connections have significantly positive t-statistic values corrected for multiple testing, blue are negative (in the MGH schizophrenia > control, in the RSS old > young). Degree of significance is indicated by the opacity of the lines. Color saturation of regions shows the number of connections involving that region. For the RSS (a) DFA, (b) fPC and (c) fMT are shown. RSS DMC is not shown because there were too many significant connections to visualize. For the MGH (d) DFA (e) fPC and (f) fMT are shown. MGH DMC is not shown because there were no significant connections.*

exclusively positive, indicating an increase in the older group. Decreases in DFA were exclusively intra-hemispheric, many of which involved left frontal regions. There were three significant RSS fPC connections, all of which were intra-hemispheric. The RSS fMT connectogram shows exclusively negative associations, many of which involved the right medial orbitofrontal cortex.

In the MGH study, all significant DFA connections indicated negative associations with schizophrenia, most of which involved only the left hemisphere and especially frontal and temporal regions. MGH fPC connections were both positive and negative. All three negative fPC significant connections were inter-hemispheric. All five significant fMT connections were negative. Three of them involved frontal regions.

Discussion

This study presents a framework for comparison of ROI-based functional and structural connectivity to identify group differences. Given two groups of subjects, each of which has T1, DWI and fMRI images, networks were constructed, and then compared uni- and bi-modally for their ability to explain group differences. The t-statistic based analysis of each connection identified which network types contribute most to group differences, and between which areas of the brain these differences occur.

There are a growing number of types of structural and functional brain connectivity available. The methods described in this paper can be used to compare multiple types of connectivity, both in uni-modal studies and for integrated analyses. Visualizations of significance of connections help to identify important connections and groups of connections and compare them to existing knowledge of group differences. With the proposed framework two proof of concept studies were conducted comparing structural and functional connectivity.

Bi-modal network comparison plots

The bi-modal network comparison plots in Figure 2.3 give important insights into the investigated network types and the relationships between them. They simultaneously show both uni- and bi-modal distributions, which makes it easy to consider both at the same time. Viewing all connectivity types in the same plot consolidates the information, making comparisons easier.

Global group differences can sometimes be seen in the 1D histograms of each network type. For example, in the mean-network plot of the RSS, DMC obviously has group differences, indicating that elderly subjects have higher cost paths than middle-aged subjects. Even when global group differences were not obvious in the mean-network plots, differences were sometimes found using the t-statistic plots. For example, in the MGH, DMC and DFA showed no obvious group differences in the mean-network plots, but did show global negative shifts in the t-statistic plots, suggesting that patients with schizophrenia have lower cost paths with reduced FA. The decrease in DFA is consistent with previously observed white matter abnormalities [116] and decreased DFA [138] in patients with schizophrenia. The decrease in minimum cost in the schizophrenia group is unexpected, but might be explained by the

inclusion of age as a covariate. As can be seen in the RSS DMC histograms, DMC is highly influenced by age. Patients with schizophrenia were on average older than controls. Including age as a covariate would have removed the effect of age differences, but it is possible that the regression overcompensated for this variable and that the global decrease is not representative of the true role of minimum cost in schizophrenia. To determine the true effects of schizophrenia on DMC, the analyses should be repeated on an age-matched sample. Both mean-network and t-statistic plots provide useful information when examining connectivity metrics in relation to group differences.

The 2D part of the mean-network plots show bi-modal relationships between connectivity types. In both studies, the patterns seen in the mean-network plot show a similar pattern, indicating that the mechanism governing the global functional and structural differences may be inherent to the connectivity metrics themselves, and not related to the subject groups being studied. For example, both fPC and fMT are increased where DMC is near zero. DMC is usually near zero between adjacent regions because there is no distance between them, and hence minimal travel costs. This close proximity may also explain the increase in functional connection weight, since adjacent regions likely have similar blood-oxygen dynamics near their border and hence greater correlation.

The bi-modal view can also be used to make inferences about differences in connection types from the same modality. For example, global group differences are much lower in magnitude in fPC than in fMT. The difference in the derivation of fPC and fMT is that fPC uses partial correlation to estimate the direct connection between specific regions [166], whereas fMT uses full Pearson correlation. Thus, global group differences are greater in indirect connections than in direct connections, which may affect sensitivity of the metric to specific effects. fPC and fMT are both well-established widely used connectivity metrics, and the choice of which to use depends on the research question one wishes to answer [126].

We decided to represent the bi-modal part of the network comparison plots with 2D histograms. The relationship between structure and function can also be visualized using scatter plots [100]. While the same general trends can be seen in histograms and scatter plots, in places with high density, points in scatter plots will overlap and thus be not differentiable, in which case scatter plots are unable to show differences in

density. By using a histogram, differences in density can be shown using color density. Another disadvantage of scatter plots is that overlap of points makes seeing group differences difficult. When points from one group cover points from another group, it may appear as though only one group is important. 2D histograms can better represent the degree of each group's influence by representing each group by a given color, where the degree of overlap is indicated by combining the two colors. This is seen in the RSS mean-network plot, where the elderly subjects are represented by blue, the middle-aged subjects by red and overlap is represented as magenta. It is clearly visible that high DMC is dominated by elderly subjects, and low but non-zero DMC is dominated by middle-aged subjects. Moderate and near-zero DMC is equally represented by both groups. Group visualization is in most cases, however, limited to two groups since more colors would likely make it harder to differentiate where each group has influence. The bi-modal network comparison plot could also be used with continuous variables. For example, age can be modelled continuously rather than using age groups. In this case, rather than computing group mean networks, one could simply make 1D and 2D histograms of structural and functional weights over all subjects, but color each part of the histogram according to the mean age associated with all points in a given connection weight range. If a gradient of color is seen, then this indicates that connectivity changes globally with age. Rather than plot the t-statistic related to group differences, one could plot the regression coefficient associated with age.

The data presented here indicated no global functional group differences, neither in 1D nor in 2D. However, with other data the 2D histograms might be useful in identifying important group differences involving both functional and structural connectivity. It is possible that little or no group differences are obvious uni-modally, but that they become obvious when viewed bi-modally. The connectivity types used here also did not show an obvious relationship between functional and structural t-statistics, however if such a relationship did exist, the 2D representations would help to see it. Such relationship would indicate that connections with significant structural differences tend also to have strong functional differences.

Worm plots

The worm plots in Figure 2.4 give important insights into regional changes in connectivity. Worm plots reflect global changes in connectivity, but often also show cluster level changes. The global changes in DMC in both studies and in DFA in the MGH study were also seen in the worm plots by the uni-directional shifts of each group of connections. All clusters in the worm plots were shifted to different degrees, indicating a relative importance of each cluster. Even when global network changes were not observed, shifts in regional groupings of connections became apparent in the worm plots. fPC and fMT had positive and negative shifts for both studies, as did DFA in the RSS. fMT and DFA both had large shifts, whereas fPC cluster shifts were minimal. This suggests that fPC is less sensitive to group differences than the other metrics. As in the bi-modal network comparison plots, this reflects the removal of the influence of other regions in a given correlation. A thorough psychological analysis of group differences identified in the worm plots is beyond the scope of this study and is limited by small sample sizes. However, we believe that epidemiological studies with high statistical power would benefit from analysis using worm plots.

As with the bi-modal network comparison plots, the worm plot can be used to represent continuous variables rather than groups. For example, if age was modeled continuously, one could simply replace the sign of the t-statistic in the y-axis with the sign of the coefficient associated with age. As with age groups, the continuous version of the plot would show the association of age with grouped connections.

If one was to judge a network's ability to separate groups purely based on global network differences and individual significant connections, it would be easy to dismiss a network as insensitive to group differences. However when looking at regional groupings of connections it may become apparent that group differences do exist. The worm plot provides a mid-level analysis, more specific than the global differences seen in the bi-modal network comparison plots, but more general than looking only at specific significant connections. The worm plot extracts important relationships that are otherwise invisible to global or individual connection based analysis.

Connectograms

The connectograms in Figure 2.6 visualize significant differences in specific connections in a 2D representation, where nodes are grouped by location in the brain. This enables quick identification of individual significant connections, significant groups of spatially-related connections and nodes with many significant connections. In both the RSS and MGH studies, the connectograms provided a clear and easily interpretable representation of significant connections in the DFA, fPC and fMT networks. Again, similar to the bi-modal network comparison plots and worm plots, one can use connectograms to visualize the association of connections with a continuous variable by determining the color of a connection by the sign of the coefficient associated with it.

Nodes with many significant connections are immediately obvious in connectograms. For example the left and right temporal poles (TeP) in the RSS DFA connectogram and the right medial orbitofrontal cortex (MOf) in the RSS fMT connectogram are easy to spot because they have several highly significant connections associated with them. The left hippocampus (Hip) in the RSS DFA also has several significant connections associated with it, which can be spotted by the region's increased color saturation, however it is less obvious because crossing connections make it difficult to see how many connections are coming from that region. Regions with many significant connections might be less obvious in a 3D representation of brain connectivity, depending on from which angle it is viewed. This would arise because a 3D representation must be viewed as a 2D projection, which might result in an important region being surrounded by unrelated connections and regions that are spatially far away, but appear in that orientation to be nearby. Additionally, 3D representations can potentially misrepresent the data. For example, if two nodes overlap in a specific orientation, they may be interpreted as a single node, with connections from both nodes extending from the same spot. This confusion can be avoided by using connectograms.

The use of connectograms also made it easy to spot networks that have many significant connections that are primarily uni- or bi-lateral. For example, most significant connections in the MGH DFA network are uni-lateral negative associations with schizophrenia in the left hemisphere, which is consistent with the reduction of left hemisphere dominance seen in schizophrenia [10]. Also, the RSS DFA network has an

abundance of positive inter-hemispheric connections and negative intra-hemispheric connections, suggesting that aging is associated with increased FA along inter-hemispheric minimum cost paths and decreased FA along intra-hemispheric minimum cost paths. An interesting avenue of future research might be to reconstruct the minimum cost paths found by SAMSCo to see if this unexpected increase can be explained by differing minimum cost paths in the old and young subjects.

A limitation of the connectogram is that there is an upper limit to the number of significant connections that it can show. The RSS DMC network had so many significant connections that useful inferences could no longer be made using a connectogram. This issue is also a limitation of 3D representations of brain connectivity. In such cases, one might consider using a matrix representation [17, 23, 198]. In this representation the connections never overlap, and thus all connections can be shown simultaneously. The disadvantage of a matrix representation, however, is that regions with several significant connections might be less obvious, since to identify them one must scan an entire row or column of a matrix and count the number of significant connections.

Methodological considerations

Image preprocessing and network generation

Subject motion is an important issue to address in any neuro-imaging study. This is especially so in functional connectivity studies. Head motion has a significant effect on connectivity. It increases connectivity estimates over short distances, decreases them over long distances, reduces modularity and can inflate the effect of age on connectivity [157]. When preprocessing our fMRI data, we addressed subject motion by regressing out six motion parameters. Alternative approaches include 24 motion parameter nuisance regression, targeting volumes affected by motion and using independent component analysis, all of which are thoroughly evaluated by Pruim et al. (2015) [147] for their ability to both remove motion-related artifacts and to preserve the signal of interest. Compared to other approaches, regressing out either six or 24 motion parameters only minimally reduced the impact of motion artifacts and was not very reproducible. However, using six parameters had minimal loss of temporal degrees of freedom. They also examined data scrubbing, which is a widely-used

approach that removes volumes affected by motion [146]. Although this approach is effective in removing variations induced by motion, it also results in a significant loss of temporal degrees of freedom and is less reproducible than many of the methods based on independent component analysis [147]. Given that subject motion can confound studies by inducing group differences, it is important to carefully choose an appropriate method of dealing with motion. Global signal regression, which was employed in this study, can reduce motion-related group difference [146]. It can remove false variance present in resting-state functional connectivity data, but it has also been linked to a negative bias in correlations computed from fMRI data [146]. Because of this, its use in functional connectivity studies is controversial and future studies must carefully examine the risks and benefits before deciding whether to use it or not.

Regarding choice of structural connectivity measures, it is important to note that both measures (DMC and DFA) are products of the SAMSCo framework, which always produces a fully connected graph in which each pair of regions has an associated connection weight, even when no physical connection is present. This reflects the possibility that regions may communicate with each other by sending signals via intermediate regions. On the other hand, more traditional definitions of structural connectivity, such as those based on streamline tractography, represent direct connections only and as such result in sparse matrices where only direct connections have non-zero values [175]. It is important to keep in mind whether a structural or functional network measure represents direct or indirect connectivity, since this can have a profound impact on the interpretation of the results.

Defining regions of interest

An important consideration when building brain connectivity networks is the method used to segment the cortex and sub-cortex [88]. Segmentations are a macroscopic representation of microscopic neuronal architecture, the relationship between which is not fully understood. This makes the choice of scale and algorithm complex. This study used an anatomical segmentation of the cortex and sub-cortex into anatomical regions, which has also been done in previous studies [37, 60, 183]. It is important to note that anatomical segmentations are one of many potential segmentation strategies. Zalesky et al. (2010) [217] used random segmentations to show that the scale of segmentation (i.e. the size and number of segmented regions) and the angular resolution of DWI data

affect the topological attributes of structural networks. Randomly segmented regions do not generally correspond to specific anatomical or functional regions, and thus may not be suitable to answer questions where regions should represent known areas of functional specialization. Cammoun et al. (2012) [25] found a compromise between anatomic and random segmentation by subdividing FreeSurfer regions into smaller regions on multiple scales. Both Zalesky et al. (2010) [217] and Cammoun et al. (2012) [25] acknowledge that while segmentation scale affects the outcome of network studies, both coarse and fine segmentations have benefits and drawbacks, and thus choice of scale should be made depending on the research question.

The segmentations discussed thus far do not use fMRI to delineate borders between regions. This may result in regions which are not functionally distinct. Several groups are working on methods of using functional data to segment grey matter. For example, Blumensath et al. (2013) [21] uses region-growing in fMRI data to find subject-specific functionally homogeneous parcels which are spatially contiguous and disjoint. The method was reproducible within subjects, however there was no correspondence between subjects' segmentations, which precludes between-subject direct comparison of connectomes using such a segmentation. Shen et al. (2013) [163] used a group-wise clustering algorithm to produce functionally homogeneous and non-overlapping parcels that correspond across subjects, thus allowing between-subject comparisons. These methods, unlike the anatomical methods, produce segmentations that estimate functionally segregated regions.

The anatomical methods and the two functional methods discussed above produce 'hard parcellations' [170], where regions are represented by non-overlapping groups of contiguous voxels. In some cases, hard parcellations may not be an appropriate representation of true functional parcellations and connectivity patterns. Previous studies have suggested that multiple overlapping functional networks exist [166]. Thus a brain region might be involved in multiple networks, in which case the time series of that region would be a mixture of signals. In such cases, hard parcellations are unable to adequately address the mixture of signals, since all voxels within a region are assigned the same weight. High-dimensional independent component analysis, on the other hand, takes signal mixtures into account by defining nodes as (potentially overlapping) spatial maps of functionally related voxels [12, 170]. Overlapping spatial maps can also be produced using seed-based functional connectivity maps [192] and

temporal functional modes [166]. Because spatial maps are often composed of multiple groups of contiguous voxels, and spatial maps often overlap with each other, each network typically describes non-contiguous and overlapping parts of the brain. Depending on the research question, one could represent graph nodes by individual networks. If contiguous regions are desired, each contiguous portion of a network could be described by a separate node. In either case, connectivity can then be estimated between pairs of regions and represented as a graph. The graph could subsequently be analyzed using the methods described in this paper.

Another potential concern related to segmentation is regions with unique internal connectivity patterns. Van den Heuvel and Hulshoff Pol (2010) [192] have shown that voxels in one hemisphere of the motor strip have maximum correlation with voxels in approximately the same location in the contralateral hemisphere. Previous studies have shown that connectivity gradients exist in some parts of the brain [166]. These unique connectivity features are poorly represented by distinct regions that assume uniform intra-region connectivity. It is important to keep this in mind when interpreting the results of connectivity analyses.

The question of segmentation strategy is not trivial and must be considered with great care. Choice of segmentation method and resolution can have a profound influence on network characteristics [43]. It is essential to realize that a poor segmentation can inappropriately group functionally unrelated voxels into the same region, or can split voxels with homogeneous signals into multiple regions.

Whether using a 'hard parcellation' or a non-contiguous and overlapping segmentation, if one wishes to analyze multiple subjects simultaneously, it is essential that segmentations correspond across subjects [166, 170]. If this basic requirement is met, then the visualizations methods presented in this paper can be applied to graphs produced with the discussed segmentations, provided that a logical grouping of nodes is provided. That being said, it is essential to realize that even though the visualizations may show interesting results, poor segmentations can obscure true connectivity patterns and interpretation of results.

Grouping regions of interest

Another issue related to segmentation is how to group regions. Regions can be grouped anatomically [60], which was the strategy used in this study. Regions can also

be parcellated using graph-theory based methods. For example, Betzel et al. (2013) [18] used a Markov process to group nodes on multiple scales based on connectivity obtained from diffusion data and evaluated each scaled based on several metrics derived from structural or functional connectivity. In another study, Yeo et al. (2011) [215] used a clustering approach to group nodes using resting-state fMRI data and found node groups that were similar to resting-state networks. Previous studies have shown that functionally-determined networks are highly interpretable and are reproducible across sessions [36] as well as across sites and datasets [167], and as such may provide a reliable parcellation to be used in graph-based brain connectivity studies. The cortical parcellation from Yeo et al. (2011) [215] was used by Betzel et al. (2014) [17] to assess changes in functional an structural connectivity across the lifespan and Sripada et al. (2014) [177] to determine whether attention-deficit/hyperactive disorder causes developmental lag within the connectome as children grow older. In both cases, the borders of ROIs within each group corresponded well with the borders of each of the parcellations. A functionally defined parcellation could be used to group regions from a segmentation that does not have corresponding borders, such as an anatomically-defined segmentation. However, this may not be the best option if one or more ROIs have significant overlap with two networks.

It is important to note that applying an existing cluster-based parcellation to a new dataset assumes that the parcellation is representative of the new data set. It is possible that the composition of node groups changes with age or in different psychiatric states. In the case of task-based fMRI, such as in the MGH data set, it is questionable whether resting-state-network-like groupings are an appropriate choice. To circumvent these issues, study-specific node groups could be computed. However, there is the question of what sample size is required to obtain a reliable estimate of parcellations. Additionally, multiple scales may offer feasible node groups, the use of which likely requires justification in the context of the research question being asked. In spite of the uncertainty that is involved in using data-driven groupings of regions, their functional basis makes them worthy of consideration in future studies assuming that these uncertainties are taken into account when interpreting results.

Whether region groups are decided anatomically, in a data-driven manner, or in another manner, the groupings can easily be used in worm plots and Connectograms

to draw conclusions about within- and between-group connectivity. While these figures cannot simultaneously represent node groups of different scales and compositions, they can be used on each scale separately.

Multiple testing correction

The methods in this paper used mass univariate testing [198] to look for group differences in brain connectivity on global, lobe-level and individual connection levels. The large amount of tests involved in this approach must be addressed by using some form of multiple testing correction. We addressed this by calculating an "effective number of independent tests" and using that number in a Bonferroni correction [125]. Several similar methods exist [70], along with alternatives such as permutation testing [106].

Even with a liberal method of multiple testing correction, few or no significant tests may be found. While this is largely due to the large number of tests involved, the problem can be magnified by low signal-to-noise ratios in data, which will weaken observed statistical relationships. In these cases, a coarser level of analysis can increase statistical power. For example, the network-based statistic method thresholds individual test statistics of a network, identifies resulting connected components and calculates a p-value for each component. By considering sub-networks rather than individual connections, the network-based statistic gains statistical power, especially when signal-to-noise ratios are low.

Another alternative to mass univariate testing is to use graph theoretical measures [114, 154], which can also be used to study group differences and associations with continuous variables, such as age and neurological test scores [17, 31, 60, 62, 218]. While the use of graph theoretical measures is a promising area of research, great caution must be exercised when using them to describe group differences or changes relative to a continuous variable. Deficiencies in the construction of input networks, including inappropriate choice of regions defining nodes, might affect graph theoretical measures and their interpretation, and their abstract nature makes it difficult to determine whether observed associations are due to true changes in connectivity or due to confounds [166].

Yet another alternative to mass univariate testing is "seed partial least squares correlation" [115], which combines the ROI correlation matrices of all subjects and

performs singular value decomposition to produce new matrices that can provide information about which seed region contributes most to group differences. It is important to note two differences between the correlation matrices from the partial least square method and those used in this study. Firstly, it works with correlations of voxels, and thus requires that all subjects' brain scans are in the same space, which ignores the individual anatomical and functional differences that exist between subjects [210]. This can be overcome by considering regional time-series instead of voxel time-series, in which case subjects do not need to be in the same space. The second difference is that the partial least squares method considers correlations between two mutually exclusive sets of time-series, and thus correlations between some pairs of time-series are not considered.

The three alternatives to mass univariate testing described here, namely the network-based statistic, graph theory measures and seed partial least squares correlation, are viable alternatives that one might consider when there is a concern about statistical power or signal to noise ratio. They are, however, incapable of identifying individual significant connections. Both univariate testing and methods on a coarser scale are worth considering when feasible and appropriate.

Along with mass univariate testing, the methods presented in this paper might be affected by the effects of multiple testing when considering multiple connectivity metrics. In this study we did not control for multiple comparisons of connectivity metrics because the connectivity metrics that we used are likely highly dependent. That combined with the fact that we only compared four metrics would result in minimal effects of multiple testing correction. However, it is important to realize that not correcting for multiple tests might inflate the false positive rate. Future studies that aim to compare multiple connectivity metrics should evaluate the degree of dependence that exists between metrics and choose an appropriate method of multiple testing correction, especially if the comparisons are used to decide on a metric that best suits their research question.

Alternatives to graph-based connectivity

This paper was primarily concerned with connectivity modelled by graphs, where ROIs define nodes and relations between nodes define edges. There are, however, other ways of defining connectivity. For example, functional connectivity is often examined

using independent component analysis [24], (fractional) amplitude of low-frequency fluctuation [221] and dual regression [54]. These methods produce spatial maps of voxels with similar dynamics. Spatial maps of FA and MD can also be created from diffusion MRI data. Both measures are used to assess the health of the white matter tracts that are at the core of brain connectivity [113, 168, 206, 208, 211]. White et al (2009) [211] discovered white matter "potholes", which are FA hypo-intensities that are spatially unique to each subject. While pothole locations often do not overlap between subjects, the occurrence of potholes tends to be higher in subject groups than in controls [206, 208, 211].

The visualizations presented in this paper were not designed to be used with voxel-wise connectivity metrics. The worm plot, however, could be easily used to visualize the results of voxel-wise connectivity studies by representing the statistical test associated with each voxel within a network as a point in the plot. Points can then be grouped by the networks to which they belong. The bi-modal connectivity plots could technically be used with spatial map data. However, to show a bi-modal relationship there should be a one-to-one correspondence between points in the functional and structural maps. Although you can relate corresponding functional and structural voxels to each other, voxel-wise relationships between diffusion and functional maps are rarely of interest in connectivity studies. Rather, the interest lies in the relationship between functionally connected grey matter regions and the white matter tracts that connect them. One could use the bi-modal plots to show relationships between spatial maps originating from the same modality, although this then becomes a uni-modal comparison. For example, one could plot the relationship between z-scores from FA pothole analysis and z-scores of radial diffusivity or mean diffusivity to determine whether a subject group's FA potholes have corresponding drops in other measures of white matter integrity. Unlike the worm and bi-modal network plots, the connectogram cannot be used with voxel-wise data since it is inherently meant to represent data that is represented as a graph. Of course, one could use the spatial maps from voxel-wise analysis to define regions of interest and subsequently use them to derive graphs, which could then be visualized using all of the presented graphs, but this would then no longer be a voxel-wise analysis.

Whether examining connectivity via graph-based methods or using a voxel-wise approach, an important consideration is whether to use spatial normalization. Spatial normalization requires non-linear registration to a common reference space, thus

potentially losing important information related to subjects' unique anatomical features. The use of spatial normalization assumes spatial overlap of functional activation or white matter abnormalities across subjects. This assumption is often not the case [210, 211]. An advantage of graph-based connectivity is that a common set of nodes is the basic requirement to be able to compare subjects. Thus spatial normalization is not a requirement, even though it is sometimes still used. Some voxel-wise methods such as amplitude of low-frequency fluctuation and dual regression are also capable of generating subject specific connectivity maps in subject space. Group voxel-wise comparisons would still need to be carried out in standard space, but the registration can then be done on the subject-specific maps. In this case, connectivity estimation is not affected by normalization. Whether using spatial normalization or not, both spatial map methods and graph-based methods are invaluable tools in the study of brain connectivity.

Future directions

This paper focused on methods for integrated analysis and visualization of structural and functional connectivity, and provided a proof of concept in rather small pilot studies. In the future we will apply the methodology to larger samples, and will use it to evaluate new methods of defining connectivity.

Conclusions

A method for integrated analysis and visualization of structural and functional connectivity differences has been proposed. In two pilot studies it could be shown that the approach enabled analysis of group differences, namely between elderly and middle-aged subjects as well as between patients with schizophrenia and controls. The method provides a way to evaluate connectivity metrics against each other for use both uni- and bi-modally.

Acknowledgements

We would like to offer our sincerest thanks to all those involved in the collection of the RSS and MGH datasets. Hazel Zonneveld was a great help in assembling the RSS data used in this study. Ryan Muetzel provided valuable input in various analysis steps.

3

Differential patterns of age-related cortical and subcortical functional connectivity in 6-to-10 year old children: A connectome-wide association study

Carolyn D. Langen, Ryan Muetzel, Laura Blanken, Aad van der Lugt, Henning Tiemeier, Frank Verhulst, Wiro J. Niessen, Tonya White

Under revision

Abstract

Typical brain development is characterized by specific patterns of maturation of functional networks. Cortico-cortical connectivity generally increases, whereas subcortico-cortical connections often decrease. Little is known about connectivity changes amongst different subcortical regions in typical development. This study examined age- and sex-related differences in functional connectivity between and within cortical and subcortical regions using two different approaches. The participants included 411 six- to ten-year-old typically developing children sampled from the population-based Generation R study. Functional connectomes were defined in native space using regions of interest from subject-specific FreeSurfer segmentations. Connections were defined as: (1) the correlation between regional mean time-series; and (2) the focal maximum of voxel-wise correlations within FreeSurfer regions. The association of age and sex with each functional connection was determined using linear regression. The preprocessing included the exclusion of children with excessive head motion and scrubbing to reduce the influence of minor head motion during scanning. Cortico-cortical associations echoed previous findings that connectivity shifts from short to long-range with age. Subcortico-cortical associations with age were primarily negative in the focal network approach but were both positive and negative in the mean time-series network approach. Between subcortical regions, age-related associations were negative in both network approaches. Few connections had significant associations with sex. The present study replicates previously reported age-related patterns of connectivity in a relatively narrow age-range of children. In addition, we extended these findings by demonstrating decreased connectivity within the subcortex with increasing age. Lastly, we show the utility of a more focal approach that challenges the spatial assumptions made by the traditional mean time series approach.

Introduction

Understanding typical brain development is critical to understanding the mechanisms behind neuropsychiatric disorders. Mental health in adulthood is highly dependent on brain development beginning in the womb and continuing throughout adolescence and into adulthood. One theory is that the neurobiological underpinnings of mental illnesses are largely driven by miswired brain connectivity originating in childhood [48]. Through an understanding of typical connectivity, we can identify aberrant patterns associated with neuropsychiatric disorders.

Brain connectivity changes dramatically in the early years of life. In infancy, the brain's short-range connections are dominant [48, 69]. Throughout childhood and adolescence, brain connectivity becomes increasingly distributed, with long-range connections becoming stronger and short-range connectivity decreasing [48, 51, 151].

Connectivity between subcortical and cortical regions has been shown to decrease with age in children [27, 78, 156, 181]. However, other studies have found the opposite effect [156, 171]. Age-related differences in connectivity between subcortical and cortical regions are accompanied by stronger cortico-cortical connectivity in older children [181]. There have been few studies examining the role of connections between different subcortical brain structures in children. Gaining a better understanding of the age-related development of subcortical connectivity provides an important baseline for the study of childhood psychopathology.

Development of brain connectivity is increasingly being studied using whole-brain connectomes derived from resting-state functional MRI (rs-fMRI) [48, 151]. Connectomes represent brain connectivity between pairs of grey matter ROI's [23, 154]. Since connectome approaches evaluate networks within the entire brain, they are well suited to evaluate the major changes taking place in typical neurodevelopment.

In this study we utilized two connectome approaches to evaluate age and sex associations in a large group of school age children across the functional connectome. First, we used the correlation of the mean time series for brain regions involved in a given connection to express uniform and homogenous connectivity. However, connectivity in some regions becomes increasingly focal during development [49], which we captured with a new measure of connectivity that determines the focal maxima of correlations between ROIs. Each approach measures different aspects of

connectivity, which can help parse whether connectivity differences in development involve larger brain regions or tend to be more focal within an ROI.

Considering the mixed findings in the literature related to cortical and subcortical connectivity, we aimed to determine age related differences in connectivity between pairs of cortical and subcortical regions. In addition, we were interested in determining how connectivity patterns differ with age between pairs of subcortical regions. This has not yet been investigated in previous studies. Previous studies examining rs-fMRI connectivity in typical development included subjects with a broad age range or had small to moderate sample sizes ($n < 200$ in most cases) [27, 51, 78, 151, 156, 171, 181]. Thus, to reduce heterogeneity, which could contribute to the mixed findings, we used a large sample of six-to-ten year-old children from a population-based cohort. By focusing on a narrow age range in a large sample, we aimed to shed new light on brain development within a narrow period of childhood. This age range is particularly interesting because it is a period in which the brain, behavior and cognition are rapidly maturing [127, 135]. This critical phase in development can provide clues into typical brain function, which can then be extended to evaluate mechanisms governing psychopathology.

Materials and Methods

Participants

The participants of this study included a subgroup of children participating in the Generation R Study, which is a large, population-based prenatal cohort study in Rotterdam, the Netherlands [108]. Magnetic resonance imaging (MRI) scans were obtained in a total of 1,070 children between 6 and 10 years of age. The protocol for recruitment and study design is described in detail elsewhere [207]. General exclusion criteria consisted of severe motor or sensory disorders (deafness or blindness), neurological disorders, moderate to severe head injuries with loss of consciousness, claustrophobia, and contraindications to MRI. Out of 1,070 children who visited the research center for an MRI, 964 children underwent an rs-fMRI scan. Of those children, 227 were screened as having problem behaviors using the Child Behavior Checklist (see description below) and were excluded from the analyses. Furthermore,

subjects were excluded due to excessive head motion (n=88), failed registrations (n=21), failed or low quality cortical segmentations (n=126), less than 125 volumes left after data scrubbing (n=5) and an incidental finding (n=1). The final dataset included 411 subjects. Informed consent was obtained from parents, and all procedures were approved by the Medical Ethics Committee of the Erasmus MC, University Medical Center Rotterdam.

Behavioral and IQ assessment

The children were assessed for behavioral and emotional problems using the Child Behavior Checklist (CBCL/1½-5), which is a questionnaire filled out by their mothers [2]. The CBCL is a 99-item inventory covering various behaviors reported by parents. It uses a Likert response format (i.e. "not true", "somewhat true" and "very true"). The CBCL was used to select children without problem behavior to ensure that associations were independent of major behavioral problems. This was accomplished by excluding participants with a score above the clinical cutoff on any syndrome, DSM-oriented, or broadband scale, according to Dutch norms [186]. Further, to minimize the potential for residual confounding, the square root of the sum of all items was used to compute a total problem score to be used as a covariate in analyses.

Two subtests from a Dutch non-verbal IQ test (i.e. Snijders-Oomen Niet-verbale intelligentie test, revisie [184]) were conducted, as described in Ghassabian et al. [72]. The mosaics subtest assessed spatial visualization abilities. The categories subtest assessed abstract reasoning abilities.

MR-Image Acquisition

Magnetic resonance imaging data were acquired on a General Electric MR-750 3-Tesla whole-body scanner (General Electric, Milwaukee, WI) using a standard 8-channel, receive-only head coil. A three-plane localizer was run first and used to position all subsequent scans. Structural T1-weighted images were acquired using a fast spoiled gradient-recalled echo (FSPGR) sequence (TR = 10.3 ms, TE = 4.2 ms, TI = 350 ms, NEX = 1, flip angle = 16°, matrix = 256 x 256, field of view (FOV) = 230.4 mm, slice thickness = 0.9mm). Echo planar imaging was used for the rs-fMRI session with the following parameters: TR = 2000 ms, TE = 30 ms, flip angle = 85°, matrix = 64

x 64, FOV = 230 mm x 230 mm, slice thickness = 4 mm. In a previous study the number of TRs necessary for functional connectivity analyses was determined, and therefore the first set of acquisitions acquired 250 TRs (acquisition time = 8min 20sec). After it was determined that fewer TRs provided stable networks of higher quality (less motion), the number of TRs was reduced to 160 (acquisition time = 5min 20) [209]. Children were instructed to keep their eyes closed and not to think about anything in particular during the rs-fMRI scan.

MR-Image Processing

Anatomical Image Processing

Predefined ROIs were defined in native space and used as the anatomical regions to quantify time-series data for brain-wide connectivity analysis. A total of 34 cortical regions and seven subcortical ROIs were defined in each hemisphere of the brain in native space from T1-weighted images using the FreeSurfer analysis suite () [57]. Details about the FreeSurfer data processing and quality control in the Generation R Study are described elsewhere [134]. The FreeSurfer image, including the cortical and subcortical labels were registered to the rs-fMRI data by applying the transformation matrix resulting from a 12 degree of freedom affine registration of the T1-weighted image to the rs-fMRI data [80]. Thus, all time-series for analyses were extracted from native fMRI space.

Resting-State Image Processing

Resting-state fMRI data were preprocessed using a combination of tools from the Analysis of Functional NeuroImages package (AFNI) [28], the Functional MRI of the Brain Software Library (FSL) [111], and in-house software written in Python version 2.7.3. For the rs-fMRI's acquired with 250 TRs, only the first 160 volumes were used so that all time courses contained the same amount of information. Preprocessing of the rs-fMRI began with slice-timing correction, motion correction, removing the first four volumes, and 0.01Hz high-pass temporal filtering. Next, the six motion correction parameters, the mean white matter signal and mean cerebral spinal fluid (CSF) signal were regressed out of each voxel's time course [64]. Finally, data scrubbing was used

to further compensate for motion, removing volumes with excessive movement [144, 145] since head motion during scanning can amplify developmental differences in connectivity [144]. This effect is significantly reduced after compensating for movement [48].

Given geometric distortions resulting from susceptibility artifacts, some ROIs were excluded from the analyses. In order to identify affected ROIs, FSL's Brain Extraction Tool [165] was used to create a brain mask from the rs-fMRI. The proportion of voxels in each ROI that intersected with the brain mask was computed for each subject. Overlap between voxels believed to represent true signal (i.e., within the brain mask) was found to be low in ROIs known to be affected by susceptibility artifacts. ROIs with a mean overlap across subjects of less than 90% were visually inspected and those ROIs with consistently low overlap were excluded from the analyses (entorhinal cortex, frontal pole, inferior temporal gyrus, lateral orbitofrontal cortex, medial orbitofrontal cortex, and temporal pole). In the remaining ROIs, only voxels in the intersection of the ROI and the brain mask were included in the analyses. See Table 3.1 for a listing of included ROIs.

Brain-wide Connectivity Analysis

Brain-wide connectivity analyses were conducted in rs-fMRI native space, after the FreeSurfer labels were mapped to the rs-fMRI data. The labels and preprocessed rs-fMRI data were used to calculate pairwise region-to-region functional connectivity. Before calculating functional connectivity, a 3 x 3 x 3 voxel median spatial filter was applied to the preprocessed rs-fMRI to increase the signal to noise ratio. Two types of functional connectivity matrices were calculated. First, the connection weight for each pair of ROIs was calculated using a Pearson correlation coefficient of the mean time-series between all pairs of ROI's (MeanTS). For the second approach, Pearson correlation coefficients were computed between all pairs of voxels within two ROIs, and the pair with the highest Pearson correlation coefficient was selected to represent the connection between those two ROIs. We coin this approach the "Anatomic and Local Peak Activity Correlation Analysis" (ALPACA). The first approach represents connectivity which is homogeneous over a pair of ROIs, whereas the second approach represents the peak connectivity which is localized to focal areas within a pair of ROIs.

For both types of connectivity, only voxels that were part of the fMRI brain mask were considered. This minimized voxels affected by geometric distortions from

Table 3.1: *Regions used in connectome analysis, grouped by location in the brain.*

Cluster	Region	Abbreviation
Frontal (Fro)	Caudal anterior cingulate cortex	Cac
	Caudal middle frontal gyrus	Cmf
	Frontal pole	FrP
	Lateral orbitofrontal cortex	LOf
	Medial orbitofrontal cortex	MOf
	Paracentral lobule	PCe
	Pars opercularis	POp
	Pars orbitalis	POb
	Pars triangularis	PTr
	Posterior cingulate gyrus	PCi
	Precentral gyrus	PrC
	Rostral anterior cingulate gyrus	RAC
	Rostral middle frontal gyrus	RMF
	Superior frontal gyrus	SFr
Occipital (Occ)	Cuneus	Cun
	Lateral occipital gyrus	LOc
	Lingual gyrus	Lin
	Pericalcarine cortex	Pcc
Parietal (Par)	Inferior parietal lobule	IPa
	Postcentral gyrus	PoC
	Precuneus	Pcn
	Superior parietal lobule	SPa
	Supramarginal gyrus	SMa
Subcortical (Sub)	Accumbens area	Acc
	Amygdala	Amg
	Caudate	CaN
	Hippocampus	Hip
	Pallidum	Pal
	Putamen	Pu
	Thalamus	Tha
Temporal (Temp)	Banks of superior temporal sulcus	BSt
	Entorhinal cortex	Erh
	Fusiform gyrus	Fus
	Inferior temporal gyrus	ITe
	Insula	Ins
	Isthmus of cingulate gyrus	ICG
	Middle temporal gyrus	MTe
	Parahippocampal gyrus	Phc
	Superior temporal gyrus	STe
	Temporal pole	TeP
	Transverse temporal gyrus	TrT

influencing the connection weight. Prior to statistical analyses, to satisfy normality assumptions for parametric statistics, Pearson correlation coefficients were converted to the Z distribution using the Fisher R-to-Z transformation.

Statistical Analysis

Statistical analyses were conducted with the statsmodels [160], scipy [140] and numpy [195] packages in Python (v2.7). For each connection, two regression models were fitted, one for MeanTS and one for ALPACA. In both cases, age, sex and the CBCL total problem score were included as independent variables, and main effects were examined for age and sex. The CBCL total problem score was included to account for residual behavioral differences among included children. To control for multiple testing, the number of effective independent tests/connections, M_{eff}, was computed for both ALPACA and MeanTS according to the method outlined in [125]. The threshold of significance was determined using the Sidak correction, $\alpha_{corr} = 1 - (1 - \alpha)^{(1/M_{eff})}$, where $\alpha = 0.05$. We additionally conducted a separate analysis in which interaction between age and gender was tested by adding an interaction term to the model. Multiple testing was controlled using the same thresholds as in the main-effects model.

Visualization

Connectograms [196] were used to visualize associations of age and sex with functional connectivity. Connectograms are used in brain connectivity analyses to show relationships between ROIs in a circular two-dimensional representation. ROIs are positioned around the outside of the circle. A given connection is represented by a line between the associated ROIs, where color and thickness are used to indicate specific properties of a connection. In this study, ROIs were grouped by anatomy (see Table 3.1 for groupings) and by hemisphere. Only connections with significant associations are shown. Red and blue represent positive and negative associations with age or male > female and female > male in the case of sex, respectively. Increased color intensity represents increased significance. Connectograms are often easier to interpret than three-dimensional representations of connectivity in anatomical space [120].

Worm plots were used to directly compare groups of connections between MeanTS and ALPACA [120]. Each point represents the association between the variable of

interest and a specific connection. Connection-age association significance is on the y-axis, which is the negative log of the p-value, multiplied by the sign of the association and a scaling factor that is used to ensure that the line representing significance is at the same location for both connectivity types. Connections were ordered along the x-axis according to the anatomical group to which their ROIs belonged (see Table 3.1 for the list of ROIs belonging to each group). Groups were ordered by their mean associations with ALPACA. Within each group of connections, points were ordered by their association, which produces a worm-like shape. This allows easy comparison of association strengths and distributions between connectivity types. The ordering was performed separately for each type of connectivity, which means that the order of connections likely differs between connection types. Points that are outside of the dashed lines indicate connections with significant associations after correction for multiple testing.

Results

Numerous age-related connections had significant associations that survived correction for multiple testing. These are shown in connectograms in Figure 3.1 and are summarized in Table 3.3 for age and Table 3.4 for sex. Negative associations with age (i.e. weaker connection strength in older children) were dominant, including 24 of 48 (50%) connections in MeanTS and 66 of 84 (79%) in ALPACA. A large proportion of negative associations with age were found in subcortical-to-subcortical connections, including 18 of 24 (75%) in MeanTS and 38 of 66 (58%) in ALPACA. Significant age associations with cortical-to-subcortical connections were primarily positive in the MeanTS approach (17 of 19 connections, 89%) but negative in all 22 of ALPACA's significant associations with age. This suggests that functional connectivity between subcortical and cortical regions increases homogenously over the entire volume of the involved regions, but decreases focally with age. Positive associations involved all lobes except for the occipital lobes in both approaches and subcortical regions in ALPACA. No significant interactions between age and sex were found for either ALPACA or MeanTS in any of the connections, once corrected for multiple testing. T-tests and Pearson correlations also showed no significant relationship between age and IQ, sex and IQ as well as age and mean displacement. There was a significant

Table 3.2: *Sample characteristics (n=411).*

Characteristic	Value
General	
Age at MRI (years)	8.05 ± 0.99
Sex (M/F)	205 / 206
Non-verbal IQ	103.77 ± 14.40
Handedness (Right/Left/Unknown)	372 / 38 / 1
Ethnicity	
Dutch (n)	316
Non-western (n)	68
Other western (n)	27
FMRI motion parameters	
Average RMS Relative (mm)	0.11 ± 0.08

Pearson correlation between age and mean displacement (-0.15, $p<0.05$), however we adjusted for motion as described in the methods section.

The age connectograms were relatively symmetric, suggesting that both homogeneous and focal age-related differences occur similarly in both hemispheres in the brain. Specific connections with symmetric age associations are shown in Figures 3.1D and 3.1E, where symmetry is intra-hemispheric (i.e. both ROIA,left-to-ROIB,left and ROIA,right-to-ROIB,right are significant), inter-hemispheric (i.e. both ROIA,left-to-ROIB,right and ROIA,right-to-ROIB,left are significant), or both. The nucleus accumbens played a central role in symmetry in negative associations, which were primarily in connections between subcortical regions in both network approaches. Positive symmetry involved frontal, temporal, parietal and subcortical regions.

Figure 3.2 shows the distribution of connection weights grouped by lobe using a worm plot [120]. Most subcortical/parietal and subcortical/frontal connection associations with age were positive in MeanTS but negative in ALPACA. In other words, in this group of edges homogeneous functional connectivity increases with age, however, there are focal areas where functional connectivity decreases with age. There were few connectivity differences between sex using both the ALPACA and MeanTS approaches. MeanTS had a total of five significant associations with sex, including three in which connectivity in males was larger than in females (left isthmus

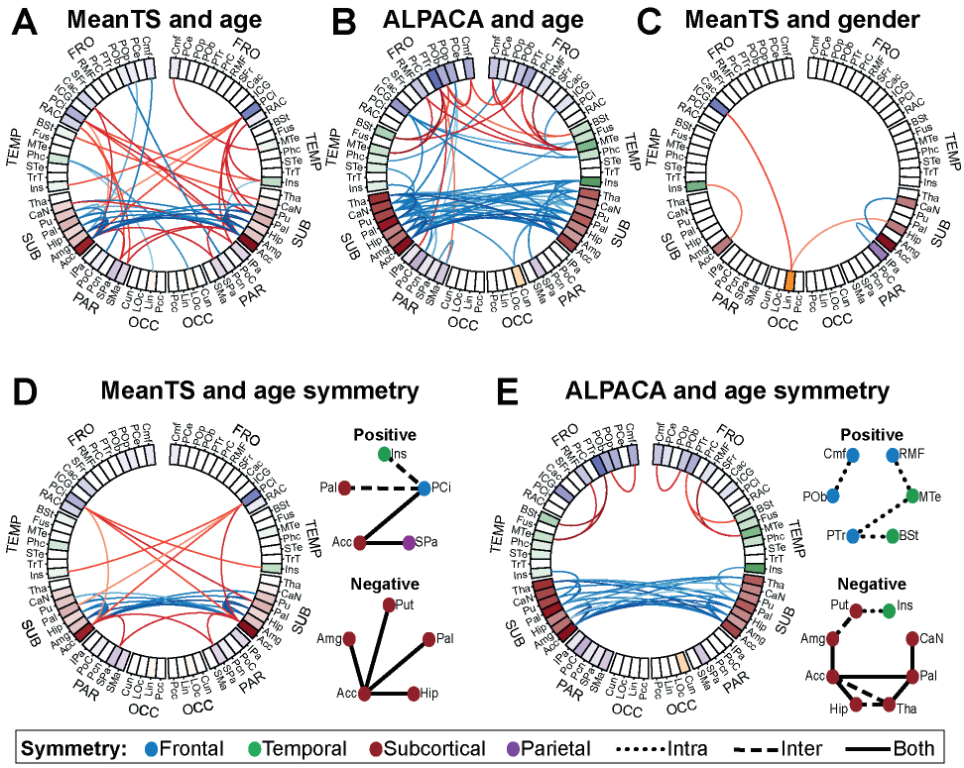

Figure 3.1: *Connectograms [196] showing connections with a significant association of (A) MeanTS with age (B) ALPACA with age and (C) MeanTS with sex. There were no connections with significant associations with sex and ALPACA, therefore the corresponding connectogram is not shown. Brain regions are divided according to location in the brain, including frontal (FRO), temporal (TEMP), subcortical (SUB), parietal (PAR) and occipital (OCC). They are arranged in a circle. Regions from the left hemisphere are on the left side of the diagram. Significant connections between two regions are plotted as red (positive age associations, or male > female) and blue (negative age associations, or female > male) lines, where color intensity indicates relative significance. The opacity of each region indicates the relative number of significant associations that each regions has. The age associations had a great deal of symmetry in both networks, as shown in (D) for MeanTS and (E) for ALPACA. The connectograms in (D) and (E) show the subset of connections that had intra-hemispheric (i.e. left-left and right-right connections were both significant) and/or inter-hemispheric (i.e. left-right and right-left connections were both significant) symmetry. These connections are also illustrated more abstractly and simply to the right of the connectograms, where regions are represented by circles, connections are represented by lines and the appearance of each line indicates the type of symmetry.*

Table 3.3: *Location of significant associations with age.*

	Hemisphere			
	Left	**Right**	**Between**	**Total**
ALPACA	**30**	**20**	**34**	**84**
Positive	**8**	**5**	**5**	**18**
Fro/Fro	2	1	1	**4**
Fro/Par	2	0	0	**2**
Fro/Temp	4	4	4	**12**
Negative	**22**	**15**	**29**	**66**
Fro/Par	1	0	0	**1**
Fro/Sub	3	0	1	**4**
Fro/Temp	0	1	3	**4**
Occ/Sub	0	2	1	**3**
Par/Par	1	0	0	**1**
Par/Sub	3	2	0	**5**
Sub/Sub	12	6	20	**38**
Sub/Temp	2	4	4	**10**
MeanTS	**13**	**12**	**23**	**48**
Positive	**5**	**7**	**12**	**24**
Fro/Par	2	1	0	**3**
Fro/Sub	2	3	5	**10**
Fro/Temp	0	2	2	**4**
Par/Sub	1	1	4	**6**
Sub/Temp	0	0	1	**1**
Negative	**8**	**5**	**11**	**24**
Fro/Par	1	0	1	**2**
Fro/Sub	1	0	0	**1**
Occ/Temp	1	0	1	**2**
Sub/Sub	5	4	9	**18**
Sub/Temp	0	1	0	**1**

cingulate/left lingual, left accumbens/left insula and left lingual/right hippocampus) and two where females had greater connectivity than males (right accumbens/right caudate

Table 3.4: *Location of significant associations with sex.*

	Hemisphere			
	Left	**Right**	**Between**	**Total**
MeanTS	**2**	**2**	**1**	**5**
Positive	**2**	**0**	**1**	**3**
Fro/Occ	1	0	0	**1**
Occ/Sub	0	0	1	**1**
Sub/Temp	1	0	0	**1**
Negative	**0**	**2**	**0**	**2**
Par/Sub	0	1	0	**1**
Sub/Sub	0	1	0	**1**

and right accumbens/right inferior parietal cortex). ALPACA did not identify any significant associations after correction for multiple testing. This suggests that sex-related differences in connectivity are homogeneous across the involved ROIs rather than focal.

Discussion

In this study we examined age- and sex differences in functional connectivity by applying two different, but complementary approaches to measure functional connectivity. Both connectivity approaches revealed both common and different patterns of connectivity in relation to age, and relatively similar patterns of connectivity between boys and girls. Significant associations between connectivity and age revealed a concentration of negative associations with age between pairs of subcortical regions and positive associations between pairs of cortical regions. The age associations generally displayed left-right symmetry. Additionally, when connections were grouped anatomically, group-wise shifts in associations with age were found. The two different connectivity indices were overall highly consistent; however there were a number of connections where they diverged, suggesting that in a subset of connections, functional connectivity changes with age either homogeneously or focally over the involved ROIs, but not both.

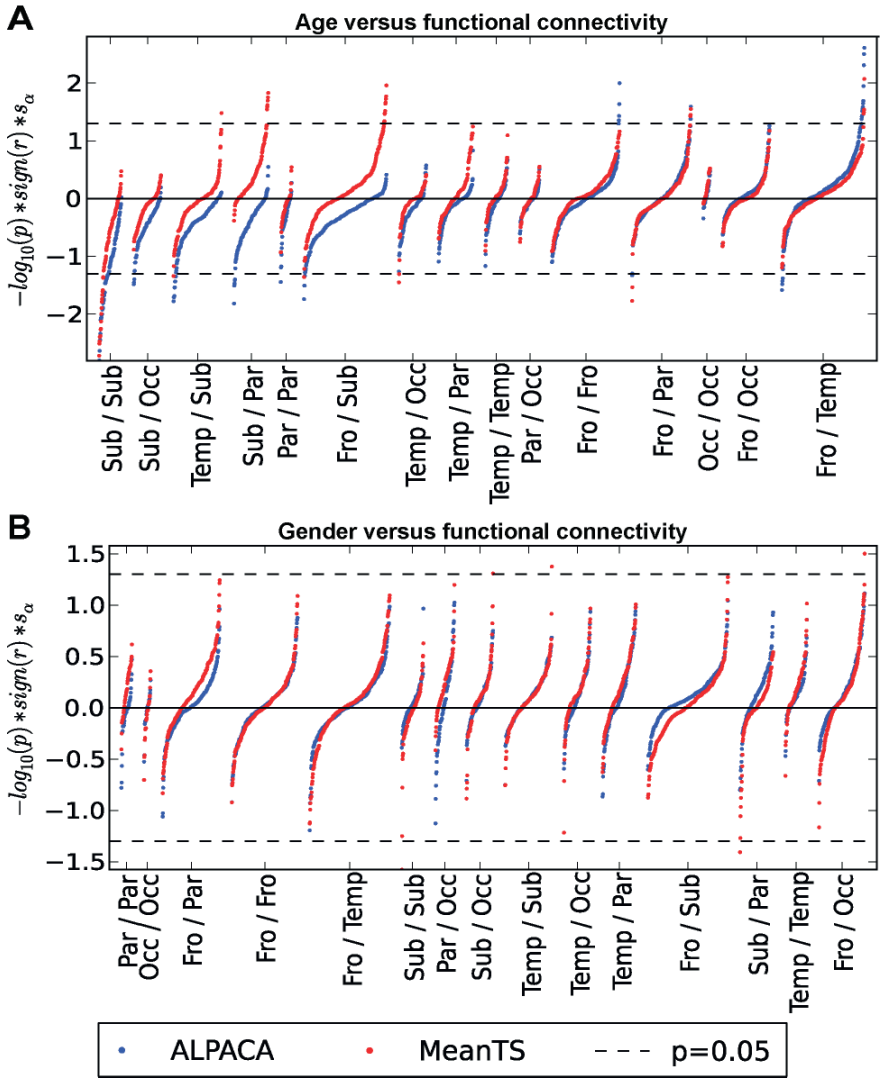

Figure 3.2: *Worm plots [120] of association of functional measures with age and sex. Connections are split into groups based on the location of the associated regions, including frontal (Fro), temporal (Temp), subcortical (Sub), parietal (Par) and occipital (Occ). Connections within each group are ordered by association strength, producing worm-like shapes. Order of groups on the x-axis is ordered by mean association strength in ALPACA. On the y-axis is the negative log of the p-value, multiplied by the sign of the test, multiplied by a scaling factor. Each point outside of the dotted lines represents a significant association of age or sex with a specific connection.*

Connectivity increases in the cortex and decreases in the subcortex with age

Both methods derived several cortico-cortical connections that were positively associated with age. This is consistent with a recent study that found that cortico-cortical connectivity increases during development in children from seven to 18 years of age [171]. Our findings expand upon this finding by demonstrating that age-related increases in connectivity are present in a narrow age-range in young children while utilizing two different methods for deriving connectivity indices. This increase in connectivity parallels an increase in volume of the frontal, temporal and parietal lobes, which has been reported to occur between the ages of six to ten years of age [124]. Thus, the increased volume, which may be a result of synaptogenesis and arborization, may also result in increasing cross-talk between brain regions. Previous studies have found that functional connectivity increases with age in long-range connections and decreases in short-range connections [51, 151]. This is partially consistent with our observations, since many of the identified significant positive associations were in connections between regions in different lobes and/or hemispheres, and were thus medium to long-range connections. We did, however, find a small number of both long-range connections that decreased with age and short-range connections that increased with age. Thus, maturation of brain connectivity may be region dependent, with many long-range connections increasing with age, whereas some show decreases. While the regions with positive associations differed between the two connectivity types, both support the notion of generally increasingly distributed networks with age. Our observations are particularly interesting because we focused on a narrow age range, whereas many previous studies focused on relatively large age ranges [151]. It is remarkable that such striking connectivity differences with age can be observed even a narrow age range in school-age children. This is likely a result of the rapid neurodevelopment that occurs during this age range.

Age associations with connections between cortical and subcortical regions differed between network approaches. MeanTS had a mix of positive and negative associations, while ALPACA had exclusively negative associations with age, adding new insight into the nature of previously observed changes in connectivity with age. The negative associations in ALPACA suggest that focal connectivity between cortical and subcortical regions decreases with age, which is consistent with studies reporting

negative associations with age in connections between subcortical and cortical regions in typical development [27, 78, 156, 181]. However, [171] found primarily positive as well as some negative age associations between cortico-subcortical connections, and [156] found that the thalamus had both positive and negative association with age in development. Our results in MeanTS, which is an expression of functional connectivity that is homogenous over the involved regions, also support the presence of subcortical-to-cortical connection associations in both directions. Under the rubric of specific functional brain networks or cortico-subcortical feedback loops associated with neurodevelopment (i.e., the cortico-cerebellar-thalamic-cortical circuit (CCTCC)) [9, 190], the presence of both positive and negative associations between cortical and subcortical regions may be expected. Maturing feedback loops involving similar functions would show increasing connectivity with age, whereas those involved in different functions would show less age-related functional connectivity. Significant differences of cortico-subcortical functional connectivity with age are also parallel to previously observed increases in size of the frontal, temporal and parietal lobes as well as some subcortical regions [124].

While there is a wealth of developmental studies examining cortical-to-cortical connections, and to a lesser extent subcortical-to-cortical connections, there is a gap in the literature regarding age-related differences in the connectivity between different subcortical structures. In this study, we found that all significant associations of connectivity between subcortical regions with age were negative for both network types. Our findings between subcortical structures may reflect networks transforming from local to distributed during development, as was shown by [51]. However, their study focused on cortical and cerebellar regions, and did not report on subcortical/subcortical connectivity.

Structural MRI studies of subcortical structures examined how volumes of subcortical regions change over time [124]. These changes include an inverted U-shaped pattern in the volume of the caudate with peaks at 7.5 and 10.0 years of age in females and males, respectively; an increase in hippocampal size in males only and an increase in the size of the amygdala in girls only. The amygdala, hippocampus and caudate were involved in subcortical connections with negative associations with age, which was true for both networks for the amygdala and hippocampus, and only for ALPACA in the caudate. As these regions have been shown to increase in volume

during childhood and subsequently decrease during adolescence [173], their communications with other subcortical regions likely also change during development. It is thus possible that in the presence of later maturing cortical structures in young children (i.e., prefrontal cortex) [124, 132], subcortical structures rely on within-system connectivity. As the cortex matures and its connections to the subcortex strengthen [32], this previous subcortical reliance on highly integrative connectivity may be relaxed. Such an imbalance in timing of development has been previously proposed for cortical/limbic connectivity [26, 91]. Given the importance of various subcortical structures and their cortical connections with different psychiatric disorders (e.g., Cortico-cerebellar-thalamic-cortical loop in Schizophrenia, caudate motor in ADHD, thalamus/basal ganglia/primary sensory networks) [27], having a better understanding of differences within and between cortical and subcortical regions is a crucial foundation for future efforts studying connectivity differences related to psychopathology.

An interesting finding in this study was inter- and intra-hemispheric symmetry in age associations. Symmetry in the negative associations in both network types was primarily between subcortical regions with the nucleus accumbens playing a central role, whereas positive symmetry involved frontal, temporal, parietal and subcortical regions. This suggests that many bilateral connections within and between hemispheres are developing simultaneously. The fact that many subcortical connections with the accumbens area had negative associations with age in both network types might be related to development of the reward center of the brain. The accumbens has been linked to risk-taking behavior in adolescents [68], but previous studies have not directly investigated the development of subcortical connection to the amygdala in children. Our results suggest that activity is increasingly directed by cortical regions rather than subcortical regions. Asymmetry in brain connectivity has previously been observed in lateralization studies [5, 47, 97]. Adolescent and adult brains are highly lateral across several resting state networks, with several brain regions showing a decrease in lateralization with age [5]. In children, language networks become increasingly left-lateralized throughout development [84, 97], whereas visuospatial networks become right-lateralized [84]. Although lateralization of the brain may be related to asymmetric association of functional connectivity with age, this relationship has not been studied directly, nor can it be definitively assumed.

Lateralization can increase even if the association with age is significant on both sides of the brain. While symmetry in functional connectivity has been widely studied, the symmetry of associations with functional connectivity have not. Examination of association symmetry could be informative in future studies. For example, individual deviations from the symmetry pattern found in typical development could be used as a marker of psychopathology.

Sexual Dimorphism

Five connections had significant associations surviving correction of multiple testing of MeanTS with sex. ALPACA did not have any associations with sex. Together these results suggest that sex-related differences in functional connectivity are likely more uniform across the involved regions, rather than being localized to spatially focal peaks. These results could alternately suggest that MeanTS is a more robust measure of sexual dimorphism. Previous studies of sex-related differences in resting-state functional connectivity are sparse in this age range. A recent study did not find any sex differences in the age range of 7-12 [171]. Additionally, diffusion tensor MRI study in children aged six to ten found no significant sex-related differences in measures of white matter integrity [137]. Both studies support our observation of few connectivity differences between sexes in this age range.

The lack of observed sex differences in functional connectivity during development in both our study and previous studies are surprising given that studies of structural connectivity have found sex differences in relation to cognition and/or intelligence in children and adolescents. Several previous studies have found sex differences in structural connectivity [89, 158, 164], however, a recent DTI study in the current cohort did not show sex differences [136]. Sex differences have also previously been observed in neuroanatomical studies. For example, longitudinal structural MRI studies have shown sex differences in grey matter volume in the frontal, parietal and temporal lobes, as well as in the caudate, amygdala and hippocampus from childhood throughout adolescence [124]. In this study, all of these regions with the exception of the amygdala had connections with significant associations with sex. Given that previous work present conflicting views on sex differences in connectivity and related grey matter volumes, and since our study found a small number of connections with sex differences in only one of the two functional networks studied, it seems that sex

differences in functional connectivity are subtle and limited in typically developing children in this age range. Measureable sex differences in the brain may emerge or become unmasked with development, with differences between boys and girls may become more apparent during adolescence and young adulthood.

Defining functional connectivity by peak activation versus over an entire region

As described above, both network types were generally in agreement with each other and with the existing literature. In some specific connections, some differences were apparent across method with respect to associations in specific connections. In the case of such differences, this suggests that the nature of the development of functional connectivity is not the same for all regions. For example, MeanTS did not have significant associations with age in fronto-frontal connections, whereas ALPACA's positive associations with age were exclusively found in fronto-frontal, fronto-temporal and fronto-parietal connections. This is in line with findings of an earlier study that suggested that cortical connections become increasingly focal with age [49]. This is in contrast to age associations with the posterior cingulate, which were positive in MeanTS but not ALPACA. This suggests that developmental changes in posterior cingulate connectivity are distributed across the entire structure rather than localized in a focal region. Previous studies have shown that connectivity in the default mode network changes during development, including connections involving the posterior cingulate [50, 182].

Increasingly diffuse connectivity with age was also found in cortical-to-subcortical connections, which were primarily positive in MeanTS but exclusively negative in ALPACA. This thus suggests a focal to diffuse trajectory with age. Such a trajectory in subcortical-to-subcortical connections was not found since their age associations were exclusively negative in both network types.

It is interesting to consider the differences between the two network types in the context of the underlying neuronal architecture. If connectivity with grey matter is more diffuse, with connecting neurons covering a more extensive surface of an ROI, then a more diffuse representation, such as MeanTS, would better capture changes in functional connectivity (e.g., a 'shared pathway'). On the other hand, if nerve fiberindividual axonal pathways between two regions start and end in focal gray matter

locations, then a focal representation of functional connectivity, such as ALPACA, may target critical regions of connectivity.

There are additional factors that must be kept in mind interpreting results involving ALPACA. For example, ALPACA's focal approach may be more flexible in identifying the location of activation because it does not average over entire regions, which can blur the signal. This may be advantageous in relation to both structural and functional variability because it may not always be sensible to assume the same spatial activation patterns across individuals. On the other hand, ALPACA does not guarantee that the activation detected across individuals corresponds to the same focal connection. For example, it may be that a large region has more than one focal peak in connectivity. ALPACA may thus choose one peak for some subjects and another for others, in which case comparison across individuals would not involve the same connection. Additionally, in some cases, weaker functional connectivity has been related to some forms of psychopathology (e.g. autism [85] and depression [92]). In this situation, finding the local maximum may not be desirable in the context of better explaining the neurobiological underpinnings of psychopathology or identifying novel biomarkers because the local maxima may not necessarily reflect the reduced connectivity across the involved regions. Given the benefits and drawbacks and the underlying assumptions of each network type, using both ALPACA and MeanTS simultaneously in future studies may result in greater insights into different aspects of functional connectivity and make inferences of whether a given connection has a diffuse or focal connectivity pattern.

Strengths and limitations

While most studies on developmental functional connectivity focus on broad age ranges with moderate sample sizes [151], many of which used task-based fMRI rather than resting state fMRI, our study focused on a narrow age range and benefited from increased statistical power due to the large cohort. The children included in this study were sampled from a population-based cohort and were representative of the general population, which helped to mitigate the common issue of selection bias of children with higher than average IQ or greater socioeconomic status. An additional strength of this study is that, by keeping our analysis in native space, our results were not influenced by inter-subject registration, which has frequently been used in previous

studies and has been shown to blur cortical areas [56, 210]. This study also effectively used "brain-wide" visualizations to display large amounts of connectomic information, namely in the connectograms and worm plots. In addition, we present both novel findings as well as replication of observations from earlier studies, the latter being important in neuroscience, which is a field plagued by many underpowered studies that do not replicate [139, 141].

As previously mentioned, we used a FreeSurfer anatomical segmentation to define our regions of interest. Anatomical segmentations have also been used in several previous studies [25, 60, 183]. This approach benefits from a subject-specific segmentation in native space, which does not require inter-subject registrations. Studies that include inter-subject registrations are vulnerable to misregistration [48]. This approach may, however, fall short in the event that ROIs are not functionally specific or homogeneous. Choice of segmentation can affect the results of connectomics studies [43]. Functionally-defined ROIs can be obtained using fMRI. Existing methods define regions to be either non-overlapping [21, 163, 215] or overlapping [12, 169, 170, 192]. For example, [215] used functional MRI to define a cortical segmentation that maximized functional specialization within regions across subjects. The borders of the resulting functional ROIs were significantly different from the anatomically-defined ROIs used in this study. Thus, a functional ROI may intersect with several anatomical ROIs. Additionally, an anatomical ROI could be composed of several functionally distinct regions or may be part of a larger functional region. Because MeanTS averages signals over ROIs, some of which are quite large, imprecise boundaries would likely be less of a problem than they would be for ALPACA. However, in the case of large anatomical regions, where only a part of the ROI is active, the MeanTS approach would average over the entire region, which would not reflect activity in the active region. The ALPACA approach would circumvent this by choosing the highest activation and the number of voxels involved in calculating the correlation coefficient are always the same.

Functional connectivity studies, and particularly those involving pediatric populations, are frequently impacted by motion artifacts, which can erroneously increase long-range connectivity and decrease short-range connectivity [48, 59, 146]. Given that younger children tend to move more than older children, this can have an impact on developmental studies. In this study, we corrected for motion using the

"scrubbing" method [144, 145], where corrupted volumes are removed. While this method significantly reduces the effect of motion [146], it is but one of many strategies [48]. Among the drawbacks of the scrubbing method are the loss of data within subjects, and the unequal degrees of freedom across subjects [146].

Another issue relevant to connectome-wide association studies is multiple testing correction. This study calculated the "number of effective tests" for each network type based on the covariance in the data, and used this number to adjust the significance threshold. Some of the differences in associations between the two networks investigated in this study could be simply due to the threshold chosen for each network. This is one of many similar methods commonly used in genetics studies to approximate permutation testing [162]. Permutation testing has been used previously in connectomics [106], but remains a computationally expensive method of multiple testing correction. Another option is to reduce the number of tests by using measures such as the network-based statistic [216], or to consider graph theoretical measures that produce node- or graph-level values [114, 154]. This approach has been used in several studies [17, 31, 60, 62, 218], however it fundamentally shifts the research focus from identification of relevant connections to the interpretation of measures that often do not have a known relation to neuro-biology [166]. Lastly, this study included individuals from the general population, rather than solely recruiting 'typically developing' children from the community. We utilized a common behavioral and emotional problem inventory to exclude children with high levels of behavior problems to maximize comparability of these data with the existing literature. While most behavioral and emotional problems are robustly measured by this parent-report instrument, the children themselves may arguably be better informants for some types of problem behavior (e.g., internalizing vs externalizing problems). However, even with some misclassification of problem behavior, the population-based nature of the present sample is highly useful in that it greatly increases the generalizability of findings across all individuals of the population, rather than only the 'typically developing' individuals.

Conclusion

The current study provides both replication and novel findings for age-related maturation of intrinsic connectivity. Replication of findings is noteworthy given our large sample size

and narrow age range, coupled with critique regarding less than optimal reproducibility and replication in the field of neuroimaging. Cortico-cortico connectivity was found to increase with age, while connectivity between subcortical regions decreased with age. Some cortico-cortical connections became increasingly focal with age, whereas other cortico-cortical and most cortico-subcortical connections became more diffuse with age. Additionally, we demonstrate the utility of native-space analyses of connectivity and offer examples of how the data can be efficiently and intuitively displayed. Future studies should explore using different anatomical or functional parcellations to determine to what extent the connectivity patterns are influenced by ROI boundaries.

Acknowledgements

This study was supported by the Netherlands Organization for Health Research and Development (ZonMw) TOP project number 91211021. Supercomputing computations were supported by the NWO Physical Sciences Division (Exacte Wetenschappen) and SURFsara (Lisa compute cluster,). The Generation R Study is conducted by the Erasmus Medical Center in close collaboration with the School of Law and Faculty of Social Sciences of the Erasmus University Rotterdam, the Municipal Health Service Rotterdam area, Rotterdam, the Rotterdam Homecare Foundation, Rotterdam and the Stichting Trombosedienst & Artsenlaboratorium Rijnmond (STAR-MDC), Rotterdam. We gratefully acknowledge the participation of the children and their parents. The general design of Generation R Study is made possible by financial support from the Erasmus Medical Center, Rotterdam, the Erasmus University Rotterdam, ZonMw, the Netherlands Organisation for Scientific Research (NWO), and the Ministry of Health, Welfare and Sport.

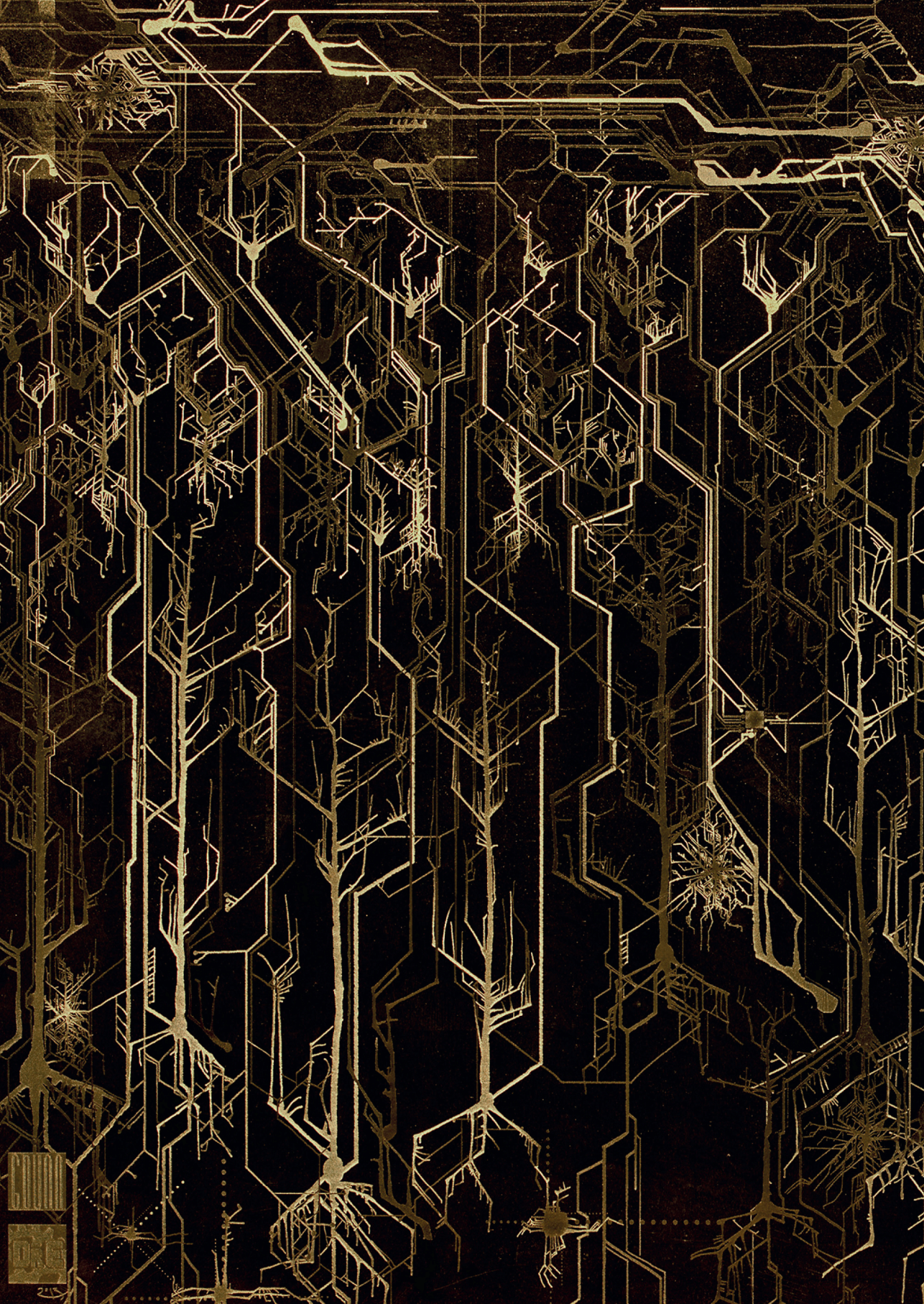


PART II
DISCONNECTION

4

The structural disconnectome: A pathology-sensitive extension of the structural connectome

Carolyn D. Langen, Meike W. Vernooij, Lotte G.M. Cremers, Wyke Huizinga, Marius de Groot, M. Arfan Ikram, Tonya White, Wiro J. Niessen

IEEE International Symposium on Biomedical Imaging (ISBI), 2017

Abstract

Brain connectivity is increasingly being studied using connectomes. Typical structural connectome definitions do not directly take white matter pathology into account. Presumably, pathology impedes signal transmission along fibres, leading to a reduction in function. In order to directly study disconnection and localize pathology within the connectome, we present the *dis*connectome, which only considers fibres that intersect with white matter pathology. To show the potential of the disconnectome in brain studies, we showed in a cohort of 4199 adults with varying loads of white matter lesions (WMLs) that: (1) Disconnection is not a function of streamline density; (2) Hubs are more affected by WMLs than peripheral nodes; (3) Connections between hubs are more severely and frequently affected by WMLs than other connection types; and (4) Connections between region clusters are often more severely affected than those within clusters.

Introduction

Understanding connectivity is essential to uncover the intricate workings of the brain. Grey matter brain structures are connected by white matter fibres, the health of which is crucial to brain function. It is hypothesized that disruptions in these connections may affect cognition and other outcomes [200]. Our understanding of connectivity has been deepened through the introduction of connectomics. A connectome is a graph in which nodes represent regions of interest (ROIs) and edges represent connections between them [174]. In the structural connectome, edges represent the degree to which regions are joined by nerve fibres. This information is typically derived from diffusion weighted images (DWIs) by estimating fibre pathways using tractography. Relevant edge characteristics include fibre density, or average diffusion measures along tracts, such as fractional anisotropy (FA) or mean diffusivity (MD).

While traditional measures of structural connectivity have been used to estimate changes in the brain across subjects [120, 152], direct investigation of the effect of pathology has largely focused on grey matter damage [31]. Since connections are largely composed of white matter fibres, pathology such as white matter lesions (WMLs) are very likely to affect the structural connectome. So far, the effect of WMLs have been studied mainly using hypothetical lesioning [44]. Another study used WMLs derived from patient data to estimate an altered connectome from connectivity data derived from healthy controls [117]. While the method is useful when patient diffusion data is not available, it requires non-linear registrations into standard space and relies on an arbitrarily defined formula to compute reduced structural connectivity. A direct study of the effect of WMLs on connectivity derived from subject data could provide new information that is not captured by traditional connectivity measures.

Conventional connectivity measures of connectivity may not adequately describe the impact of WMLs. For example, consider two axons, A and B, where B is shorter than A and both have identical lesioned portions. Suppose that lesions have a negative effect on signal transmission, which may include decreased transmission speed, increased refractory period or increased minimum required stimulus. The net effect will be the same for both A and B because they both have the same length of lesioned fibre. However, the effect will not be equally represented by conventional connectivity measures. WMLs will cause a change in mean diffusion measures [200], but the measured effect will be lower in case A because the effect is averaged over a greater

length. With increasing length, mean measures will converge to the value of a normal fibre. In the case of streamline density, there is no guarantee that WMLs disturb diffusion enough to result in a detectable reduction. Other measures should thus be considered to adequately represent WMLs in connectomes.

In this study we expand on the disconnectome map [63, 191] with the introduction of the *structural disconnectome*, a variant of the connectome in which only streamlines that pass through white matter pathology are considered. By examining abnormal streamlines separately, the effect of pathology on the connectome can be studied directly. We characterize the WML disconnectome in older adults from a population-based setting and compare it to the connectome to answer the following questions: (i) Are strong connections more strongly affected by WMLs than weak connections? (ii) Are highly connected ROIs more strongly affected by WMLs than sparsely connected ROIs? and (iii) Which types of connections are most affected by WMLs? By answering these questions we demonstrate the potential of the disconnectome to study the effects of white matter disease on connectivity and provide motivation for its use in the future.

Methods

Data

4199 subjects from the population-based Rotterdam Study [103], aged 45 to 100 (2346 females, mean age 63) were included. Magnetic resonance images (MRI) were acquired on a 1.5 tesla GE Signa Excite scanner, including: (1) A T1-weighted (**T1w**) structural scan (TR = 13.8ms, TE = 2.80ms, TI = 2000ms, 96 slices, slice thickness 1.6mm); (2) A T2-weighted fluid-attenuated inversion recovery (**FLAIR**) sequence (TR = 8000ms, TE = 120 ms, TI = 400ms, 64 slices, slice thickness 2.5mm); and (3) A diffusion-weighted spin echo echo-planar **DWI** (TR = 8575ms, TE = 82.6ms, axial FOV 210×210mm, slice thickness 3.5mm, 35 contiguous slices, maximum b-value 1000s/mm^2 in 25 non-collinear directions with three unweighted volumes).

Image Processing

DWIs were processed as described in [39]. Briefly, volumes were co-registered. Rotation components were used to realign gradient vectors. Diffusion tensor images (DTI) were estimated using ExploreDTI's Levenberg Marquardt estimator, including upsampling to 1mm isotropic. FA was calculated from the DTI. **WMLs were segmented** using an automated approach: (1) T1w data was segmented into grey matter, white matter and cerebrospinal fluid using a k-Nearest-Neighbour classifier [201]; and (2) tissue segmentation maps and FLAIR intensity values were used for WML delineation [38]. **The T1w image was parcellated** into 83 ROIs using FreeSurfer [55]. The parcellation was further segmented into 234 ROIs using the connectome mapper toolkit [33]. The WML mask and ROIs were affinely transformed to DTI space.

Network generation

Estimated tensors were used to reconstruct deterministic streamlines using the diffusion toolkit [203] with an angular threshold of 45°, an FA threshold of 0.2, and one seed per grey and white matter voxel. The streamlines were smoothed using a spline filter (step length = 0.5mm).

As illustrated in Fig. 4.1, a connectome (G_{NS}) was created by defining nodes as ROIs and connections as pairs of ROIs, with connection weight defined as the number of streamlines intersecting both ROIs, normalized by dividing by the ROIs size. A disconnectome (G_{PAS}) quantified the *proportion of affected streamlines* (PAS) as the fraction of streamlines that pass through the WML mask, where the numerator and denominator were normalized. Mean group networks, M_{NS} and M_{PAS}, were created. Only connections found in at least 60% of subjects were included to optimize the balance between false positive and false negative connections [42].

Network metrics

Weighted node degrees of all networks were calculated. The PAS of a node was defined as the normalized number of affected streamlines extending from the corresponding ROI divided by the node's weighted degree in G_{NS}. In Fig. 4.1, the degrees of nodes (purple, green, orange) was (2,3,3) in G_{NS} and (1,0.5,1.5) in G_{PAS}

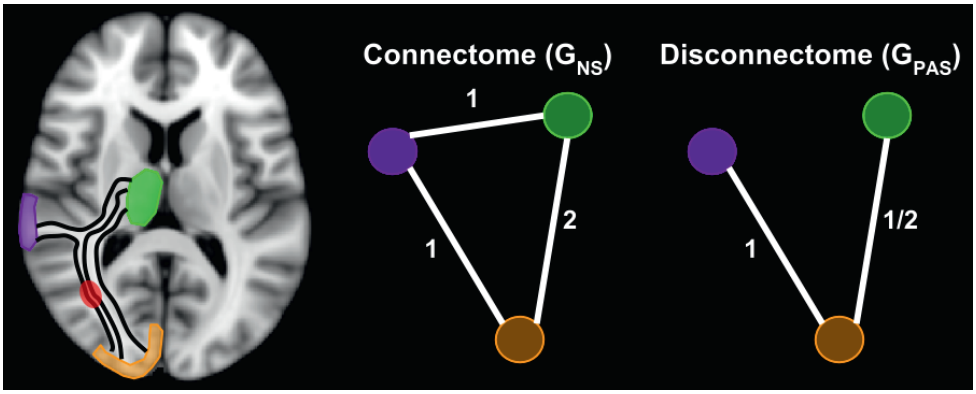

Figure 4.1: *In this schematic example, three ROIs are considered, shown in green, orange and purple. ROIs are connected by streamlines, which are depicted in black. In this example a WML, drawn in red, affects two streamlines. The edges of the connectome, G_{NS}, are defined by the number of streamlines connecting each pair of ROIs. The edges of the disconnectome, G_{PAS}, are defined by the number of streamlines affected by WMLs divided by the total number of streamlines. (Best seen in color.)*

and the node PAS was (0.5,0.33,0.67). Nodes were classified as hubs if their degrees were greater than or equal to the 85th percentile in M_{NS}, and as periphery nodes otherwise. Edges were classified as rich-club, feeder and local edges if they involved two, one or zero hubs, respectively [44]. Louvain node clustering was used to group nodes into highly interconnected modules.

Results

The mean connectome and disconnectome are shown in Fig. 4.2. The pattern of edge weights is remarkably different between both graphs, where heavily-weighted edges are primarily in and between the frontal and temporal lobes of the connectome, whereas in the disconnectome they involve occipital, subcortical and some temporal regions. These incongruencies are also observed in networks of individual subjects. Fig. 4.3 shows the relation between connectivity, disconnectivity and WML volume in both edges and nodes. The Spearman correlation of connectome and disconnectome edges of all subjects were positive, however they attenuated with increasing WML volume (Fig. 4.3 upper). The subject with the greatest WML volume (98 cm^3) had a correlation of

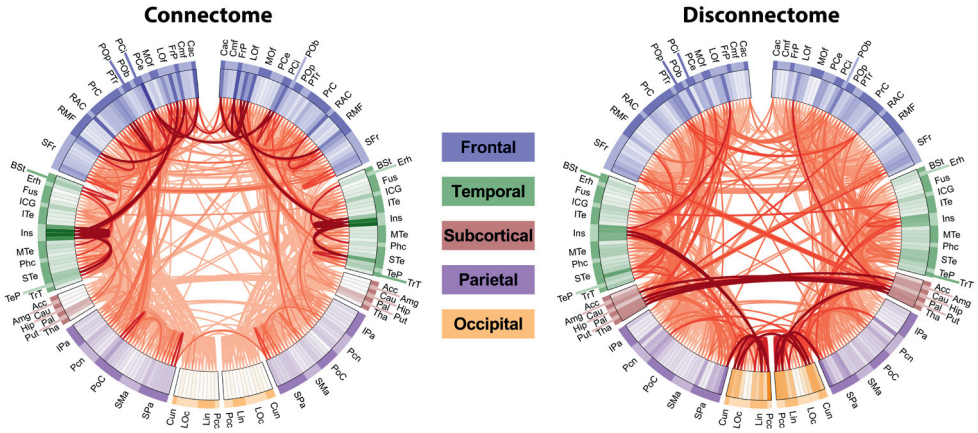

Figure 4.2: *The mean graphs as connectograms. ROIs are aligned around the edge and grouped according to their parent FreeSurfer region, indicated by the color in the outer ring. The inner ring indicates the connectome degree and disconnectome node PAS. Increased edge weight is represented by increased line color saturation.*

0.28 ($p < 10^{-16}$) when all connections were considered. The correlation was 0.02 ($p = 0.57$) when only connections with PAS>0 were considered. These results suggest that the relationship between a connection's number of streamlines and the degree of disconnection is minimal.

The correlation of nodal degree and PAS was greater with increasing WML volume (Fig. 4.3 lower). The subject with the highest WML load had a correlation of 0.53 ($p < 10^{-17}$) when all connections were considered. The correlation was 0.50 ($p < 10^{-14}$) when only connections with PAS>0 were considered. In other words, the communication pathways of nodes which are better connected to the rest of the brain are generally more vulnerable to WMLs.

Hub nodes were almost exclusively found in the frontal and temporal lobes. Edges were grouped according to how many hub nodes they involved. Characteristics of edge groupings are show in Fig. 4.4. Across subjects, paired t-tests between edge groups showed differences in both within-group mean PAS (Fig. 4.4A) and within-group fraction of affected connections (Fig. 4.4B). These results suggest that edges with increased hub involvement are both more severely and more frequently affected by WMLs.

The distribution of PAS across connections in the mean disconnectome within and between modules is shown in Fig. 4.5. In all but two modules the difference between

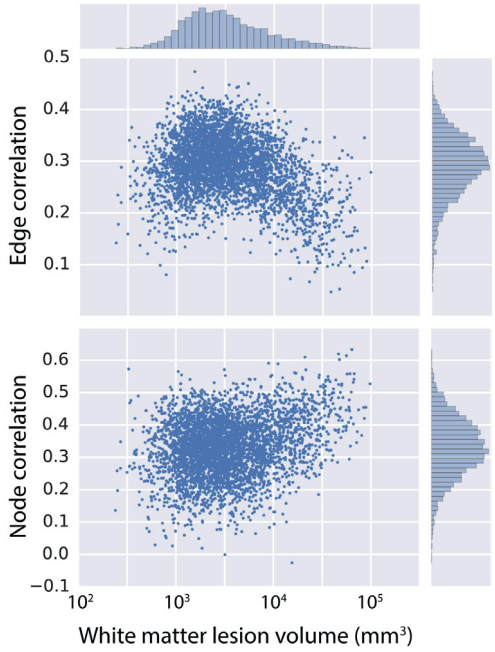

Figure 4.3: *Relationship between connectivity, disconnectivity and WML volume. Correlations were computed between the connectome and disconnectome of each subject for both edges (upper) and nodes (lower), the distributions of which are shown in the histograms on the y-axis. The x-axis histogram shows the distribution of WML volume across subjects. The scatter plots show the relationship between the correlations and WML volume.*

inter- and intra-module PAS was negative. The two positive differences were in the two modules with greatest hub composition, reflecting the previous observation that hubs take part in connections with greater PAS.

Discussion

In this proof-of-concept study among a large sample of community-dwelling subjects with varying WML load, we introduced the concept of the disconnectome and used it to show the extent to which WMLs affect brain connectivity. We found that nodes with a high degree are more likely to be involved with connections affected by WMLs, whereas edges with a high streamline density are not more affected by WMLs than

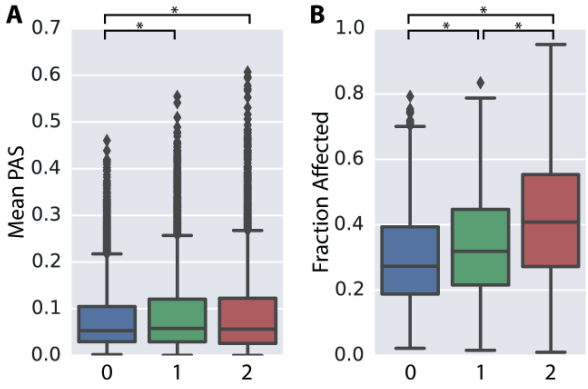

Figure 4.4: *Distribution of affectedness per edge type. (A) Mean PAS per subject in each edge group. (B) Fraction of connections with* $PAS > 0$ *per subject within each edge group.*

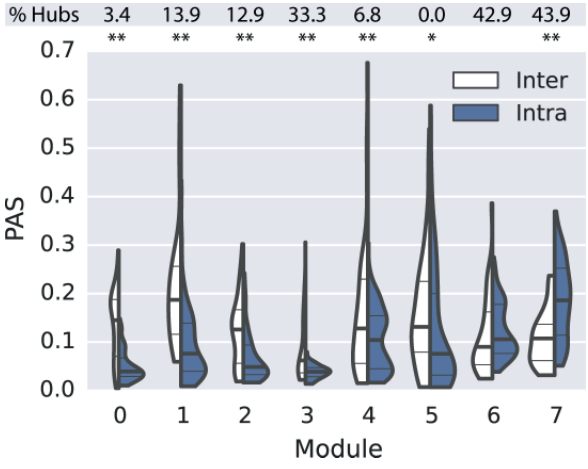

Figure 4.5: *Distribution of intra- (blue) and inter- (white) module affectedness per module. The median is shown by a thick line and the 25th and 75th percentile are shown by thin lines. * and ** indicate* $p < 0.05$ *and* $p < 10^{-6}$ *in paired Welch's t-tests, respectively. Modules are ordered according to t-test outcome. Percentage of hub nodes in a module is shown along the top of the figure.*

those with low density. Additionally, connections between hubs are most affected by WMLs and connections between peripheral nodes are least affected. Connections between modules are generally more affected than those within modules. Surprisingly, connections with highest PAS primarily involved interhemispheric subcortical and intrahemispheric occipital connections, whereas WMLs develop most frequently on tracts between frontal and both parietal and occipital regions [40]. Overall, these observations provide clues into the mechanism and spread of WMLs, suggesting that, with the exception of a small subset of connections, WMLs are found primarily in regions of high connectivity without preference for streamline density.

This study showed that valuable insights about brain connectivity can be gained by studying the disconnectome. Future studies could benefit from including the disconnectome in their analyses. For example, studying the disconnectome in relation to health outcomes such as cognitive deterioration can shed light on how structural connectivity affects functioning and yield new information about differences between disorders. Previous studies have shown that brain hubs and their connections play crucial roles in several neurological and psychiatric brain disorders [193]. It would be interesting to see whether some hubs are more affected by pathology than others in one disorder versus another.

The disconnectome could also confirm findings of lesion simulation studies. The effect of WMLs on connectomes was previously simulated by deleting edges and examining the effect on graph theory measures [44]. While this revealed valuable insights into the potential effects of lesioning on brain networks, the conclusions were theoretical since real lesion data was not incorporated. A study of the effects of real WMLs on network measures would provide complementary information to these theoretical insights, e.g. where lesions appear in practice and the relative importance of specific connections to network function. Furthermore, studying disconnectomes would provide a continuous measure of lesion effects, whereas the simulation considered only the binary case (i.e. undamaged fibres versus those with complete loss of function).

Another study examined the effects of grey matter lesions on simulated functional connectivity [7]. Simulations of the effect of WMLs on functional connectivity could be validated using the disconnectome and real functional data. Studying the disconnectome and functional connectome together may help to clarify the complex relationship between structural and functional connectivity.

Conclusion

Although conventional connectomes have made invaluable contributions to the understanding of the human brain, they do not directly measure disconnection resulting from white matter pathology. The newly introduced disconnectome, which reflects the percentage of streamlines that pass through pathology, can increase our understanding of the effect of pathology on the brain. The use of disconnectomes has the potential to deepen the understanding of disorders, such as schizophrenia and neurodegeneration, and normal processes, such as ageing.

5

The heritability of connectivity and disconnectivity of the brain in a population-based study

Carolyn D. Langen, Gennady Roshchupkin, Hieab H. Adams, Marius de Groot, Frans Vos, Meike W. Vernooij, M. Arfan Ikram, Wiro J. Niessen

IEEE International Symposium on Biomedical Imaging (ISBI), 2017

Abstract

We present the largest population-based heritability study of the human brain structural connectome, including a pathology-sensitive extension, the *dis*connectome. The disconnectome maps the effect of white matter lesions throughout the brain. The connectome and disconnectome were generated from diffusion-weighted images of 4111 subjects from the Rotterdam Study aged between 45 and 99 years. Graph theory measures were derived for both the connectome and disconnectome. Genotypes were used to derive genetic relationship matrices between individuals for heritability analyses. High measures of heritability, from 33% to 51%, were found across all connectivity measures. The disconnectome showed more significantly heritable connectivity measures than the connectome, suggesting that the new proposed measure may reveal additional or complementary information about the genetic architecture of the human brain.

Introduction

Healthy white matter is essential to brain function. Damage to white matter tracts may affect cognition and other outcomes [200]. In recent years, brain connectivity has been modeled by the connectome, which is a graph in which nodes represent regions of interest (ROIs) and edges represent connections between them [174]. In the case of structural connectivity, edges are assigned weights which reflect the degree to which regions are connected by nerve fibres. They are typically derived from diffusion weighted images (DWIs) by estimating fibre pathways using tractography. Traditional measures of structural connectivity include the number of fibres connecting pairs of ROIs and mean diffusion measures between them.

Given that connectivity is mediated via white matter tracts, one would expect that white matter pathology such as white matter lesions (WMLs) has a significant effect on the brain. However, the connectome does not take WMLs directly into account. Previous studies have modelled WMLs in the connectome using hypothetical lesioning [44] and by estimating altered patient connectomes from connectivity data derived from healthy controls [117]. While these studies have yielded useful insights, they are both forced to make assumptions about the degree to which lesions affect a given connection. Modelling the topology of disconnection in the brain may yield new knowledge with regards to how and where pathology affects brain connectivity. In order to directly study disconnection, this study defines the structural ***dis***connectome, which extends the disconnectome map [63, 191] and reflects the location of white matter pathology within the connectome.

A better understanding of the genetic underpinnings of brain connectivity and disconnectivity can help to identify the mechanisms that control communication within the brain, including those that give rise to neurological and psychiatric illness [185]. Current multi-center efforts showed that is it possible to discover genetic variants that influence the volume of several brain regions [3, 19, 94, 95]. To power such analyses requires data from tens of thousands of individuals. Also, the choice of appropriate neuroimaging measurements (phenotypes) is critical to identify target genetic variants while performing genome-wide association analysis. Alternatively, genetic heritability analysis summarizes the strength of genetic influences on a phenotype and requires much less data. Effectively, the powerful heritability paradigm allows the prioritization of neuroimaging measurements for future genome-wide association studies.

In this work, we aimed to determine the heritability of measures derived from the connectome and disconnectome in the general population. This allows us to localize the genetic underpinnings of both normal connectivity and the relation with white matter lesions.

Methods

Participants and Imaging

This study involved 4111 unrelated subjects from the Rotterdam Study, an ongoing large population-based cohort study of participants that are 45 years and older living in the Ommoord suburb of Rotterdam, the Netherlands [96]. Brain MRI was implemented in the study protocol from 2005 onwards [103]. Magnetic resonance images (MRI) were acquired on a 1.5 tesla GE Signa Excite scanner, including: (1) A T1-weighted (**T1w**) structural scan (TR = 13.8ms, TE = 2.80ms, TI = 2000ms, 96 slices, slice thickness 1.6mm); (2) A T2-weighted fluid-attenuated inversion recovery (**FLAIR**) sequence (TR = 8000ms, TE = 120 ms, TI = 400ms, 64 slices, slice thickness 2.5mm); and (3) A diffusion-weighted spin echo echo-planar **DWI** (TR = 8575ms, TE = 82.6ms, axial FOV 210×210mm, slice thickness 3.5mm, 35 contiguous slices, 25 non-collinear directions at b = 1000s/mm^2 and three volumes at b = 0).

Image Processing

DWIs were processed as in [39]. Briefly, volumes were co-registered. Rotation components were used to realign gradient vectors. Diffusion tensor images (DTI) were estimated using ExploreDTI's Levenberg Marquardt estimator, including upsampling to 1mm isotropic voxels. FA was calculated from the DTI. **WMLs were segmented** using an automated approach: (1) T1w data was segmented into grey matter, white matter and cerebrospinal fluid using a k-Nearest-Neighbour classifier [201]; and (2) the segmentation maps from step one and the FLAIR intensity values were used for WML delineation [38]. **The T1w image was parcellated** into 83 ROIs using FreeSurfer [55]. The WML mask and ROIs were affinely registered to DTI space.

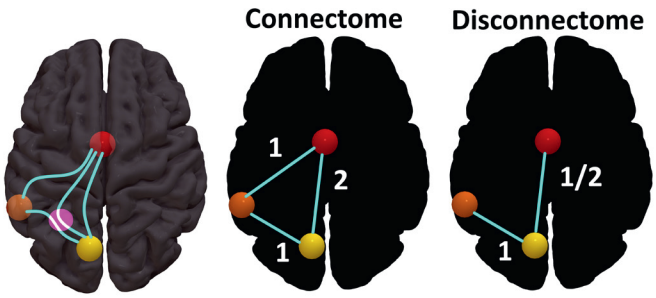

Figure 5.1: *In this schematic example, three ROIs are considered, shown in red, orange and yellow. ROIs are connected by streamlines, which are depicted in cyan. In this example a WML, drawn in pink, affects two streamlines. The edges of the connectome, G_{NS}, are defined by the number of streamlines connecting each pair of ROIs. The edges of the disconnectome, G_{PAS}, are defined by the number of streamlines affected by WMLs divided by the total number of streamlines. (Best seen in color.)*

Network generation

Estimated tensors were used to reconstruct deterministic streamlines using the diffusion toolkit [203] with an angular threshold of 45°, an FA threshold of 0.2, and one seed per grey and white matter voxel. The streamlines were smoothed using a spline filter (step length = 0.5mm).

As illustrated in Fig. 5.1, a connectome (G_{NS}) was created by defining nodes as ROIs and connections as pairs of ROIs, with connection weight defined as the number of streamlines intersecting both ROIs, normalized by dividing by ROI volume. A disconnectome (G_{PAS}) quantified the *proportion of affected streamlines* (PAS) as the fraction of streamlines that pass through the WML mask.

Network metrics

Several graph theory measures were computed from the connectome as described in [154], including the shortest path length between all pairs of nodes, weighted degree, closeness centrality, nodal clustering coefficient, number of triangles around a node, characteristic path length, global efficiency, mean clustering coefficient, mean number of triangles and the total weight. Similar measures were derived from the disconnectome. On the edge level this included *shortest path disruption*,

Table 5.1: *Heritability of global and nodal measures*

Measurement	Heritability (%) Max	# significant
Global		
Connectome		
Characteristic path length	14	0
Global efficiency	**34***	1
Total weight	**34***	1
Mean clustering coefficient	**34***	1
Mean number of triangles	**40***	1
Disconnectome		
Global PAS	19	0
Mean nodal PAS	**37***	1
Mean nodal integration disruption	**38***	1
Mean clustering coefficient	**35***	1
Mean number of triangles	5	0
Nodal		
Connectome		
Closeness centrality	**35***	1
Clustering coefficient	17	0
Number of triangles	32	0
Degree	**41***	4
Disconnectome		
Clustering coefficient	**41***	2
Number of triangles	**37***	2
PAS	**44***	5
Integration disruption	**40***	10

*Significant heritability estimates based on FDR threshold

$\hat{l}_{i,j} = \sum_{u,v \in p(i,j)} d_{u,v}$, where u, v, i and j are nodes, $p(i,j)$ is the shortest path between i and j defined over the connectome and $d_{u,v}$ is the PAS between u and v. On the

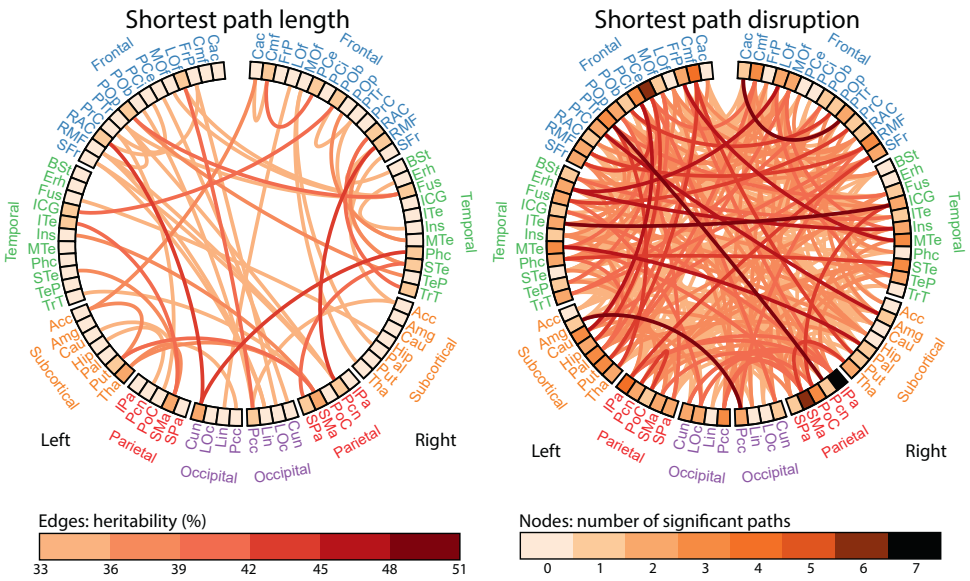

Figure 5.2: *Heritability of shortest path length and disruption. Regions of interest (ROIs) are grouped by lobe. Lines in the center correspond to edges with significant heritability. The color in the outer ring corresponds to the number of paths with significant heritability associated with a given ROI.*

nodal level this included PAS (i.e. the fraction of streamlines extending from an ROI which are affected by WMLs), *integration disruption* (i.e. the average shortest path disruption across all paths related to an ROI), clustering coefficient and number of triangles. Global disconnectome measures included integration disruption (i.e. the average shortest path disruption across all paths), mean nodal clustering coefficient, mean nodal number of triangles, mean nodal PAS and global PAS (i.e. the proportion of all streamlines which are affected by WMLs).

Heritability analysis

Heritability (h^2) is the proportion of total phenotypic variance accounted for by additive genetic factors, and is quantified by comparing the observed phenotypic covariance matrix with the covariance matrix predicted by the genetic relationship matrix (GRM). In the case of high heritability, the covariance of a trait is greater among genetically similar

individuals.

We used Massively Expedited Genome-wide Heritability Analysis (MEGHA) [71] to estimate heritability in our population. This method allows fast and accurate estimates of heritability across thousands of phenotypes based on genome-wide genotype data of common genetic variants from unrelated individuals. As previously described [4], a GRM matrix was constructed using the 1000 Genomes imputed genotypes, filtered on imputation quality ($R^2 < 0.5$) and allele frequency ($MAF < 0.01$). We calculated pairwise genetic relatedness between 4111 individuals. We removed participants with more than 0.025 genotype similarity, resulting in a final study population of 3255 subjects. The threshold was chosen based on a previous study [213]. The analysis was then performed in the remaining unrelated subjects while correcting for age and sex. An inverse Gaussian transformation was also applied to ensure normality of the graph theory measurements.

To correct for multiple comparisons across all connectome and disconnectome measurements, we used the standard False Discovery Rate (FDR) correction algorithm [214] at $q = 0.01$, resulting in a p-value threshold of 0.000 49.

Results

WMLs were found in all subjects with a mean, median and standard deviation of 5.6 ml, 2.8 ml and 8.7 ml, respectively. The range of values was from 0.2 ml to 88.8 ml. WMLs were 57% heritable.

Graph measures were found to be significantly heritable in both the connectome and disconnectome. The global measures were similarly heritable between both types of connectivity (Table 5.1), where the highest heritability was for mean number of triangles in the connectome (40%) and mean nodal integration disruption in the disconnectome (38%). Nodal measures were much more heritable in the disconnectome than in the connectome (Table 5.1). All disconnectome measures were significant, where the highest heritability was 44% in the PAS of the pericalcarine cortex, whereas only two connectome properties had significant heritability. This included closeness centrality in the lateral orbitofrontal gyrus (35%) and degree in four nodes, with maximum heritability in the superior temporal gyrus (41%).

Moreover, on the level of edges, while both types of connectivity were heritable, path

measures in the disconnectome were much more heritable than those in the connectome over the whole brain (Fig. 5.2). In general, the edge heritability was distributed quite uniformly over all brain regions. However, in the disconnectome, the inferior parietal lobule and paracentral sulcus have noticeably more significantly heritable edges. This could potentially mean that WML pathology has stronger genetic architecture that affects the paths to these regions.

Discussion

In this work we investigated the heritability of brain connectivity and disconnectivity in 3255 unrelated healthy adult subjects. We showed that these measures are highly heritable. Furthermore, our work demonstrates that the proposed disconnectome measures are relevant phenotypes for genetic studies.

Although the subjects in this study were all community-dwelling individuals, they all expressed WMLs to some degree. This is a common finding in aging [105]. While exact mechanisms are poorly understood, they are generally believed to reflect cumulative vascular damage and are related to cognitive deterioration.

The construction of the disconnectome as presented in this study is limited by the fact that diffusion in lesions differs from that in healthy tissue. This in turn can impede tractography and thus result in underestimated disconnection. Nevertheless, our method found a considerable location-specific genetic link with WML-related disconnectivity in the brain.

The heritability of the disconnectome suggests that the presence of WML across connections between brain regions is not random, but rather it has its own genetic architecture. WMLs are known to be associated with the risk of stroke, decreased cognitive function and dementia [45]. Therefore understanding which genes affect the particular disconnectome properties can give insight into etiology of these complex diseases.

Conclusion

This is the first population based genetic analysis of high-dimensional connectivity and disconnectivity properties in the brain. The disconnectome provides a way to localize the effects of WMLs to specific connections or regions in the brain. This study showed that disconnectome measures may be complementary or even superior endophenotypes than the classical connectome, suggesting their value for further genetic association analysis. The genetic determinants underlying these heritability estimates have yet to be identified by future association analysis.

6

White matter disconnection is associated with cognitive impairment

Carolyn D. Langen, Lotte G. M. Cremers, Marius de Groot, Tonya White, M. Arfan Ikram, Wiro J. Niessen, Meike W. Vernooij

In preparation

Abstract

Previous studies have linked age-related white matter hyperintensities (WMHs) to cognitive impairment globally. We aimed to determine this relationship in specific connections. Brain connectivity and WMH-related disconnectivity were derived from 3744 participants of the population-based Rotterdam Study. Connectivity was represented by the diffusion-tensor connectome, whereas the disconnectome represented disconnectivity due to WMH. The relationship between (dis)connectivity and cognitive measures was estimated using linear regression. Lower disconnectivity and higher connectivity corresponded to better cognitive function. There were many more significant associations in the disconnectome than in the connectome. Most connectome associations attenuated when disconnection was included in the model. WMH-related disconnectivity was especially related to executive functioning. Increased cognitive speed corresponded to increased connectivity in specific connections independent of WMH presence. WMH-related disconnectivity explains more variation in cognitive function than does connectivity. Efficient wiring in some connections is important to information processing speed independent of WMH presence.

Background

White matter pathology is increasingly being linked to cognitive impairment. Macroscopic white matter changes assessed using imaging include white matter atrophy and white matter hyperintensities (WMHs). These imaging markers have been associated with cognitive decline [45, 81], impairment in gait [179], depression [35], and an increased risk of stroke and dementia [45]. These observations have resulted in the disconnection hypothesis, which states that a loss of white matter connectivity will lead to a loss of communication between different cortical regions resulting in loss in function [66, 67, 82, 121]. Support for the disconnection hypothesis has grown with studies showing that reduced microscopic white matter connectivity, operationalized by diffusion-tensor imaging (DTI) measures, relates to worse brain function [121, 142].

Yet, previous work has almost invariably been performed on a global level, and surprisingly little is known about direct, spatial effects of pathology and loss of connectivity on a local level on brain function such as cognition. We recently showed a location-specific link between WMH-related disconnectivity and reduced functional brain connectivity [121]. However, the association of local white matter (dis)connectivity and specific cognitive domains is as yet unknown.

In order to study location-specific disconnectivity, it is necessary to understand how brain regions are connected. Thanks to advances in methods to acquire and process magnetic resonance images (MRIs), these connections can now be used to build networks called connectomes. The structural connectome quantifies the degree of connectivity between grey matter regions of interest (ROIs) and is generally estimated by tracking streamlines (or 'tracts') through the white matter using DTI [174]. It has been successfully used to estimate group differences [120, 152] and associations with age [17] and atrophy [218]. However, traditional measures of structural connectivity, such as streamline density and tract-specific diffusion measures, do not directly reflect disconnection, and as such may not adequately represent the extent to which pathology, such as WMHs, affects connectivity [152]. Studies of connectivity in brains with pathology may therefore benefit from a datastructure which models pathology-related disconnection directly, on a local level.

Previous studies have attempted to model disconnection by generating altered connectomes, where the weight of a given connection is decreased to simulate the effects of lesions [44, 117]. This, however, assumes that we know the effect of a lesion

on any given connection. In reality, the degree to which a lesion inhibits the function of a white matter tract is unknown. For this reason we developed the structural disconnectome [119], a subject-specific adaptation of the structural connectome in which only white matter tracts passing through WMHs are taken into account. It thus estimates the damage to each connection in subject space.

In this study we used the disconnectome to investigate the relationship between white matter disconnectivity and cognition in a population-based setting. We hypothesized that the disconnectome will be significantly linked to measures of cognitive function, more so than gross measures like total white matter hyperintensity volume and connectome-based measures.

Methods

Setting

This study involved participants of the Rotterdam Study, an ongoing large population-based cohort study of participants that are 45 years and older living in the Ommoord suburb of Rotterdam [96]. Brain MRI was implemented in the study protocol from 2005 onwards [104] and 5430 non-demented participants without contraindications to MRI were eligible for scanning from 2006 to 2011. In total, 4841 participants were scanned. Similar to [30], subjects were excluded in the case of incomplete acquisition (n = 53), presence of artifacts in the DWI (n = 112), presence of cortical infarcts detected in MRI (n=160), history of clinical stroke (n=116) and missing cognition data (n = 524). Participants were further excluded if the grey matter parcellation failed (n = 45) or if the tissue segmentation (see below) was visually judged to be of low quality (n = 87). An additional 30 subjects were excluded due to insufficient dementia screening, resulting in 3714 participants for the analyses.

The Rotterdam Study has been approved by the medical ethics committee according to the Population Study Act Rotterdam Study, executed by the Ministry of Health, Welfare and Sports of the Netherlands. Written informed consent was obtained from all participants.

Image acquisition and processing

Multisequence MRI was performed on a 1.5 tesla General Electric Signa Excite scanner. A quality assurance protocol ensured that the system remained unchanged (i.e. no major updates or upgrades) during the period of inclusion. The scanning sequence included a T1-weighted image (T1w, TR = 13.8 ms, TE = 2.80 ms, TI = 400 ms, 96 slices of 1.6 mm), a T2-weighted fluid-attenuated inversion recovery (FLAIR) sequence (TR = 8000 ms, TE = 120 ms, TI = 2000 ms, 64 slices of 2.5 mm), a proton density weighted image (PD, TR = 21,300 ms, TE = 17.3, 90 slices of 1.6 mm) and a spin echo echo-planar DWI (TR = 8575 ms, TE = 82.6 ms, axial field of view = 210 $\times$ 210 mm, 35 contiguous slices of 3.5 mm, maximum b-value 1000 mm^2/s in 25 noncollinear directions with three unweighted volumes). We refer to [103] for additional details about the image acquisition. A technical issue between February 2007 and May 2008 resulted in 1220 subjects being scanned with swapped phase and frequency encoding directions in the diffusion sequence, resulting in a mild ghosting artifact in the phase encoding direction [39]. This was included as a potential confounder in the statistical analyses.

Tissues were automatically segmented from structural MRIs into grey matter, white matter and cerebral-spinal fluid [201]. The tissue segmentation and FLAIR image were used to automatically segment WMHs [38], after which the full tissue segmentations were manually inspected and corrected in case of errors. WMH segmentations were moved to diffusion space using an affine transform [80]. Grey matter ROIs were delineated by first parcellating the T1w image into cortical and subcortical parcels using FreeSurfer [55]. Parcellations were then affinely transformed to diffusion space.

DWI volumes were co-registered to reduce the effect of eddy currents and subject motion. This resulted in rotation parameters, which were used to correct the gradient vectors. Diffusion tensor images (DTIs) and diffusion parameters, such as fractional anisotropy and mean diffusivity, were computed using a nonlinear Levenberg Marquardt estimator [123].

Definition of connectivity and disconnectivity

Fiber assignment by continuous tracking was used to estimate streamlines from the DTIs using the Diffusion Toolkit [203]. The edges of the connectome were defined by

the number of streamlines intersecting the ROIs associated with the edge. The edges of the disconnectome were defined as the proportion of a given connection's streamlines that pass through at least one WMH voxel. Both networks were constructed and the connectome's global efficiency measure [154] was computed using the NetworkX Python package [86]. Global efficiency is a measure of how well a network is able to exchange information between ROIs.

Measures of cognitive function

For details of the cognitive test battery we refer to [30]. Briefly, this battery included: (1) The 15-Word Learning Test (WLT), which includes immediate recall, delayed recall and word recognition to investigate memory [20]; (2) The Stroop Test, which includes reading, color-naming, and interference tasks and assesses executive function and information processing speed [74, 75]; (3) The Letter-Digit Substitution Task (LDST), which assesses information processing speed and executive function [194]; (4) the Word Fluency Test (WFT), which assesses executive function [205]; and (5) the Purdue Pegboard Test, which measures fine motor speed [46]. The Stroop test outcomes were inverted such that higher scores corresponded to better performance, which is the case with the other tests. A composite cognitive score, the g-factor, was computed using a principal component analysis on the z-scores of: (1) the delayed recall score of the 15-Word Learning Test; (2) the Stroop Interference Test; (3) the Letter-Digit Substitution Task; (4) the Word Fluency Test; and (5) the Purdue Pegboard Test [102].

Statistics

Linear regression was used to assess the global and local relationship between connectivity and WMH-related disconnectivity as determinants and cognitive measures as outcomes, using several models. Global models estimated the relationship for: (1) WMH volume, (2) global efficiency; and (3) WMH volume and global efficiency in the same model including an interaction term. Similarly, for each edge, models were fit with: (1) the edge value in the disconnectome; (2) the edge value in the connectome; and (3) the edge value in both the disconnectome and connectome including an interaction term. Only edges which existed in 60% of subjects were included in the analysis based on a previous study that found that this threshold reflects a balance

between false positives and false negatives [42]. All models included age, gender, supratentorial intracranial volume and encoding direction as covariates. Before fitting each model, all connectivity variables, disconnectome edges, and WMH volumes were standardized by subtracting the median and dividing by the interquartile range. In the standardization of edge measures, the mean and interquartile range was computed across all edges and subjects. The p-values of the coefficients of the connectivity measures were adjusted using the False Discovery Rate method [214] in order to correct for multiple comparisons.

Results

Sample characteristics

Table 6.1 shows the characteristics of the participants in this study. Mean age was 62.4 and 56.1% were female. The median (standard deviation) WMH volume was 5.2mL (7.6mL), and the mean (standard deviation) MMSE was 28.2 (1.8). The g-factor explained 49.4% of the variance in the separate cognitive tests.

WMH volume and connectome-derived global efficiency in relation to cognition

The Spearman correlation between WMH volume and global efficiency was 0.04 ($p < 0.05$ before multiple testing correction). Table 6.2 shows the relationship between the global efficiency, WMH volume and cognitive measures. All relationships were significant ($p < 0.05$), except for global efficiency in relation to WFT and all three WLT subtasks. For all significant relationships, lower WMH volume and higher global efficiency corresponded to higher cognitive measures, both when WMH volume and global efficiency were modeled separately and when they were included in the same model. The coefficients for global efficiency generally reduced in the combined model, but remained significant. The interaction term between WMH volume and global efficiency in the combined model was not significant for any of the cognitive measures.

Table 6.1: *Sample characteristics.*

Characteristics	Total (N = 3714)
Age, years	62.4 (10.6)
Sex, F	2083 (56.1)
Cognitive test results	
Letter-Digit Substitution Task, num. of correct digits	30.9 (6.9)
Purdue Pegboard Test, num. of pins placed	10.5 (1.9)
Stroop 1: reading, s	16.7 (3.2)
Stroop 2: color naming, s	22.9 (4.4)
Stroop 3: interference, s	46.5 (15.8)
Word Fluency Test, number of animals	23.3 (6.0)
WLT, delayed recall	7.8 (2.9)
WLT, immediate recall (mean of 3 trials)	7.9 (2.1)
WLT, recognition	13.5 (1.8)
Intracranial volume, mL	1121.1 (114.8)
MMSE	28.2 (1.8)
White matter lesion volume[a], mL	5.2 (7.6)

Continuous variables are presented as means (standard deviations) and categorical variables as n (%).

[a] White matter lesion volume is presented as median (inter-quartile range).

Cognition in relation to individual connections

Figure 6.1 shows the relationship between the disconnectome, connectome and g-factor. In all but one edge, higher connectome edge weights corresponded to higher g-factor. Higher disconnectome edge weights corresponded to lower g-factor in all cases. Disconnectome edges were more than 8 times more frequently associated with g-factor than connectome edges (Table 6.4). When modeled separately, the connectome model had 28 significant associations that on average explained 36.2% of the variance in the g-factor, whereas the disconnectome had 232 significant associations, which on average explained 36.4% of the variance. The model which included both connectome and disconnectome edges explained on average 36.4% of the variance in the g-factor, where the connectome had six significant connections and the disconnectome had 157. The disconnectome edge associations were fairly symmetric, where the bilateral superior frontal gyri and putamen were involved in the greatest number of significant associations.

The connection-specific relationships with the other cognitive scores are shown in

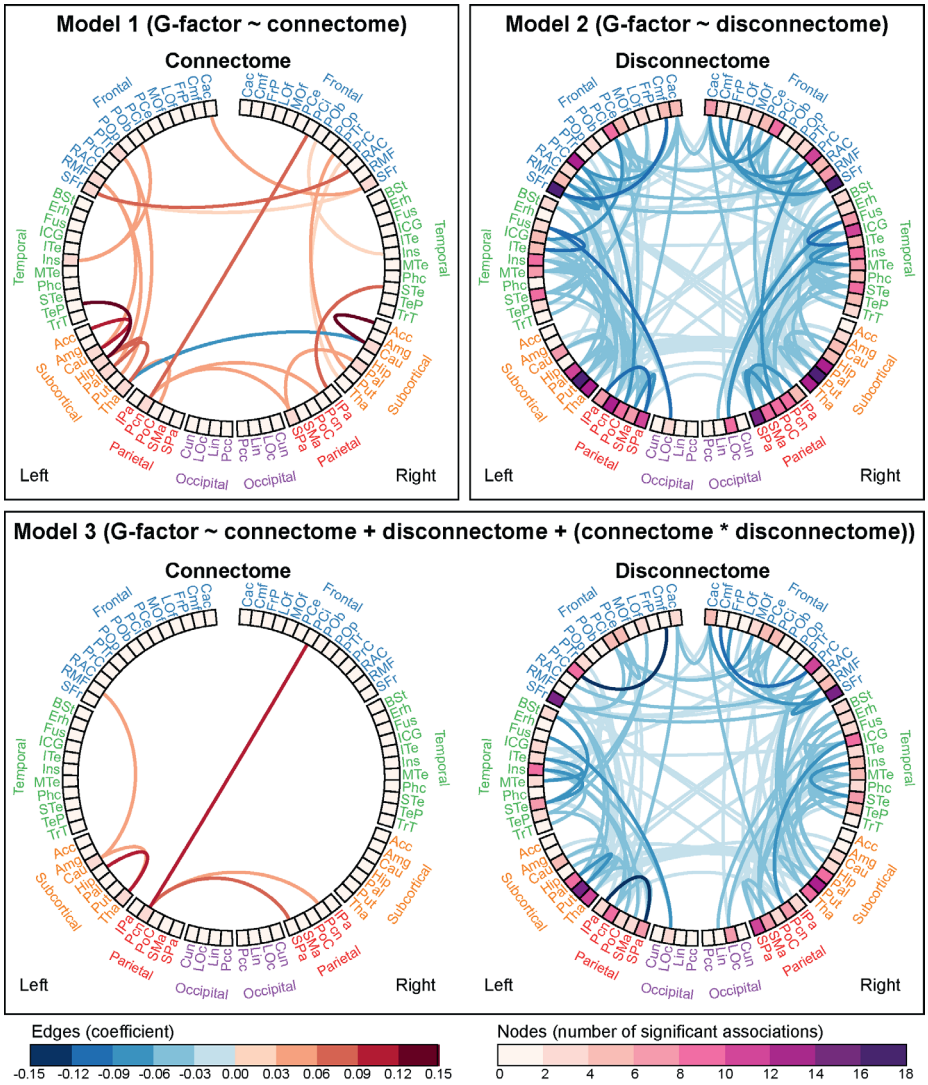

Figure 6.1: *Relationship between g-factor and connections as connectograms. Only significant associations ($p < 0.05$) are shown. ROIs are arranged around the outside of the diagram, grouped by lobe. ROIs are colored according to the number of significant associations that involve them. Connections (edges) are represented by lines between ROIs, which are colored according to the value of their regression coefficient, where red indicates positive correlations and blue represents negative correlations. The connectograms in the top row show the connectome and disconnectome when they are modelled separately. In the bottom row they are modelled together. For the ROI abbreviations refer to Table 6.3*

Figure 6.2 to Figure 6.5 and summarized in Table 6.4. As with the g-factor, the associations were much more widespread in the disconnectome than in the connectome. In most cases higher connectome edge weights corresponded to better cognitive measures, whereas higher disconnectome edge weights corresponded to worse cognitive measures. The interaction between the connectome and disconnectome was not significant in any of the edges for any of the cognitive measures. The disconnectome had many more associations with all cognitive tests than the connectome (Figure 6.2 to Figure 6.5), and the connectome associations attenuated or disappeared after adjusting for the disconnectome (Figure 6.4). Many of the disconnectome associations remained intact after adjusting for the connectome (Figure 6.5). All significant connectome edge associations involved parietal or subcortical regions. In both the connectome and disconnectome, the occipital lobe had relatively few significant associations with all cognitive measures.

Discussion

This study investigated the relationship between structural brain connectivity, WMH-related disconnectivity and cognition in a population-based sample of adult subjects. WMH-related disconnectivity explained cognitive impairment much better than connectivity measures, both on a global level and locally in the disconnectome.

On the global level, we found that total WMH volume as well as the connectome's global efficiency were both related to cognitive functioning. These results support and extend earlier findings that larger WMH load and lower global efficiency correspond to worse general cognition [187]. On a domain level, we found that global efficiency in connectivity was associated with the Stroop test, Purdue pegboard test and LDST, but not with the WLT and WFT. This suggests that efficiency of the brain is important with regards to information processing speed, fine motor speed and some aspects of executive function, but that memory and executive control may be less dependent on efficiency. This relationship cannot be explained by lesion formation, since the association with efficiency remained after adjusting for WMH volume and because global efficiency and WMH volume were not correlated. Previous studies also found that global efficiency was associated with speed-related cognitive function [122, 187] and executive function [122], independent of WMHs.

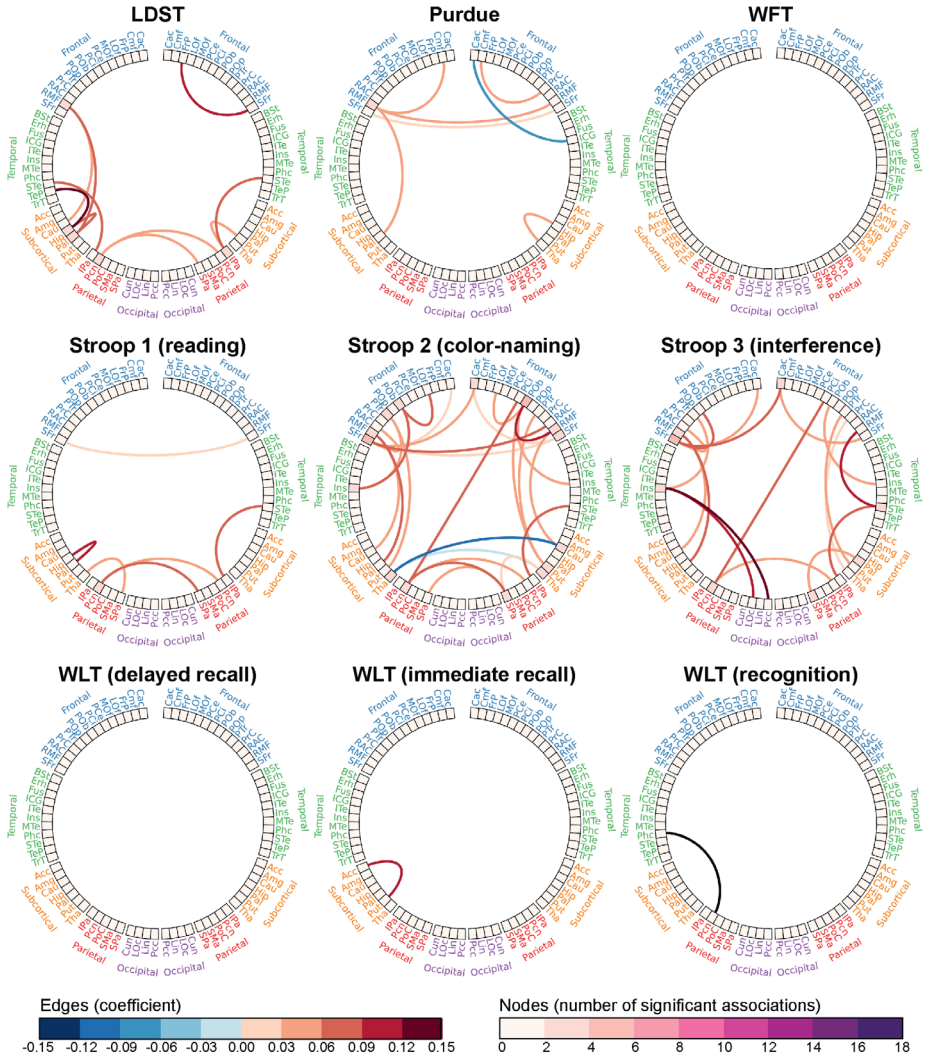

Figure 6.2: *Connectograms of all cognitive tests in relation to the connectome, where the disconnectome is not included in the model. Only significant associations ($p < 0.05$) are shown. ROIs are arranged around the outside of the diagram, grouped by lobe. ROIs are colored according to the number of significant associations that involve them. Connections (edges) are represented by lines between ROIs, which are colored according to the value of their regression coefficient, where red indicates positive correlations and blue represents negative correlations. For the ROI abbreviations refer to 6.3. Abbreviations: LDST = Letter-Digit Substitution Test; Purdue = Purdue pegboard test; WFT = Word Fluency Test; WLT = 15-Word Learning Test.*

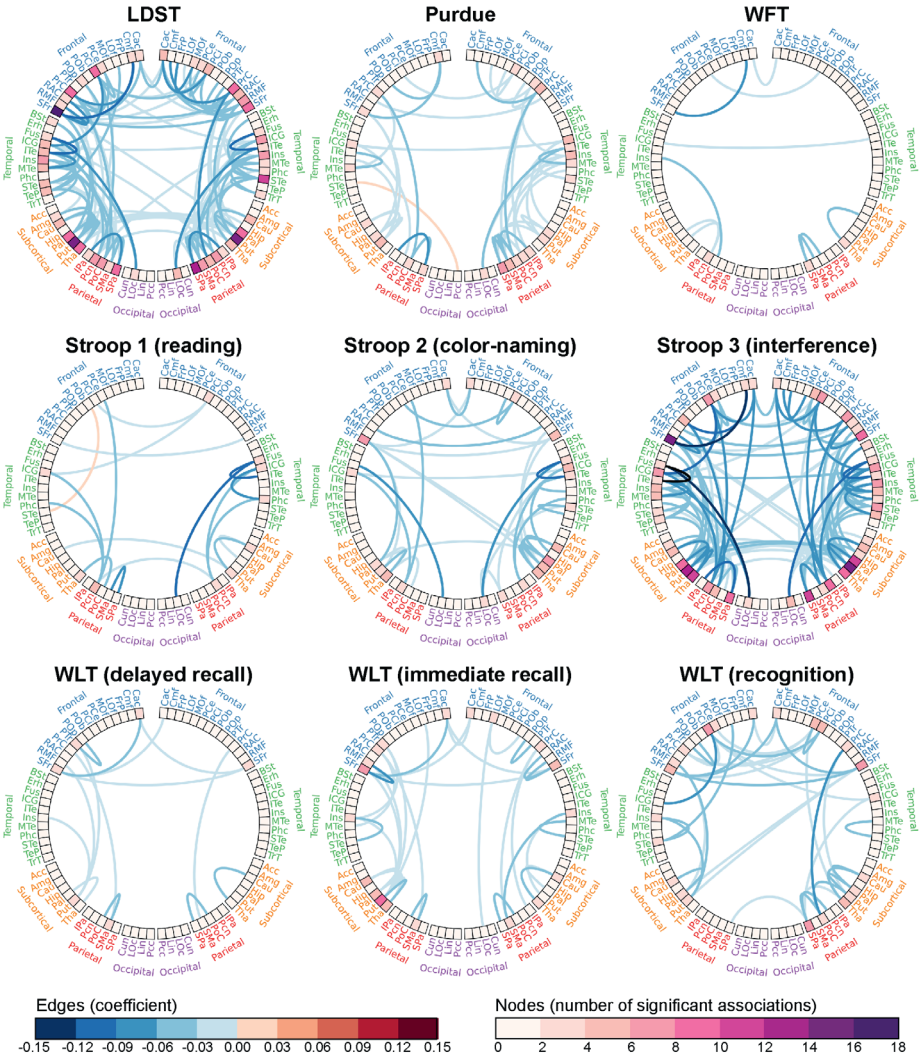

Figure 6.3: *Connectograms of all cognitive tests in relation to the disconnectome, where the connectome is not included in the model. Only significant associations ($p < 0.05$) are shown. ROIs are arranged around the outside of the diagram, grouped by lobe. ROIs are colored according to the number of significant associations that involve them. Connections (edges) are represented by lines between ROIs, which are colored according to the value of their regression coefficient, where red indicates positive correlations and blue represents negative correlations. For the ROI abbreviations refer to 6.3. Abbreviations: LDST = Letter-Digit Substitution Test; Purdue = Purdue pegboard test; WFT = Word Fluency Test; WLT = 15-Word Learning Test.*

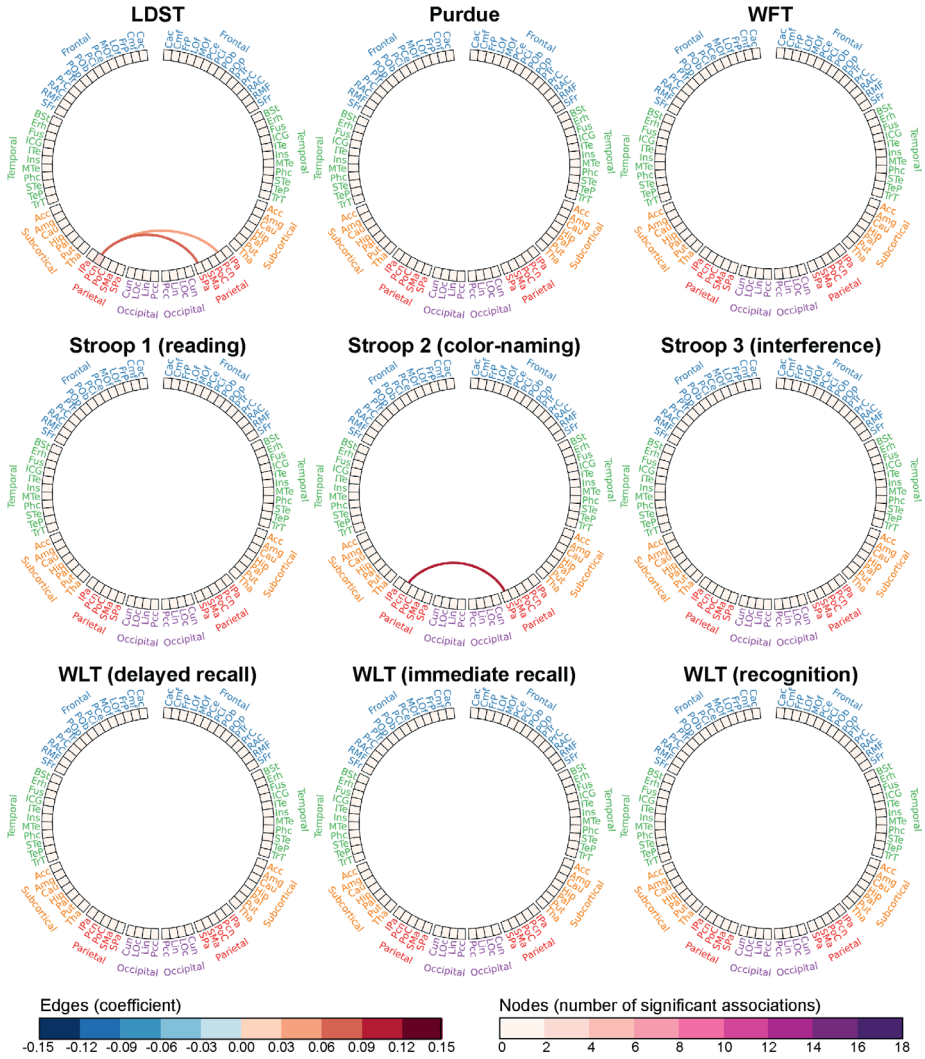

Figure 6.4: *Connectograms of all cognitive tests in relation to the connectome, where the disconnectome is also included in the model. Only significant associations ($p < 0.05$) are shown. ROIs are arranged around the outside of the diagram, grouped by lobe. ROIs are colored according to the number of significant associations that involve them. Connections (edges) are represented by lines between ROIs, which are colored according to the value of their regression coefficient, where red indicates positive correlations and blue represents negative correlations. For the ROI abbreviations refer to 6.3. Abbreviations: LDST = Letter-Digit Substitution Test; Purdue = Purdue pegboard test; WFT = Word Fluency Test; WLT = 15-Word Learning Test.*

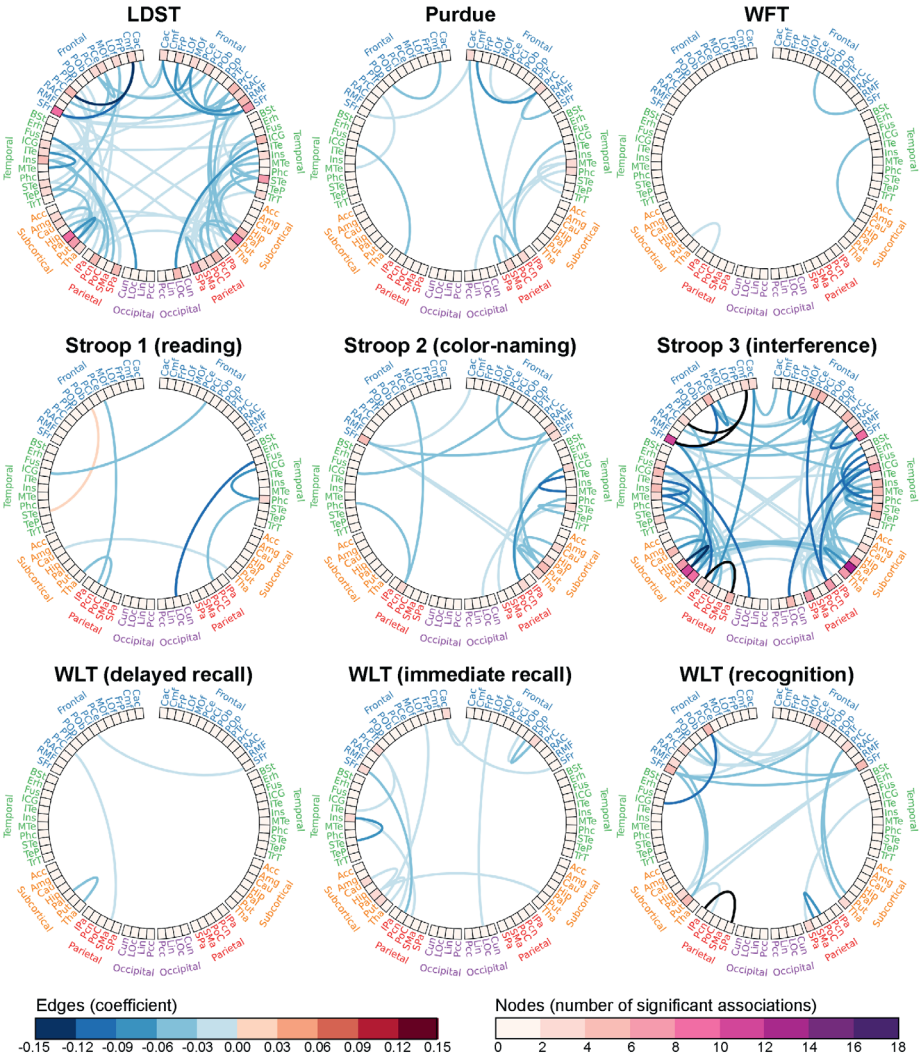

Figure 6.5: *Connectograms of all cognitive tests in relation to the disconnectome, where the connectome is also included in the model. Only significant associations ($p < 0.05$) are shown. ROIs are arranged around the outside of the diagram, grouped by lobe. ROIs are colored according to the number of significant associations that involve them. Connections (edges) are represented by lines between ROIs, which are colored according to the value of their regression coefficient, where red indicates positive correlations and blue represents negative correlations. For the ROI abbreviations refer to 6.3. Abbreviations: LDST = Letter-Digit Substitution Test; Purdue = Purdue pegboard test; WFT = Word Fluency Test; WLT = 15-Word Learning Test.*

Similar to the global efficiency models, the edges in the connection-specific models were most often associated with the Stroop test, LDST and Purdue pegboard test, supporting the suggestion that brain connectivity is important to solving problems quickly and to some aspects of executive function. The fact that most of the connectome associations disappeared after adjusting for WMH-related disconnectivity may be unsurprising, since most significant associations involved frontal, subcortical or parietal regions and a previous study found that primarily WMH in fronto-parietal and fronto-parietal-subcortical white matter networks are associated with decline in executive function [107]. The edge associations that remained after adjusting for WMH-related disconnectivity involved only the LDST and Stroop color-naming subtask, indicating that decline in information processing speed is not the result of WMHs alone. These tests had two common connectome edge associations, namely between the left rostral middle frontal cortex and the left caudate, as well as the left precuneus and the right superior parietal cortex. This suggests that efficient wiring between these brain regions may be especially important to information processing speed independent of the effect of WMHs, particularly with regards to resisting disruptive stimuli [11] and integrating complex neuropsychological processes [194]. The LDST was additionally associated with connectome edges between the bilateral precunei, the inferior parietal cortex and the superior temporal gyrus, the caudate and thalamus and the caudate and rostral middle frontal cortex. Thus in these connections, streamline density is related to integration of complex neuropsychological processes, including visual scanning, mental flexibility, sustained attention, psychomotor speed and information processing speed [194], regardless of whether WMHs are present or not.

We expressed WMH-related disconnectivity in the disconnectome, taking into account potential disruptions of fibres due to WMH load. The disconnectome yielded many more signficant associations with cognitive function than the connectome. These associations remained after adjusting for the weight of the connectome edges. Taken together, these results provide location-specific support for the disconnection hypothesis by providing a mapping between lesioned connections and worse brain functioning. The associations of WMH-related disconnectivity with worse cognitive function corroborate previous studies' findings that loss of structural connections related to decrease in brain function [45, 187, 200]. However, the specific localization of WMH-related loss of executive function extended beyond the previously found

associations with fronto-parietal and fronto-parietal-subcortical white matter networks [107]. Our results indicate that WMHs in connections between all lobes are associated with executive function, especially with respect to the LDST and Stroop interference test, which had similar patterns of associations. Interestingly, among subcortical connections, those involving the putamen, thalamus and pallidum were most frequently associated with all cognitive tests except the Stroop reading test and WFT, whereas connections with the caudate and amygdala were minimally affected, and those with the accumbens and hippocampus were not affected at all. This is in contrast to a previous study that found that lesions in the caudate were associated with deficits in executive control, attention, memory and drive, whereas those in the putamen and pallidum were less associated with cognitive deficits [16]. This discrepancy may be the result of differences in lesion location: our study focused on WMHs, whereas Benke et al. studied lesions in grey matter tissue. Thus while damage to the putamen and pallidum may have less impact on cognition than damage to the caudate, damage to subcortical communication pathways has more impact with regards to putamen and pallidum than the caudate.

Important strengths of our study are large sample size in a population-based cohort with a wide range of ages. This provided the statistical power to yield important insights into the aging process. Our use of the connectome and disconnectome also allowed us to gain a greater resolution in investigating the disconnection hypothesis. Combined with a wide range of cognitive tests, this allowed for a connection-specific mapping between connectivity, disconnectivity and specific cognitive functions. We should also consider potential limitations. As we included only participants who finished all cognitive tests in order to construct the g-factor, we may have selected subjects that performed relatively well and thus introduced selection bias. If anything, this will likely have led us to underestimate the association between disconnectivity and cognitive functioning. Another limitation is the cross-sectional design, precluding any conclusions on directionality of the associations. The study was further limited by low angular resolution diffusion data as well as the use of DTI and deterministic tractography. While newer and higher-resolution protocols would be of benefit, the data comes from a long-running population-based study which began before such acquisition protocols became available. While DTI and deterministic tractography are often unable to deal with crossing fibres and challenging brain geometry, more

sophisticated methods, such as probabilistic tractography, require a long processing time and may be more difficult to interpret. If anything, we believe our results indicate the added value in the disconnectome, and serve as a stepping stone for future research that applies more advanced acquisition and processing techniques.

The implementation of the disconnectome as presented in this study depends on subject-specific tractography in order to estimate disconnection. However, WMHs have been shown to influence diffusion [40], and thus may impede tractography. As a consequence, the degree of disconnectivity may have been underestimated. A previous study mitigated the effect of lesions on tractography by applying subject-specific pathology masks to tractography from healthy controls to estimate changes in connectivity [117]. The effect of lesions on tractography may however differ between locations, individuals and lesion types. Thus the results from such methods may be imprecise and more difficult to interpret than for patient-specific structural connectomes. Additionally, with this approach the exact location of disconnection is not observed directly. Future work may focus on disentangling this.

Conclusion

In this large, population based study of brain connectivity and disconnectivity, we found that WMH-related disconnectivity is highly associated with cognitive dysfunction, especially in relation to executive functioning. The connectome is also related to cognition, but to a lesser extent. This association remained in a subset of connections after adjusting for the presence of WMHs.

Acknowledgements

We would like to sincerely thank all those involved in the data collection and processing of the Rotterdam Study data. Henri Vrooman provided a great deal of assistance in assembling the required datasets. This work was supported by the Netherlands Organization for Health Research and Development (ZonMW) [grant numbers 91211021, 90700435]; VPH-Dare@IT (FP7-ICT-2011-9-601055); the Netherlands Organization for Scientific Research (NWO) [grant 184.033.111];

Alzheimer Nederland [grant WE.03-2012-30], the European Union Seventh Framework Programme (FP7/2007 - 2013) [grant FP7-ICT-2011-9-601055]; Internationale Stichting Alzheimer Onderzoek (ISAO) grant number 12533; the Erasmus MC and Erasmus University Rotterdam; the Research Institute for Diseases in the Elderly (RIDE); the Ministry of Education, Culture and Science; the Ministry of Health, Welfare and Sports; the European Commission (DG XII); and the Municipality of Rotterdam.

Table 6.2: *Relationship between cognitive measures, WMH volume and global efficiency*

				Stroop				15-Word Learning Test		
	g-factor	**LDST**	**Purdue**	**Read**	**Color**	**Inter.**	**WFT**	**Del.**	**Imm.**	**Rec.**
Cognition ~ WMH volume										
R^2	0.372	0.226	0.335	0.112	0.104	0.247	0.106	0.101	0.112	0.030
WMH volume										
Coef	**-0.049**	**-0.044**	**-0.027**	**-0.030**	**-0.038**	**-0.058**	-0.022	**-0.025**	**-0.028**	**-0.033**
$CI_{0.025}$	-0.060	-0.057	-0.037	-0.045	-0.053	-0.074	-0.035	-0.037	-0.040	-0.050
$CI_{0.975}$	-0.038	-0.032	-0.018	-0.015	-0.024	-0.042	-0.009	-0.012	-0.015	-0.016
Cognition ~ Global efficiency										
R^2	0.362	0.218	0.332	0.111	0.102	0.241	0.103	0.098	0.108	0.026
Global efficiency										
Coef	**0.064**	**0.066**	0.046	0.068	**0.094**	**0.113**	-0.002	0.004	0.002	0.010
$CI_{0.025}$	0.030	0.029	0.018	0.023	0.052	0.066	-0.041	-0.033	-0.035	-0.040
$CI_{0.975}$	0.097	0.103	0.074	0.113	0.137	0.161	0.037	0.042	0.038	0.060
Cognition ~ WMH volume + global efficiency + (WMH volume * global efficiency)*										
R^2	0.373	0.227	0.336	0.113	0.107	0.249	0.106	0.101	0.112	0.029
WMH volume										
Coef	**-0.048**	**-0.045**	**-0.025**	**-0.030**	**-0.037**	**-0.049**	**-0.026**	**-0.027**	**-0.030**	**-0.036**
$CI_{0.025}$	-0.060	-0.058	-0.035	-0.046	-0.052	-0.067	-0.040	-0.041	-0.043	-0.054
$CI_{0.975}$	-0.036	-0.032	-0.015	-0.013	-0.021	-0.032	-0.012	-0.013	-0.017	-0.018
Global efficiency										
Coef	**0.041**	**0.051**	**0.031**	**0.061**	**0.084**	**0.076**	-0.006	-0.005	-0.011	-0.004
$CI_{0.025}$	0.007	0.012	0.002	0.014	0.039	0.027	-0.047	-0.045	-0.050	-0.056
$CI_{0.975}$	0.076	0.090	0.061	0.108	0.128	0.126	0.035	0.035	0.027	0.049

Bold values represent statistical significance ($p < 0.05$). The p-value has been adjusted using the Benjamini-Yukateli false discovery rate method [214].
Abbreviations: Coef = regression coefficient; LDST = Letter-Digit Substitution test; R^2 = adjusted R-squared; ($CI_{0.025}$, $CI_{0.975}$) = 95% confidence interval of the estimated coefficient; Purdue = Purdue Pegboard test; WFT = Word Fluency Test; WMH = white matter hyperintensity.
*Note: The interaction term is not included in the table because it was not significant.

Table 6.3: *Regions used in connectome analysis, grouped by location in the brain.*

Cluster	Region	Abbreviation
Frontal (Fro)	Caudal anterior cingulate cortex	Cac
	Caudal middle frontal gyrus	Cmf
	Frontal pole	FrP
	Lateral orbitofrontal cortex	LOf
	Medial orbitofrontal cortex	MOf
	Paracentral lobule	PCe
	Pars opercularis	POp
	Pars orbitalis	POb
	Pars triangularis	PTr
	Posterior cingulate gyrus	PCi
	Precentral gyrus	PrC
	Rostral anterior cingulate gyrus	RAC
	Rostral middle frontal gyrus	RMF
	Superior frontal gyrus	SFr
Occipital (Occ)	Cuneus	Cun
	Lateral occipital gyrus	LOc
	Lingual gyrus	Lin
	Pericalcarine cortex	Pcc
Parietal (Par)	Inferior parietal lobule	IPa
	Postcentral gyrus	PoC
	Precuneus	Pcn
	Superior parietal lobule	SPa
	Supramarginal gyrus	SMa
Subcortical (Sub)	Accumbens area	Acc
	Amygdala	Amg
	Caudate	CaN
	Hippocampus	Hip
	Pallidum	Pal
	Putamen	Pu
	Thalamus	Tha
Temporal (Temp)	Banks of superior temporal sulcus	BSt
	Entorhinal cortex	Erh
	Fusiform gyrus	Fus
	Inferior temporal gyrus	ITe
	Insula	Ins
	Isthmus of cingulate gyrus	ICG
	Middle temporal gyrus	MTe
	Parahippocampal gyrus	Phc
	Superior temporal gyrus	STe
	Temporal pole	TeP
	Transverse temporal gyrus	TrT

Table 6.4: *Summary of significant associations between cognitive measures, the disconnectome and connectome*

				Stroop				15-Word Learning Test		
	g-factor	LDST	Purdue	Read	Color	Inter.	WFT	Del.	Imm.	Rec.
Cognition ~ Disconnectome										
R^2	0.364	0.220	0.332	0.113	0.102	0.241	0.107	0.102	0.112	0.030
n_D	232	157	49	21	46	145	14	14	43	47
$Coef_D$	-0.035	-0.037	-0.026	-0.040	-0.037	-0.048	-0.032	-0.028	-0.029	-0.035
Cognition ~ Connectome										
R^2	0.362	0.219	0.332	0.112	0.102	0.240	n/a	0.101	n/a	0.030
n_C	28	13	7	7	29	21	0	1	0	1
$Coef_C$	0.048	0.065	0.021	0.049	0.041	0.061	n/a	0.113	n/a	-0.24
Cognition ~ Disconnectome + Connectome + (Disconnectome * Connectome)*										
R^2	0.364	0.221	0.333	0.113	0.103	0.242	0.106	0.102	0.112	0.030
n_D	157	91	20	9	23	106	5	6	20	30
$Coef_D$	-0.035	-0.035	-0.033	-0.038	-0.040	-0.052	-0.037	-0.030	-0.030	-0.035
n_C	6	2	0	0	1	0	0	0	0	0
$Coef_C$	0.065	0.070	n/a	n/a	0.099	n/a	n/a	n/a	n/a	n/a

Abbreviations: n_D = number of significant disconnectome edges, n_C = number of significant connectome edges, $Coef_C$ = connectome regression coefficient; $Coef_D$ = disconnectome regression coefficient; LDST = Letter-Digit Substitution test; R^2 = adjusted R-squared; F = F-test for model fit; ($CI_{0.025}$,$CI_{0.975}$) = 95% confidence interval of the estimated coefficient; Purdue = Purdue Pegboard test; WFT = Word Fluency Test; WMH = white matter hyperintensity

*Note: The interaction term is not included in the table because it was not significant.

7

White matter lesions relate to tract-specific reductions in functional connectivity

Carolyn D. Langen, Hazel I. Zonneveld, Tonya White, Wyke Huizinga, Lotte G. M. Cremers, Marius de Groot, M. Arfan Ikram, Wiro J. Niessen, Meike W. Vernooij

Neurobiology of aging, 2017

Abstract

White matter lesions play a role in cognitive decline and dementia. One presumed pathway is through disconnection of functional networks. Little is known about location-specific effects of lesions on functional connectivity. This study examined location-specific effects within anatomically-defined white matter tracts in 1,584 participants of the Rotterdam Study, aged 50-95. Tracts were delineated from diffusion magnetic resonance images using probabilistic tractography. Lesions were segmented on FLAIR images. Functional connectivity was defined across each tract on resting-state functional MRI by using grey matter parcellations corresponding to the tract ends and calculating the correlation of the mean fMRI activity between the grey matter regions. A significant relationship between both local and brain-wide lesion load and tract-specific functional connectivity was found in several tracts using linear regressions, also after Bonferroni correction. Indirect connectivity analyses revealed that tract-specific functional connectivity is affected by lesions in several tracts simultaneously. These results suggest that local white matter lesions can decrease tract-specific functional connectivity, both in direct and indirect connections.

Introduction

The importance of healthy white matter for brain functioning is becoming increasingly understood. White matter atrophy and white matter lesions, both markers of white matter pathology which can be assessed using imaging, have been related to cognitive decline [45, 81], impairment in gait [179], depression [35], and an increased risk of stroke and dementia [45]. White matter is organized in the brain in tracts, which connect functional brain regions with each other or project outside the brain, mostly to the spinal cord. When the integrity of these white matter tracts is compromised, one might expect that a deficit in function will follow; this has been coined the 'disconnection-hypothesis' [66]. In this hypothesis, a loss of connections in brain structure (i.e. white matter connections) directly affects brain functioning, or so-called functional connectivity (i.e. grey matter activity).

Experimental evidence from animal studies indeed suggests that functional connectivity is negatively affected by white matter disconnection [142, 197]. Evidence supporting the disconnection hypothesis in humans has been found in individual patients with tumors [159], after stroke [161, 172], after transection of the corpus callosum [112] and damage to the arcuate fasciculus resulting in non-fluent speech production in aphasia [65]. These studies, however, focused only on neurological events and conditions affecting single individuals with rare events. This relationship has not yet been confirmed on a population level for more common, yet arguably more subtle pathologies, such as white matter lesions. In the general population, white matter pathology has indeed been linked to reductions in neuronal activity on a global level [81, 219], but it is still poorly understood how pathology affects functional connectivity on a local level, i.e. specific tracts and their connecting brain regions. It is important that we gain more insight into this relation, as it may help us to understand why there is a large inter-individual variation in how white matter pathology compromises brain function. Also, it could help us predict in which brain regions white matter pathology will cause more functional deficits; which may ultimately enable prevention and earlier therapy. With this in mind, we examined the location-specific relationship between white matter lesions (WMLs) and functional connectivity within a population-based setting of middle-aged and older adults.

Material and methods

Setting

The study was embedded within the Rotterdam Study, a large population based cohort designed to investigate chronic diseases in middle-aged and older population [96]. The cohort originated in 1990 and comprised 7,983 participants aged 55 years and older. In 2000 and 2006 the cohort was expanded and now includes 14,926 participants aged 45 years and older. Brain MRI was implemented in the core study protocol from 2005 onwards. The Rotterdam Study has been approved by the medical ethics committee according to the Population Study Act Rotterdam Study, executed by the Ministry of Health, Welfare and Sports of the Netherlands. Written informed consent was obtained from all participants.

Resting state functional MRI (rs-fMRI) was piloted in 2009-2011, and implemented into the existing multi-sequence study protocol from 2012 onwards. Between January 2009 and October 2013 we obtained rs-fMRI from 2,118 participants. We excluded participants with prevalent dementia at time of scanning (n=5), insufficient screening for dementia (n=12), relative motion (i.e. the amount of movement between two consecutive timepoints) of >0.5mm (n=1) or absolute motion >3mm in any volume in the rs-fMRI (n=46), or image artefacts interfering with data extraction on any of the scans necessary for this study (e.g. due to metal artefacts, registration issues) (n=158). Furthermore, we excluded scans with cortical infarcts (n=65), because gliosis around cortical infarcts may cause automated WML segmentation to become unreliable. In total, 1,831 rs-fMRI scans were available for analysis. Of these, n=71 were excluded because of missing diffusion data, n=159 were excluded because of partially scanned occipital or temporal lobes in the rs-fMRI and n=17 were excluded because of failed cortical parcellation, yielding a total of n=1,584 for the current analysis. The Rotterdam Study has been approved by the medical ethics committee according to the Population Study Act Rotterdam Study, executed by the Ministry of Health, Welfare and Sports of the Netherlands. Written informed consent was obtained from all participants.

Image acquisition

Participants were scanned on a 1.5 tesla GE Signa Excite scanner. This included a T1-weighted image (T1w, TR = 13.8 ms, TE = 2.80 ms, TI = 400 ms, 96 slices of 1.6 mm), a T2-weighted fluid-attenuated inversion recovery (FLAIR) sequence (TR = 8000 ms, TE = 120 ms, TI = 2000 ms, 64 slices of 2.5 mm), a proton density weighted image (PD, TR = 21,300 ms, TE = 17.3, 90 slices of 1.6 mm), a spin echo echo-planar diffusion-weighted image (DWI, TR = 8000 ms, TE = 74.6 ms, axial FOV 210 $\times$ 210 mm, 39 contiguous slices of 3.5 mm, maximum b-value 1000 mm^2/s in 25 noncollinear directions with three unweighted volumes), and a rs-fMRI sequence (TR = 2900 ms, TE = 60 ms, 31 slices of 3.3 mm, 160 time points 2.9 s apart). Additional details about the image acquisition can be found in [103].

Image processing

Tissue segmentation, DWI processing and white matter tract segmentation procedures were similar to those described in [39]. Briefly, structural MRIs were automatically segmented into grey matter, white matter and CSF using a k-nearest-neighbors classifier [201]. Tissue segmentations and FLAIR intensity were used to segment white matter lesions using an automated approach [38]. Lesion segmentations were manually inspected, and corrected in the case of errors. White matter lesion segmentations were affinely transformed to diffusion space. DWI volumes were co-registered to reduce the effect of participant motion and eddy currents. The resulting rotation parameters were used to correct gradient vectors. A diffusion model was estimated from the co-registered DWI, and probabilistic tractography was used to reconstruct white matter fibers using BEDPOSTX and PROBTRACKX [14, 15], respectively, both of which are available in the FMRIB software library (FSL, http://www.fmrib.ox.ac.uk/fsl/) [111]. AutoPTX was used to identify white matter tracts [39]. For each tract this produced a tract-density image, which was then normalized and thresholded using tract-specific thresholds that were previously extensively optimized based on the reproducibility of FA measurements in 30 subjects of the Rotterdam Study [39]. Of the 26 reconstructed tracts, this study included two interhemispheric tracts (forceps major and minor) and 18 intra-hemispheric tracts (nine pairs of tracts with one tract per hemisphere). The remaining tracts were excluded

because they projected into tissues outside of the brain. AutoPtx tracks the cingulum in two parts (i.e. the cingulate-gyral and parahippocampal parts). In each hemisphere, the two parts were combined to form a single tract. Each intra-hemispheric tract had a left and right component, thus a total of 18 tracts were included in these analyses. A list of included tracts and their anatomical descriptions can be found in Supplementary Table 1. Tract-specific measurements of WML volume and white matter volume were computed after thresholding tract images as described in [39].

The rs-fMRI data was preprocessed using FSL. This included affine registration with 12 degrees of freedom of rs-fMRI volumes to the individual's T1w structural image using FLIRT, and a non-linear registration of the T1w image to a standard space template (MNI 152) using FNIRT [8]. All registrations were visually inspected and excluded if they were of poor quality. Low-frequency drifts and motion components were compensated for using MCFLIRT and temporal filtering [13, 110]. The resulting image was decomposed into several components using single-session independent component analysis. In a test set of 60 participants that were equally distributed over five age groups (aged 50-59.4y, 59.4-68.4y, 68.5-77.3y, 77.3-86.3y, 86.7+y) and gender, the components were manually (visually) classified as "good" (signal) or "bad" (noise) components. This was used to denoise the rs-fMRI data using FMRIB's ICA-based Xnoiseifier 1.06 (FIX) [83, 155].

In order to compute tract-specific functional connectivity, masks of the grey matter voxels corresponding to either end of each tract were defined. To this end, T1w images were first parcellated by FreeSurfer into cortical (34 parcels per hemisphere) and subcortical parcellations [55]. FreeSurfer cortical parcels were further subdivided into 241 regions of interest (ROIs) using the Connectome Mapper's python nipype interface [33, 77]. This parcellation resolution was chosen because the regions were relatively small, yet allowed better correspondence across participants than higher resolutions [25]. When delineating cortical ROIs, the connectome mapper labels only the voxels on the border between the white matter and cortex. The remaining cortical voxels were assigned the ROI labels of the closest labeled voxel. The entire ROI volume was affinely transformed to diffusion space. For a given unthresholded tract, ROIs that did not overlap with the unthresholded tract image in at least 90% of participants were excluded. A threshold was not used in order to ensure that projections into the grey matter, which are less dense than in the middle of the tract, are left intact. ROIs were

Table 7.1: *Tracts and their corresponding grey matter FreeSurfer ROIs.*

ROIs 1	ROIs 2
Anterior thalamic radiation (ATR L/R): Association fibers projecting from the anterior part of the thalamus to the frontal lobe	
Subcortical:	*Frontal:*
Thalamus	Frontal pole (L:1, R:1)
	Insula (L:2,3,4,R:2,3)
	Lateral orbitofrontal cortex (L:2-4, R:4)
	Medial orbitofrontal (R:1)
	Pars opercularis (L:1, R:1)
	Pars orbitalis (L:1, R:1)
	Pars triangularis (L:1, R:2)
	Rostral middle frontal (L:1-6, R:1-6)
	Superior frontal gyrus (L:1,3,5, R:1-5)
Cingulate gyrus (CGC) and parahippocampal parts (CGH) of cingulum (CG, L/R): The cingulum is composed of limbic fibers connecting cingulate gyrus, parietal lobe and frontal lobe to the parahippocampal gyrus and adjacent structures in the temporal lobe	
Frontal:	*Temporal:*
Caudal anterior cingulate (L:1, R:1)	Entorhinal (L:1, R:1)
Medial orbitofrontal (L:1, R:1)	Fusiform (L:3,4, R:3,4)
Posterior cingulate (L:1,2, R:1,2)	Isthmus cingulate (L:1, R:1)
Rostral anterior cingulate (L:1, R:1)	Parahippocampal (L:1, R:1)
Superior frontal (L:2, R:1,2)	
Forceps Major (FMA): Commissural fibers connecting the left and right occipital lobes	
Left occipital:	*Right occipital:*
Cuneus (L:1)	Cuneus (R:1,2)
Lateral occipital (L:1,3-5)	Lateral occipital (R:1-5)
Lingual (L:1,3)	Lingual (R:1-3)
Pericalcarine (L:1)	Pericalcarine (R:1,2)
Forceps Minor (FMI, L/R): Commissural fibers connecting the lateral and medial surfaces of the left and right frontal lobes	
Left frontal:	*Right frontal:*
Caudal anterior cingulate (L:1)	Caudal anterior cingulate (R:1)
Frontal pole (L:1)	Frontal pole (R:1)
Lateral orbitofrontal (L:4)	Lateral orbitofrontal (R:4)
Medial orbitofrontal (L:1,2)	Medial orbitofrontal (R:1,2)
Rostral anterior cingulate (L:1)	Pars orbitalis (R:1)
Rostral middle frontal (L:4-6)	Rostral anterior cingulate (R:1)
Superior frontal (L:1-3)	Rostral middle frontal (R:1,3-6)
	Superior frontal (R:1-4)

Inferior fronto-occipital fasciculus (IFO, L/R): Association fibers connecting the frontal lobe to the occipital and temporal lobes lateral to the posterior and inferior cornua

Frontal:
Frontal pole (L:1, R:1)
Insula (L:1-4, R:1-3)
Lateral orbitofrontal (L:1-4, R:1-4)
Medial orbitofrontal (R:1)
Pars orbitalis (L:1, R:1)
Pars triangularis (L:1, R:2)
Rostral middle frontal (L:3,5,6, R:4-6)
Superior frontal (L:1, R:1)

Occipital:
Cuneus (L:1, R:1)
Lateral occipital (L:4,5, R:2,4,5)
Lingual (L:1-4, R:1-3)
Pericalcarine (L:1, R:1,2)

Temporal:
Fusiform (L:1,2, R:1-3)
Inferior temporal (L:4, R:4)
Middle temporal (L:1, R:1)
Superior temporal (L:4, R:4)

Inferior longitudinal fasciculus (ILF, L/R): Association fibers connecting the temporal and occipital lobes

Temporal:
Banks of the superior temporal sulcus (L:2, R:1)
Entorhinal (L:1, R:1)
Fusiform (L:1-4, R:1-4)
Inferior temporal (L:1-4, R:1-4)
Insula (L:1-3, R:1-3)
Isthmus cingulate (L:1, R:1)
Middle temporal (L:1-4, R:1-4)
Parahippocampal (L:1, R:1)
Superior temporal (L:3-5, R:2-5)
Temporal pole (L:1, R:1)
Transverse temporal (L:1, R:1)

Occipital:
Cuneus (L:1, R:1,2)
Lateral occipital (L:1-5, R:1-5)
Lingual (L:1-4, R:1-3)
Pericalcarine (L:1, R:1,2)

Posterior thalamic radiation (PTR, L/R): Association fibers connecting the posterior parts of the thalamus with the occipital and parietal lobes

Subcortical:
Thalamus

Occipital:
Cuneus (L:1, R:2)
Lateral occipital (L:1-5, R:1-5)
Lingual (L:1, R:1)
Pericalcarine (L:1, R:2)

Parietal:
Inferior parietal (L:1,2, R:6)
Superior parietal (L:6,7, R:6,7)

Superior longitudinal fasciculus (SLF, L/R): Association fibers connecting: (1) the superior and medial parietal cortex to the dorsal and medial cortex in the frontal lobe; (2) the caudal-inferior parietal cortex to the dorsolateral prefrontal cortex; (3) the supramarginal gyrus to the ventral premotor and prefrontal cortex; (4) the superior temporal gyrus and superior temporal sulcus to the dorsal prefrontal cortex; and (5) the frontal lobe to the occipital lobe

Frontal:
Pars opercularis (L:2, R:1-2)
Precentral (L:2-8, R:1-6)
Superior frontal (L:8,9, R:6,7)

Occipital:
Lateral occipital (L:4)

Parietal:
Inferior parietal (L:1-5, R:1-6)
Postcentral (L:1-7, R:1-5)
Precuneus (R:4-5)
Superior parietal (L:1-5, R:1-4)
Supramarginal (L:1-5, R:1-4)

Temporal:
Banks of the superior temporal sulcus (L:1,2, R:1)
Inferior temporal (L:2-4, R:3,4)
Middle temporal (L:1-3, R: 1-3)
Superior temporal (L:1-3, R:1-3)
Transverse temporal (L:1)

Superior thalamic radiation (STR, L/R): Sensorimotor fibers connecting the thalamus to the precentral and postcentral gyri

Subcortical:
Thalamus

Frontal:
Caudal middle frontal (L:3, R:1,3)
Paracentral (L:1, R:2)
Pars opercularis (L:2, R:2)
Precentral gyrus (L:1-5,7, R:2-6)
Superior frontal (L:6-9, R:5-8)

Uncinate fasciculus (UNC, L/R): Association fibers connecting the anterior temporal lobe, hippocampus and amygdala to the frontal gyrus and lower surfaces of the frontal lobe

Frontal:
Frontal pole (L:1, R:1)
lateral orbitofrontal (L:1-4, R:1-4)
Medial orbitofrontal (L:1,2, R:1-3)
Pars orbitalis (L:1, R:1)
Pars triangularis (L:1, R:1,2)
Rostral anterior cingulate (L:1)
Rostral middle frontal (L:5,6, R:4-6)
Superior frontal (L:1, R:1)

Subcortical:
Amygdala

Temporal:
Middle temporal (L:4, R:4)
Superior temporal (L:4,5, R:4,5)
Temporal pole (L:1, R:1)

further excluded if they did not conform to commonly accepted definitions of the endpoints of the tract (see Supplementary Table 1) [202], were found in the middle portion of a tract or if it was ambiguous to which end of the tract the ROI belonged. For example, the uncinate fasciculus connects frontal and temporal regions, where the insula is positioned in the middle portion of the tract. In this case, it is unclear whether

the insula belongs to the frontal or temporal end of the tract, and the degree of connectivity with the insula is unknown. For this reason, the insula was deemed a region that would confound the results and thus was not included in the analysis of the uncinate fasciculus. Each included ROI was assigned to either end of the tract. See Supplementary Table 1 for a list of ROIs corresponding to each tract.

Functional connectivity was computed for each tract. To do this, the ROI segmentation and each white matter tract were transformed into fMRI space. Two masks per tract were formed by taking the intersection of the unthresholded tract and the identified ROIs. A mean time-series was computed across all voxels within each mask from the preprocessed fMRI data. Functional connectivity for a given tract was calculated as the Pearson correlation of the mean time-series within the two masks corresponding to the tract.

Statistical analysis

The relationship between age and both tract-specific WML volume and functional connectivity was determined using Spearman's correlation. Robust linear regression models were fit per tract to determine how both global (i.e. brain-wide, Model 1) and local (i.e. tract-specific, Model 2) WMLs affect functional connectivity across each tract using the statsmodels Python library (http://statsmodels.sourceforge.net). We used robust linear regression because it minimizes the effect of outliers on the model fitting. Model 2 additionally included the tract's white matter volume as a covariate. Model 2 measured the associations in direct connections (i.e. both functional connectivity and WML volume were from the same tract). A third model was fit to all possible pairs of tracts to determine how WMLs in indirect connections affect functional connectivity. In this model, the functional connectivity in a given tract was the dependent variable, the WML volume of a second tract was the independent variable of interest, where the white matter volume of the second tract was included as a covariate. All three models included intracranial volume, age and gender as covariates. All variables and covariates except for gender were standardized before model fitting. Given that the models had multiple outcome measures and input variables (M=18 for both functional connectivity and tract-specific WML load), there were two sources of dependence between tests. Thus, standard methods of adjusting for multiple testing in the case of dependent variables, which only consider the case of multiple outcome measures with

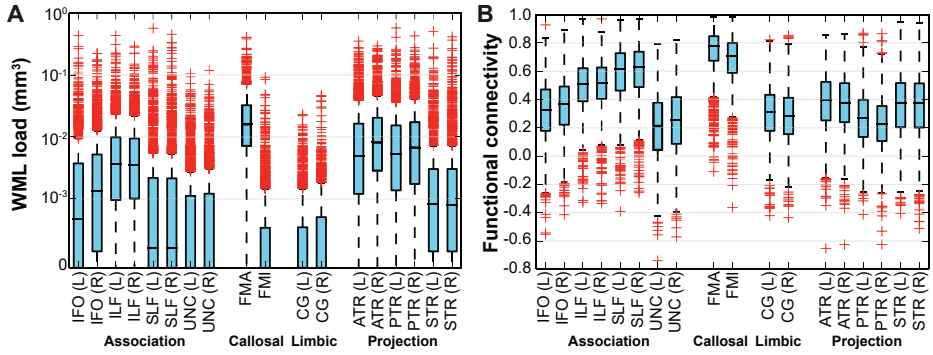

Figure 7.1: ***Distribution of tract-specific white matter lesion (WML) load and functional connectivity across participants.*** *Boxes extend from the lower to the upper quartile, where the median is indicated a line. Whiskers indicate the range of values within 1.5 times the interquartile range from the median. Red markers show individual observations outside of the whisker range. White matter tracts are listed alphabetically on the x-axis. In (A) WML load is on the y-axis and is defined as the volume of WMLs in a given tract divided by tract volume. In (B) functional connectivity is on the y-axis and is defined as the Pearson correlation of the mean timeseries within the regions on either end of a given tract.*

7

a single global dependent variable of interest, were not applicable. In order to take type I errors into account, we considered significance over a range of p-values between 0.05 and the Bonferroni threshold 0.05/M=0.0028 and evaluated significant results in each tract relative to each other.

Results

The characteristics of the study population are shown in Table 7.2. Of the 1,584 participants, the mean age was 62.6 years (standard deviation 6.5, age range 50-95 years), and 58.6% were women. The median WML volume was 4.0 mL (interquartile range 1.5 – 4.3). WMLs were concentrated primarily within the forceps major, anterior thalamic radiations, posterior thalamic radiations and inferior longitudinal fasciculi, however WML load (i.e. WML volume adjusted for tract volume), was found in all tracts (see Figure 7.1A). T-tests indicated that the mean WML load for all tracts was significantly different from zero, with the largest p-value being less than 10^{-18}. Tract-specific functional connectivity varied greatly across tracts and participants (see

Table 7.2: *Characteristics of the study population.*

Characteristics	N=1584
Age, years	62.6 (6.5, range: 50 to 95)
Female	929 (58.6)
Global white matter lesion volume, mL	4.0 (1.5 - 4.3)
Global normal-appearing white matter volume, mL	409.6 (54.6)
Intracranial volume, mL	1133.1 (111.0)

Data presented as mean (standard deviation) for continuous variables and number (percentages) for categorical variables. White matter lesion volume presented as median (interquartile range).

Figure 7.1B), where the greatest sample means were found in forceps major and minor and smallest sample means were found in the uncinate fasciculi and posterior thalamic radiations. WML volume was highly positively correlated ($p < 0.0028$) with age in all tracts, whereas functional connectivity was highly negatively correlated ($p < 0.0028$) with age in the uncinate fasciculi, cingulate gyri, and forceps minor (see Figure 7.2). Grey matter ROIs included for each tract are visualized in Figure 7.3.

The relationship between WML load and functional connectivity varied greatly across tracts and between hemispheres. Figures 7.4 and 7.5 show how functional connectivity decreased with increasing WML volume. The association between higher tract-specific WML load and lower functional connectivity in direct connections reached Bonferroni significance ($p < 0.0028$) in the left inferior fronto-occipital fasciculus whereas the relationship between global WML volume and functional connectivity did not reach Bonferroni significance in any tract (Figure 7.4). The global and local associations in several tracts approached statistical significance ($0.0028 < p < 0.05$), all of which indicated that increased WML volume is associated with decreased functional connectivity. Of the associations with $p < 0.05$, age played a highly significant role ($p < 0.0028$) only in the global model for the uncinate fasciculi and the right cingulate gyrus.

The functional connectivity of most tracts decreased with increasing WML volume in several other tracts, which is summarized in Figure 7.6 (Model 3, see Figure 7.7 for a visualization of the results in connectivity diagrams). In other words, the functional connectivity across a given tract is often negatively affected by WMLs in indirect connections. The functional connectivity across most association tracts were often

affected by WML load in association, limbic and projection tracts, where the Bonferroni threshold ($p < 0.0028$) was reached in four tracts. Of the projection tracts, the functional connectivity across only the left anterior and right superior thalamic radiation were affected by the WML volume in several tracts. The functional connectivity of the forceps major was affected by the WML volume in association and projection tracts with significance that approached the Bonferroni threshold ($0.0028 < p < 0.05$), whereas the functional connectivity in limbic tracts and the forceps minor were largely unaffected by WMLs. Bonferroni significance was reached for nine associations, three of which affected the functional connectivity in the right anterior thalamic radiation, two of which affected the functional connectivity in the superior thalamic radiation and four of which affected the functional connectivity in association tracts (Figure 7.6). The WML volume in the left inferior fronto-occipital fasciculus, right superior longitudinal fasciculus and posterior thalamic radiation each affected functional connectivity in two

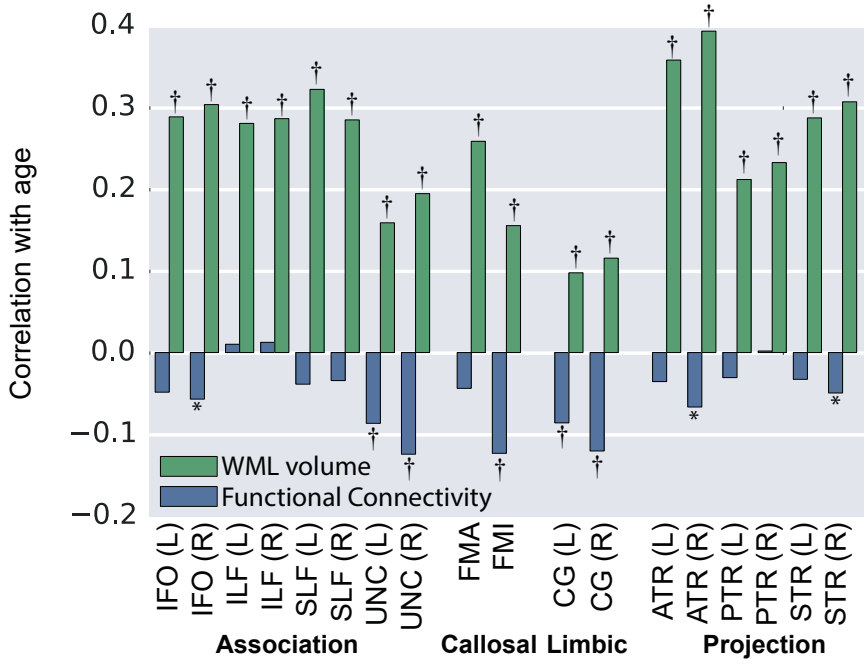

Figure 7.2: ***Correlation of functional connectivity (blue) and WML volume (green) with age.*** *† indicates Bonferroni significance (i.e. p < 0.0028). * indicates p < 0.05.*

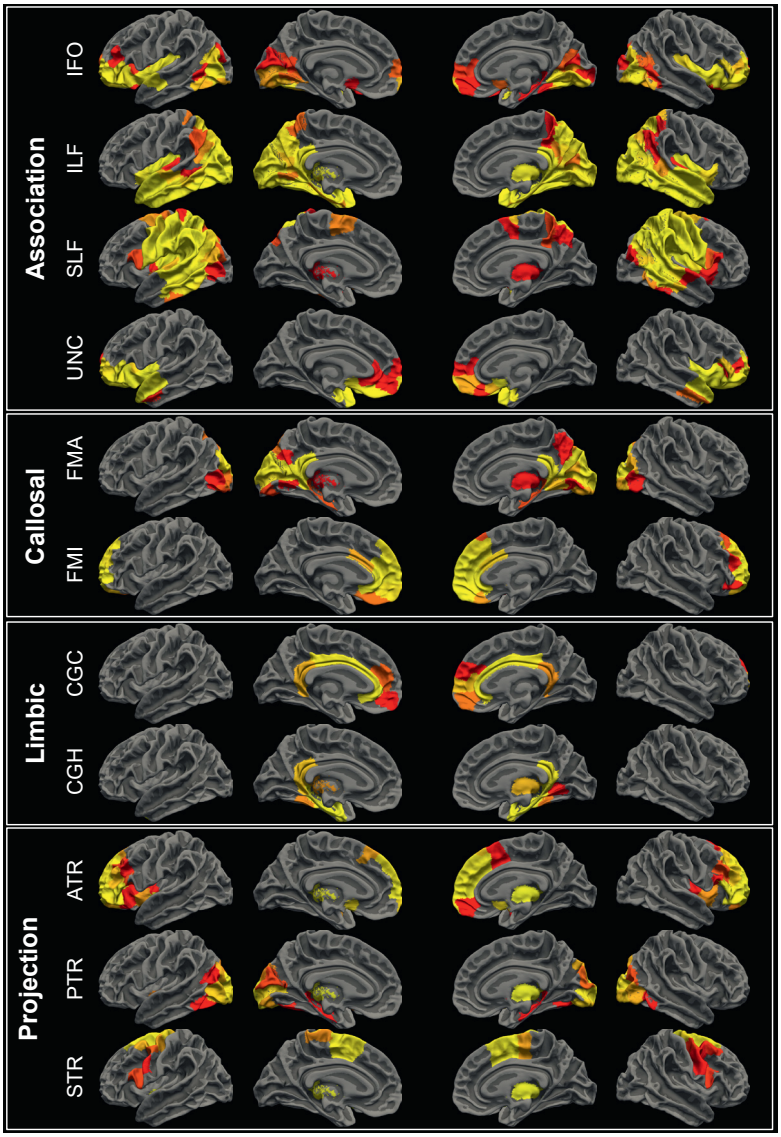

Figure 7.3: ***White matter tract overlap with grey matter ROIs.*** *Coloring indicates the percentage of subjects with overlap, where red corresponds to 90%, yellow corresponds to 100% and ROIs with overlap in less than 90% of subjects are not colored.*

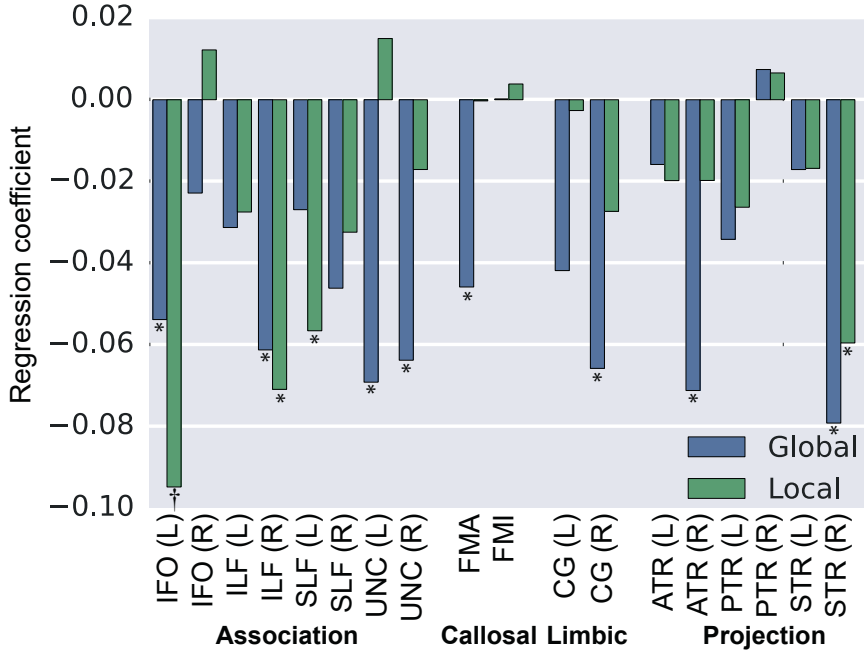

Figure 7.4: ***Model parameters in direct connections.*** *Blue and green bars show the parameters associated with global WML volume (WMLglobal) in model one and local WML volume (WMLlocal) in model two, respectively.* † *indicates Bonferroni significance (i.e. p < 0.0028).* * *indicates p < 0.05.*

tracts with Bonferroni significance. Other tracts with Bonferroni level WML effects included the bilateral cingula and left superior longitudinal fasciculus. Of the tracts with Bonferroni significance in relation to WML volume, functional connectivity was negatively associated with age in the uncinate fasciculi ($p < 0.0023$), the right anterior thalamic radiation ($p < 0.05$) and the right superior thalamic radiation ($p < 0.05$).

Discussion

In this large study among community-dwelling participants aged over 50 years, we found that a higher tract-specific white matter lesion load related to lower functional connectivity in the brain regions connecting to these tracts. This finding supports the

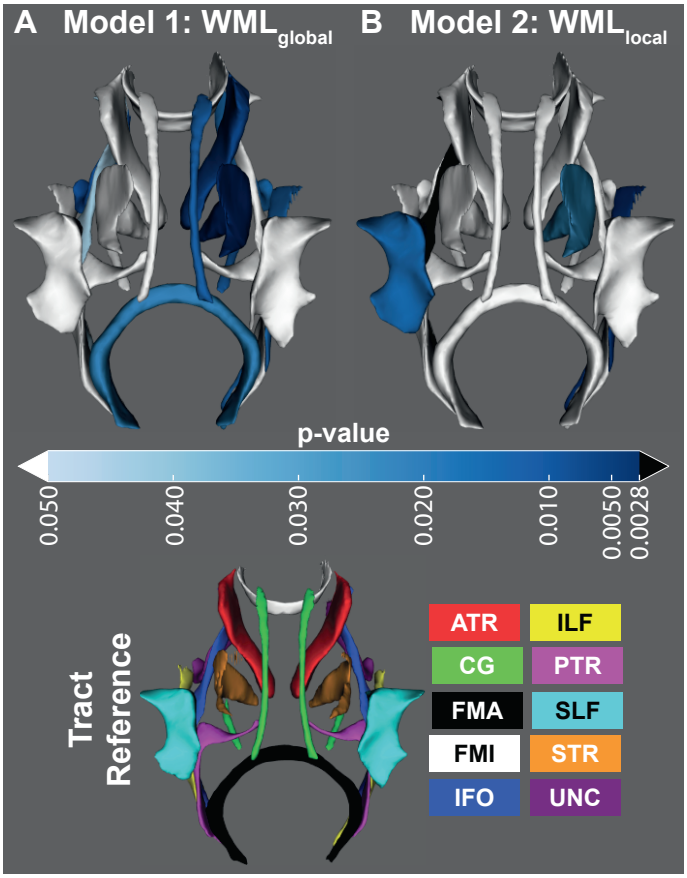

Figure 7.5: ***The association between WML volume and functional connectivity in each tract.*** *The p-values of the regression coefficient corresponding to (A) global WML volume (WMLglobal) in model one and (B) local WML volume (WMLlocal) in model two are represented by the color in each tract. Tracts that reached Bonferroni significance (i.e. p < 0.0028) are colored black. Shades of blue denote significant connections that did not reach Bonferroni significance. White denotes non-significance. The tract reference specifies the names associated with each tract.*

disconnection hypothesis and is indicative of local structural pathology directly affecting brain function. Yet, we furthermore found that tract-specific functional connectivity was also influenced by white matter load in other, not directly connected tracts. This implies that also diffuse white matter pathology, or indirect connections, may affect functional connectivity.

This study benefited from a large sample size and the fact that both DWI and rs-fMRI were acquired in the same scanning session and with consistent scanning parameters. We also used advanced probabilistic tractography and tract segmentation methods which help to spatially localize anatomical tracts in native space. Additionally, we specifically concentrated on data, such as what is typically acquired in a standard

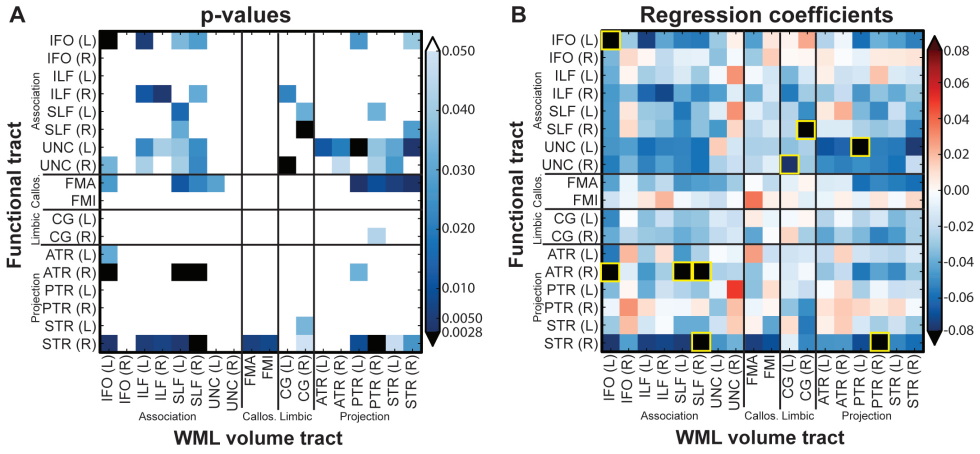

Figure 7.6: ***The effect of WMLs in indirect connections on functional connectivity.*** *Each matrix element corresponds to a single regression of model three, where the WML volume of the tract on the x-axis is the independent variable and the functional connectivity across the tract on the y-axis is the dependent variable. The color of each element represents (A) the p-value and (B) the regression coefficient. In (A), tracts that reached Bonferroni significance (i.e. p < 0.0028) are colored black, shades of blue denote significant connections (p < 0.05) that did not reach Bonferroni significance, and white denotes non-significance. In (B), negative associations are in shades of blue, positive associations are in shades of red and significant associations (p < 0.0028) are outlined in yellow. All significant associations were negative. All models included tract-specific white matter volume, age, sex and intracranial volume as covariates.*

clinical setting, where angular and spatial resolution is often limited, rather than advanced imaging protocols, to show that such methods are within the grasp of typical epidemiological and clinical studies. The study was limited by a cross-sectional design, in which it is not possible to ascertain whether WMLs cause a decrease in functional connectivity or vice versa, though the latter is biologically less likely. Also, our findings are supported by previous research that shows a reduction of functional connectivity following transection of the corpus callosum in a single participant, where the anterior and posterior commissures were left intact [112]. The analyses in this study were further limited by the fact that some tracts had a very low WML volume across participants. Although all tracts had a range of WML loads and for all tracts this load was significantly greater than zero, for some tracts WMLs were present only in a few subjects, and they were often small. For these tracts a decrease in functional connectivity may not yet be detectable. As such, we may have underestimated the

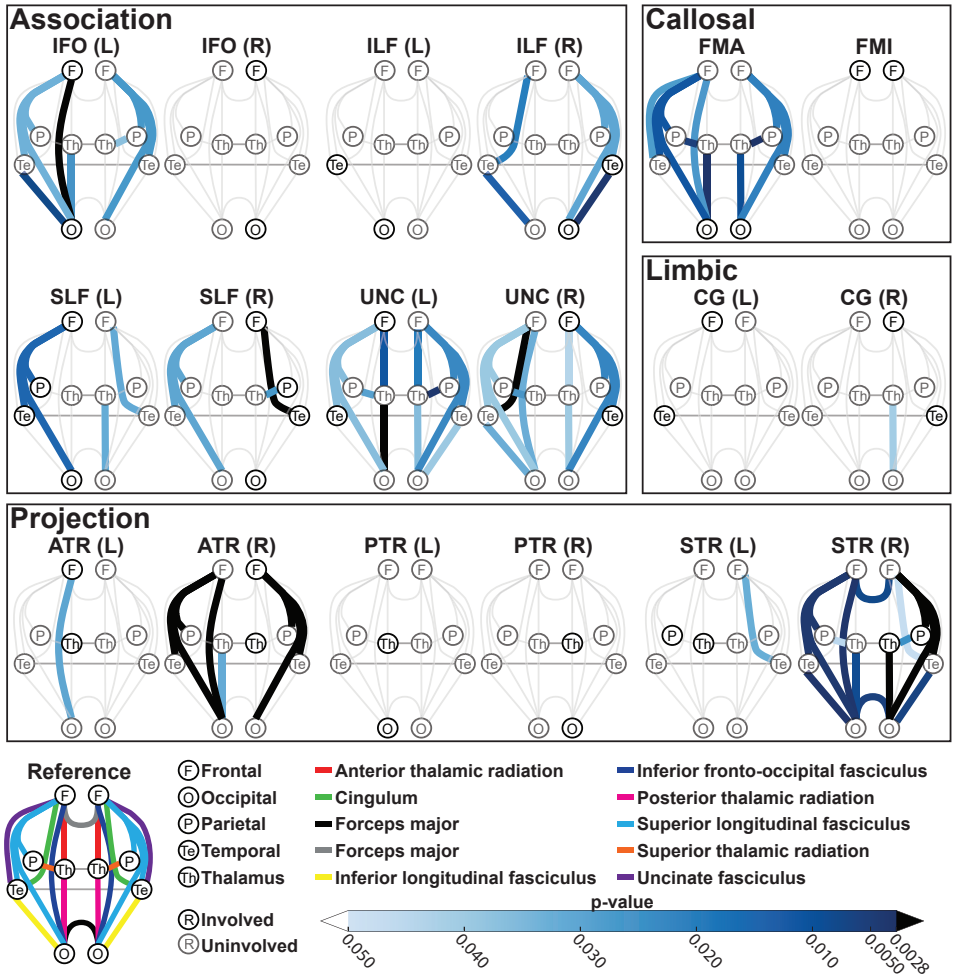

Figure 7.7: ***Visualization of the effect of WMLs in indirect connections on functional connectivity in model three.*** *The label of each connectivity diagram corresponds to the dependent tract (i.e. the tract over which functional connectivity is defined), whereas coloring within each diagram indicates the significance corresponding to tract-specific WML volume in model three. Tracts without a significant relationship are represented by a thin grey line. Note that all significant associations of WML volume with age were negative. Regions that are involved in the functional connection are opaque whereas uninvolved regions are represented by duller colors. The middle and posterior commissural fibers are shown between bilateral thalami and temporal cortices, respectively, to illustrate additional pathways that signals can potentially take.*

impact of some strategic WMLs on functional connectivity. As such, we may have underestimated the impact of some strategic WMLs on functional connectivity. Additionally, a potential limitation is our choice to use anatomically-defined white matter tracts, which is on a relatively large scale and does not take all grey matter regions into account. A broader explorative approach such as connectomics would be more inclusive and less aggregated, but would require more rigorous multiple-testing correction, and result in more uncertainty about whether observed structural connections are representative of true anatomical connectivity, and a more difficult interpretation of results in a biological or psychological context. Another limitation related to the chosen method of delineating grey matter tract endpoint masks is the fact that the method assumes that white matter tracts are comprised predominantly of bundled axons projecting from one single location to another. In reality, some fibers join and leave these bundles at various points along the tract, which could not be modeled with the approach we used.

We found that global and local WML volume had a significant relationship with functional connectivity in many of the same tracts, which reflects both the contribution of each tract to the global white matter volume and the fact that functional connectivity is believed to be an amalgamation of both direct and indirect connections. Neuronal signals can travel from one region to another via intermediate regions and thus contribute to functional connectivity; hence the WML load of one tract may influence the functional connectivity across another. Indeed, our analyses found that the functional connectivity across a given tract was also influenced by the WML load in several other tracts, and that these indirect connections were often stronger than the direct associations. We were unable to include global white matter lesion load into the direct and indirect models because of multi-collinearity issues. Because of this, we cannot conclusively claim that our results cannot be explained by systemic white matter disease burden. However, our analysis included the tracts which contain the majority of lesions, which together encompass most white matter that contributes to global WML load. Thus, these results estimate the relative contribution of WMLs in each tract, where the strongest relationships are likely driving forces in the loss of functional connectivity. This is supported by findings from animal studies. A study on rats found that after induced stroke, functional connectivity initially dropped but then was gradually restored, likely through indirect connections [197]. Another study on

monkeys found that interhemispheric functional connectivity was partially maintained after complete section of the corpus callosum when another tract, the anterior commissure, was spared [142]. In humans, patients with either complete transection or absence of the corpus callosum had at least partially intact interhemispheric connectivity [149, 188, 189], which might also arise from alternate pathways such as the anterior or posterior commissures. Thus, the brain's structural network allows brain function to be maintained via alternate pathways, even when direct connectivity is compromised. For example, the functional connectivity in the right anterior thalamic radiation (ATR) was affected by WMLs in four tracts, where the left inferior fronto-occipital fasciulus (IFO) and the bilateral superior longitudinal fasciculi (SLF) were all significant according to the Bonferroni threshold. The ATR, IFO and SLF all serve frontal regions. It is interesting that the functional connectivity of the bilateral IFO was not affected by the WML load in either the left or right ATR, suggesting that while the IFO may be an important alternate pathway for the ATR, the opposite may not be the case.

When interpreting these results, it has to be considered that age is correlated with functional connectivity and WML volume in several tracts. Given that age was included as a covariate in all models, it is remarkable that we still found several strong associations between WML volume and functional connectivity. This suggests that there is an age-independent and location-specific relation between WML volume and functional connectivity.

The results of this study have important implications with respect to cognition. Previous studies on a similar sample found that reduced global white matter integrity (estimated by diffusion measures) related to worse cognitive function [200] as well as a tract-specific link between decline in white matter integrity and decline in cognitive function, independent of tract-specific WML volume, especially in the inferior fronto-occipital fasciculus [30]. We found that the left fronto-occipital fasciculus had a significantly worse tract-specific functional connectivity with higher local WML load. White matter lesions in this tract also had a significant relationship on the functional connectivity of several other tracts. Taking into account that white matter lesions and white matter microstructure are assumed part of the same disease spectrum [40, 129], our study adds important insights to these previous findings in that it shows a local decline in brain function in relation to local white matter pathology. This provides a

potential mechanism to explain the observed cognitive decline. While this study focused on WMLs, which are easily detected in structural images, future studies including microstructural parameters, such as fractional anisotropy and mean diffusivity, might shed additional light on the location-specific relationship between white matter degeneration and functional connectivity. Such a study would, however, be limited by the fact that deviations in the value of these parameters does not necessarily indicate pathology. Also, a simple average of values across an entire tract may not adequately represent the microstructural changes that precede lesion formation.

White matter disease is highly prevalent in aging, both in terms of macrostructural changes (atrophy and lesions) as well as microstructural abnormalities, and is considered to be mainly of vascular origin [52, 143]. Given that cerebral small vessel damage and WML development are increased by hypertension, a potential treatment to prevent WMLs from developing is to control blood pressure [143, 199]. Future studies on whether WMLs can be prevented or even treated would add important insights into whether we can prevent or reduce loss of functional connectivity. Another important focus of future studies would be to determine why some tracts are more vulnerable to WML-related connectivity loss than others and to consider the importance of indirect connections on functional connectivity in relation to vascular disease.

In conclusion, we found that a higher tract-specific WML load relates to lower functional connectivity in the brain regions connecting to these tracts. This finding supports the 'disconnection hypothesis' and is indicative of local structural pathology directly implicating brain function. The results of this study provide clues into the mechanism of reduced brain functioning as a result of WMLs on a local level.

Acknowledgements

We would like to sincerely thank all those involved in the data collection and processing of the Rotterdam Study data. Henri Vrooman provided a great deal of assistance in assembling the required datasets and Martijn van den Heuvel provided valuable feedback in the concept development stage.

Disclosure Statement

No conflicts of interest exist for any of the authors.

Funding

This work was supported by the Netherlands Organization for Health Research and Development (ZonMW) [grant numbers 91211021, 90700435]; the Netherlands Organization for Scientific Research (NWO) [grant 184.033.111]; Alzheimer Nederland [grant WE.03-2012-30], the European Union Seventh Framework Programme (FP7/2007 – 2013) [grant FP7-ICT-2011-9-601055]; the Erasmus MC and Erasmus University Rotterdam; the Research Institute for Diseases in the Elderly (RIDE); the Ministry of Education, Culture and Science; the Ministry of Health, Welfare and Sports; the European Commission (DG XII); and the Municipality of Rotterdam.

8

General discussion

The collection of works presented in this thesis showed how the connectome, disconnectome and other brain (dis)connectivity measures can be used to study brain function. By developing and using new visualization techniques (Chapter 2) and data analysis techniques on these data we have shed new insight on (i) the development of the brain (Chapter 3), (ii) the relationship between structural connectivity and lesion-related disconnectivity (Chapter 4), (iii) the heritability of connectivity and disconnectivity (Chapter 5), (iv) the role that lesion-related disconnectivity plays in cognitive decline (Chapter 6), and (v) how lesions can affect functional connectivity (Chapter 7). In this final chapter the main findings of these studies are summarized and discussed.

Summary

Brain connectivity

The connectome is a large and complex data structure. Even when a coarse segmentation approach is used, there can be tens of ROIs, and thousands of connections. In addition to this, graph-theory measures can be derived on an edge-wise, node-wise or global level. As a result, statistical analysis and visualization of the connectome can be challenging. In Chapter 2, we described methods for the integrated analysis of group differences in several types of structural and functional connectivity using t-tests. We developed new visualization methods to aid in the interpretation of results. These visualizations included: (1) The *bi-modal comparison plot*, which shows uni- and bi-modal distributions of connectome edge data and can be used to effectively compare group mean networks of several network types simultaneously, including showing the overlap between groups, as well as the distribution of statistical test outcomes; (2) The *worm plot*, an extension of the Manhattan plot which compares statistical test significance across groups of edges for several connectivity measures simultaneously, allowing quick identification of both edge groups and specific edges that contribute to group differences; and (3) *Connectograms*, which are two-dimensional representations of the connectome. These visualizations helped to identify which connectivity definitions were best-suited for analyzing group differences in both aging and schizophrenia.

In Chapter 3 we used worm plots and connectograms to identify which ROIs, lobes and connections are involved in brain development. This study used two measures of functional connectivity. First, a region-wide level of activity was estimated by computing a mean time-series for each ROI. Correlation of mean time-series was then used to estimate connectivity between all pairs of ROIs. In the second approach, correlations were computed for all pairs of grey matter voxels. The highest correlation between each pair of ROIs represented the functional connectivity. The results of the study suggest that the development of connectivity occurs both over entire ROIs, but also focally.

Disconnection in the brain

Pathologies can disrupt brain function. White matter pathologies, such as white matter lesions (WMLs), can cause cortical ROIs to be partly or completely disconnected. Disconnection is not directly represented by traditional measures of connectivity, and thus may not capture the full extent of how pathology interferes with brain function. In Part II we computed direct measures of disconnectivity for populcation-based adult subjects and used them to learn about the effect of WMLs on brain function.

Chapter 4 introduced the concept of the *structural disconnectome*, which directly represents the degree to which WMLs affect brain connectivity as the fraction of streamlines which pass through WMLs. We compared the disconnectome of a population-based sample of adults to the structural connectome and found that: (1) Disconnection is not a function of streamline density; (2) Hubs are more affected by WMLs than peripheral nodes; (3) Connections between hubs are more severely and frequently affected by WMLs than other connection types; and (4) Connections between region clusters are often more severely affected than those within clusters.

The heritablity of the connectome and disconnectome was investigated in Chapter 5. We found that (dis)connectivity was 33% to 51% heritable and that disconnectome measures were both more significantly and more frequently heritable than connectome measures. This suggests that the WML-related disconnectivity provides complementary information about the genetic architecture of the human brain.

Chapter 6 examined the relationship between connectivity, disconnectivity and cognitive function using linear regression. Lower disconnectivity and higher connectivity corresponded to better cognitive function. Disconnectivity explained more variation in cognitive function than did connectivity. In most connections, connectome

associations with cognition disappeared when disconnectome measures were included. In a small subset of connections, connectome associations with speed-related cognitive tests persisted after accouting for disconnection, suggesting that efficient wiring is important to information processing speed independent of lesion presence.

The relationship between disconnection and brain function was examined on a tract-specific level in Chapter 7. White matter tracts were delineated in diffusion MRI data using probabilistic tractography. Each tract's functional connectivity was defined using resting-state functional MRI. A significant relationship between lesion load and functional connectivity was found in several tracts using linear regression. This study found that local white matter lesions can decrease tract-specific functional connectivity, both in direct and indirect connections.

Discussion

Effective connectivity and disconnectivity visualization

Abstract representations of connectivity and disconnectivity are high-dimensional, which poses unique challenges in presenting them in publications. Studies can greatly increase readers' understanding and appreciation of their insights by using effective visualizations and descriptive summary statistics. As such, the decision of how to present results should not be taken lightly.

Several visual representations of edge-measures in connectomes were compared in Chapter 2. Each representation has benefits and drawbacks. Matrix representations provide a large amount of information in a compact and uncluttered way, but individual connections and regions can easily become lost in all of the information. On the other hand, two-dimensional drawings of the brain effectively adds locational context to specific regions, but only in two dimensions, where the third dimension is lost completely. The connectogram foregoes representing the spatial location of regions in favour of a cleaner and more readable circular representation. The connectogram and brain drawings are unable to effectively show large numbers of connections simultaneously, since overlapping connections obscure the view of individual connections. For the (dis)connectome papers in this thesis we favoured the

connectogram, which provided clear summary of the edge-wise connectivity results while allowing individual highly significant connections to be highlighted.

Once an overview of the edge-wise and node-wise results is visualized, it is often useful to compare results between different types of connectivity. Previous studies have compared individual connections using scatter plots with structural connectivity on one axis, and functional connectivity on the other, where each point represents a measures on an edge-, node-, or aggregated-measure level. With increasing number of points, or when showing data from more than one group of subjects, the information contained in this type of plot becomes obscured. To circumvent this, we used bi-modal comparison plots, which included one- and two-dimensional distributions to show point density, and coloring to show relative importance of groups, thus maximizing the amount of information that can be clearly presented in one plot.

Information about distributions was also provided in worm plots in chapters 2 and 3, where data-points were grouped according to location in the brain, and arranged along the x-axis by increasing value within each group. This plot provides information about the distribution and size of data-point groups and allows the comparison across several datasets. However, the distribution information must be extrapolated from the shape of each "worm", which may not be straightforward for many readers. Chapter 4 instead used a violin plot, which shows distributions in a more intuitive way, with the limitation that it can only directly compare two datasets at a time.

Chapter 7 does not use the (dis)connectome to represent (dis)connectivity, but rather uses anatomically-defined white matter tracts. This greatly reduces the amount of data that needs to be taken into account in figures, and thus changes the considerations when choosing visualizations. The three-dimensional configuration of white matter tracts could easily be visualized in a two-dimensional plot, since only few tracts needed to be shown simultaneously. Results relating to direct connectivity could thus be visualized on the tracts themselves. However, since indirect connectivity is associated with more than one white matter tract it is less straightforward to show this information in a connectivity plot. While a simplified connectivity diagram was used to show results of indirect connectivity, in such a plot it is not immediately obvious whether lines correspond to white matter or grey matter measures. Indirect information was also shown in matrix format, which, thanks to the low number of tracts, resulted in a clear figure in which individual data-points could be easily identified and compared to

other points.

Visualizations are an effective way to convey results in a publication. The importance of visualizations must not be underestimated, since ineffective visualizations may result in important conclusions being lost in the vast array of available publications.

Challenges and considerations when using abstract data structures to represent the brain

The connectome, disconnectome and anatomically-defined white matter tracts are greatly simplified representations of brain connectivity. Even so, the abstract nature of these data structures introduces some unique challenges in their implementation, analysis, and interpretation. Studies using these data structures can be significantly impacted by decisions made at every step, from data acquisition to statistical analysis.

In the data acquisition phase, it is important to consider the MR scanner's protocol. State-of-the-art protocols are high resolution in all dimensions, including the three spatial axes. Diffusion and functional imaging can additionally have high angular and temporal resolution, respectively. High resolution data enables the use of sophisticated processing methodology, which can make results more accurate and reliable. The downside is that this data is more expensive to acquire and subjects must remain still in the scanner for extended time periods. For this reason, state-of-the-art protocols may not be suitable for studies with limited budget and involving certain subject groups. These protocols are also not suitable for long-running studies that started before the protocols were available, since upgrading protocols mid-study introduces statistical challenges with regards to comparing data pre- and post-upgrade.

Once data is acquired it must be processed. Diffusion and functional images require sophisticated methods to translate their high-dimensional data into something we can understand. However, sophistication comes at a cost. For example, in diffusion imaging, probabilistic tractography can better account for crossing, splitting or kissing fibres than can deterministic tractography. This can give a more accurate map of structural connectivity. However, it requires considerable computational resources, time, and many methods require state-of-the-art protocols. Studies constrained in any of those areas may opt for simpler methods based on deterministic tractography, which is less accurate, but much faster and requires far fewer resources to compute. The processing steps which follow also require important considerations, including which

grey matter parcellation methods to use, how to define connectivity between regions, and which graph theory measures to compute. The complexities of these considerations are thoroughly discussed in Chapter 2.

The huge amount of data contained in the connectome can make statistical analysis challenging. If one test is conducted per connection, node, and derived measure, then the total number of tests may be in the thousands. This necessitates the use of multiple testing correction. Given the interconnected nature of the connectome, the tests are not independent, and thus the Bonferroni correction is too stringent. There are a multitude of alternatives, all of which have benefits and drawbacks.

Another statistical consideration that is particularly relevant with regards to the disconnectome is how to deal with non-normal data. Previous studies have opted to do a log transformation in order to normalize their data [30, 38, 41, 118, 187, 200]. It is a common misconception that data must be normal in order to perform linear regression [125]. However, the normality assumption of linear regression refers to the *errors* of the model rather than the *variables* themselves [133]. Thus indiscriminately applying a transformation for the purposes of normalization is not necessary. In fact, it can have detrimental effects on statistical analyses, especially when a small constant is added prior to the transformation in order to ensure positive values [53].

Final remarks

While previous studies have shown that changes to structural connectivity are related to brain function, excluding disconnectivity from these analyses paints an incomplete picture. The detrimental effect of WML-related disconnection often outweighs the contribution of connectivity. This suggests that efficient wiring cannot compensate for damage to the brain's hardware. Regardless of how well the brain's circuitry is constructed, if the integrity of the connections becomes compromised, then the communication of the brain's computational units will also be compromised. White matter damage is like a short circuit in the brain. It results in a loss of function, affecting our ability to think, interact with the world and even to be ourselves. Moving forward in the field of neuroscience, it is crucial that both connectivity and disconnectivity are considered together due to their complementary relationship.

References

[1] S. Achard. A Resilient, Low-Frequency, Small-World Human Brain Functional Network with Highly Connected Association Cortical Hubs. *Journal of Neuroscience*, 26(1):63–72, 2006.

[2] T. M. Achenbach and L. A. Rescorla. *Manual for the ASEBA preschool forms & profiles: An integrated system of multi-informant assessment; Child behavior checklist for ages 1 1/2-5; Language development survey; Caregiver-teacher report form*. University of Vermont, 2000.

[3] H. H. H. Adams, D. P. Hibar, V. Chouraki, J. L. Stein, P. A. Nyquist, M. E. Rentería, S. Trompet, A. Arias-Vasquez, S. Seshadri, S. Desrivières, A. H. Beecham, N. Jahanshad, K. Wittfeld, S. J. Van der Lee, L. Abramovic, S. Alhusaini, N. Amin, M. Andersson, K. Arfanakis, B. S. Aribisala, N. J. Armstrong, L. Athanasiu, T. Axelsson, A. Beiser, M. Bernard, J. C. Bis, L. M. E. Blanken, S. H. Blanton, M. M. Bohlken, M. P. Boks, J. Bralten, A. M. Brickman, O. Carmichael, M. M. Chakravarty, G. Chauhan, Q. Chen, C. R. K. Ching, G. Cuellar-Partida, A. D. Braber, N. T. Doan, S. Ehrlich, I. Filippi, T. Ge, S. Giddaluru, A. L. Goldman, R. F. Gottesman, C. U. Greven, O. Grimm, M. E. Griswold, T. Guadalupe, J. Hass, U. K. Haukvik, S. Hilal, E. Hofer, D. Hoehn, A. J. Holmes, M. Hoogman, D. Janowitz, T. Jia, D. Kasperaviciute, S. Kim, M. Klein, B. Kraemer, P. H. Lee, J. Liao, D. C. M. Liewald, L. M. Lopez, M. Luciano, C. Macare, A. Marquand, M. Matarin, K. A. Mather, M. Mattheisen, B. Mazoyer, D. R. McKay, R. McWhirter, Y. Milaneschi, N. Mirza-Schreiber, R. L. Muetzel, S. M. Maniega, K. Nho, A. C. Nugent, L. M. O. Loohuis, J. Oosterlaan, M. Papmeyer, I. Pappa, L. Pirpamer, S. Pudas, B. Pütz, K. B. Rajan, A. Ramasamy, J. S. Richards, S. L. Risacher, R. Roiz-Santiañez, N. Rommelse, E. J. Rose, N. A. Royle, T. Rundek, P. G. Sämann, C. L. Satizabal, L. Schmaal, A. J. Schork, L. Shen, J. Shin, E. Shumskaya, A. V. Smith, E. Sprooten, L. T. Strike, A. Teumer, R. Thomson, D. Tordesillas-Gutierrez, R. Toro, D. Trabzuni, D. Vaidya, J. Van der Grond, D. Van der Meer, M. M. J. Van Donkelaar, K. R. Van Eijk, T. G. M. Van Erp, D. Van Rooij, E. Walton, L. T. Westlye, C. D. Whelan, B. G. Windham, A. M. Winkler, G. Woldehawariat, C. Wolf, T. Wolfers, B. Xu, L. R. Yanek, J. Yang, A. Zijdenbos, M. P. Zwiers, I. Agartz, N. T. Aggarwal, L. Almasy, D. Ames, P. Amouyel, O. A. Andreassen, S. Arepalli, A. A. Assareh, S. Barral, M. E. Bastin, D. M. Becker, J. T. Becker,

D. A. Bennett, J. Blangero, H. van Bokhoven, D. I. Boomsma, H. Brodaty, R. M. Brouwer, H. G. Brunner, R. L. Buckner, J. K. Buitelaar, K. B. Bulayeva, W. Cahn, V. D. Calhoun, D. M. Cannon, G. L. Cavalleri, C. Chen, C.-Y. Cheng, S. Cichon, M. R. Cookson, A. Corvin, B. Crespo-Facorro, J. E. Curran, M. Czisch, A. M. Dale, G. E. Davies, E. J. C. De Geus, P. L. De Jager, G. I. de Zubicaray, N. Delanty, C. Depondt, A. L. DeStefano, A. Dillman, S. Djurovic, G. Donohoe, W. C. Drevets, R. Duggirala, T. D. Dyer, S. Erk, T. Espeseth, D. A. Evans, I. O. Fedko, G. Fernández, L. Ferrucci, S. E. Fisher, D. A. Fleischman, I. Ford, T. M. Foroud, P. T. Fox, C. Francks, M. Fukunaga, J. R. Gibbs, D. C. Glahn, R. L. Gollub, H. H. H. Göring, H. J. Grabe, R. C. Green, O. Gruber, V. Gudnason, S. Guelfi, N. K. Hansell, J. Hardy, C. A. Hartman, R. Hashimoto, K. Hegenscheid, A. Heinz, S. Le Hellard, D. G. Hernandez, D. J. Heslenfeld, B.-C. Ho, P. J. Hoekstra, W. Hoffmann, A. Hofman, F. Holsboer, G. Homuth, N. Hosten, J.-J. Hottenga, H. E. H. Pol, M. Ikeda, M. K. Ikram, C. R. J. Jr, M. Jenkinson, R. Johnson, E. G. Jönsson, J. W. Jukema, R. S. Kahn, R. Kanai, I. Kloszewska, D. S. Knopman, P. Kochunov, J. B. Kwok, S. M. Lawrie, H. Lemaître, X. Liu, D. L. Longo, W. T. L. Jr, O. L. Lopez, S. Lovestone, O. Martinez, J.-L. Martinot, V. S. Mattay, C. McDonald, A. M. McIntosh, K. L. McMahon, F. J. McMahon, P. Mecocci, I. Melle, A. Meyer-Lindenberg, S. Mohnke, G. W. Montgomery, D. W. Morris, T. H. Mosley, T. W. Mühleisen, B. Müller-Myhsok, M. A. Nalls, M. Nauck, T. E. Nichols, W. J. Niessen, M. M. Nöthen, L. Nyberg, K. Ohi, R. L. Olvera, R. A. Ophoff, M. Pandolfo, T. Paus, Z. Pausova, B. W. J. H. Penninx, G. B. Pike, S. G. Potkin, B. M. Psaty, S. Reppermund, M. Rietschel, J. L. Roffman, N. Romanczuk-Seiferth, J. I. Rotter, M. Ryten, R. L. Sacco, P. S. Sachdev, A. J. Saykin, R. Schmidt, P. R. Schofield, S. Sigurdsson, A. Simmons, A. Singleton, S. M. Sisodiya, C. Smith, J. W. Smoller, H. Soininen, V. Srikanth, V. M. Steen, D. J. Stott, J. E. Sussmann, A. Thalamuthu, H. Tiemeier, A. W. Toga, B. J. Traynor, J. Troncoso, J. A. Turner, C. Tzourio, A. G. Uitterlinden, M. C. V. Hernández, M. Van der Brug, A. Van der Lugt, N. J. A. Van der Wee, C. M. Van Duijn, N. E. M. Van Haren, D. Van 't Ent, M.-J. Van Tol, B. N. Vardarajan, D. J. Veltman, M. W. Vernooij, H. Völzke, H. Walter, J. M. Wardlaw, T. H. Wassink, M. E. Weale, D. R. Weinberger, M. W. Weiner, W. Wen, E. Westman, T. White, T. Y. Wong, C. B. Wright, H. R. Zielke, A. B. Zonderman, I. J. Deary, C. DeCarli, H. Schmidt, N. G. Martin, A. J. M. De Craen, M. J. Wright, L. J. Launer, G. Schumann, M. Fornage, B. Franke, S. Debette, S. E. Medland, M. A. Ikram, and P. M. Thompson. Novel genetic loci underlying human intracranial volume identified through genome-wide association. *Nature Neuroscience*, oct 2016.

[4] H. H. H. Adams, V. J. A. Verlinden, M. L. Callisaya, C. M. van Duijn, A. Hofman, R. Thomson, A. G. Uitterlinden, M. W. Vernooij, J. N. van der Geest, V. Srikanth, and M. A. Ikram. Heritability and Genome-Wide Association Analyses of Human Gait Suggest Contribution

of Common Variants. *The journals of gerontology. Series A, Biological sciences and medical sciences*, 71(6):740–746, 2016.

[5] O. Agcaoglu, R. Miller, A. R. Mayer, K. Hugdahl, and V. D. Calhoun. Lateralization of resting state networks and relationship to age and gender. *NeuroImage*, 104:310–25, jan 2015.

[6] A. Alexander-Bloch, J. N. Giedd, and E. Bullmore. Imaging structural co-variance between human brain regions. *Nat Rev Neurosci*, 14(5):322–336, 2013.

[7] J. Alstott, M. Breakspear, P. Hagmann, L. Cammoun, and O. Sporns. Modeling the impact of lesions in the human brain. *PLoS Computational Biology*, 2009.

[8] J. L. R. Andersson, M. Jenkinson, and S. Smith. Non-linear registration, aka Spatial normalisation FMRIB technical report TR07JA2. *FMRIB Analysis Group of the University of Oxford*, 2007.

[9] N. C. Andreasen and R. Pierson. The role of the cerebellum in schizophrenia. *Biological psychiatry*, 64(2):81–8, jul 2008.

[10] A. Angrilli, C. Spironelli, T. Elbert, T. J. Crow, G. Marano, and L. Stegagno. Schizophrenia as failure of left hemispheric dominance for the phonological component of language. *PLoS ONE*, 4, 2009.

[11] E. AydÄśn, M. Cansu Ülgen, A. Tabo, Ö. Devrim Balaban, S. YeÅ§ilyurt, and H. Yumrukçal. Executive function and genetic loading in nonpsychotic relatives of schizophrenia patients. *Psychiatry Research*, 248:105–110, feb 2017.

[12] C. F. Beckmann. Modelling with independent components. *NeuroImage*, 62(2):891–901, aug 2012.

[13] C. F. Beckmann and S. M. Smith. Probabilistic Independent Component Analysis for Functional Magnetic Resonance Imaging. *IEEE Transactions on Medical Imaging*, 23(2):137–152, 2004.

[14] T. E. J. Behrens, H. J. Berg, S. Jbabdi, M. F. S. Rushworth, and M. W. Woolrich. Probabilistic diffusion tractography with multiple fibre orientations: What can we gain? *NeuroImage*, 34(1):144–55, jan 2007.

[15] T. E. J. Behrens, M. W. Woolrich, M. Jenkinson, H. Johansen-Berg, R. G. Nunes, S. Clare, P. M. Matthews, J. M. Brady, and S. M. Smith. Characterization and propagation of uncertainty in diffusion-weighted MR imaging. *Magnetic resonance in medicine : official journal of the Society of Magnetic Resonance in Medicine / Society of Magnetic Resonance in Medicine*, 50(5):1077–88, 2003.

[16] T. Benke, M. Delazer, L. Bartha, and A. Auer. Basal Ganglia Lesions and the Theory of Fronto-Subcortical Loops: Neuropsychological Findings in Two Patients with Left Caudate Lesions. *Neurocase*, 9(1):70–85, feb 2003.

[17] R. F. Betzel, L. Byrge, Y. He, J. Goñi, X.-N. Zuo, and O. Sporns. Changes in structural and functional connectivity among resting-state networks across the human lifespan. *NeuroImage*, 102:345–357, 2014.

[18] R. F. Betzel, A. Griffa, A. Avena-Koenigsberger, J. Goñi, J.-P. Thiran, P. Hagmann, and O. Sporns. Multi-scale community organization of the human structural connectome and its relationship with resting-state functional connectivity. *Network Science*, 1(03):353–373, 2013.

[19] J. C. Bis, C. DeCarli, A. V. Smith, F. van der Lijn, F. Crivello, M. Fornage, S. Debette, J. M. Shulman, H. Schmidt, V. Srikanth, M. Schuur, L. Yu, S.-H. Choi, S. Sigurdsson, B. F. J. Verhaaren, A. L. DeStefano, J.-C. Lambert, C. R. Jack, M. Struchalin, J. Stankovich, C. A. Ibrahim-Verbaas, D. Fleischman, A. Zijdenbos, T. den Heijer, B. Mazoyer, L. H. Coker, C. Enzinger, P. Danoy, N. Amin, K. Arfanakis, M. A. van Buchem, R. F. A. G. de Bruijn, A. Beiser, C. Dufouil, J. Huang, M. Cavalieri, R. Thomson, W. J. Niessen, L. B. Chibnik, G. K. Gislason, A. Hofman, A. Pikula, P. Amouyel, K. B. Freeman, T. G. Phan, B. A. Oostra, J. L. Stein, S. E. Medland, A. A. Vasquez, D. P. Hibar, M. J. Wright, B. Franke, N. G. Martin, P. M. Thompson, M. A. Nalls, A. G. Uitterlinden, R. Au, A. Elbaz, R. J. Beare, J. C. van Swieten, O. L. Lopez, T. B. Harris, V. Chouraki, M. M. B. Breteler, P. L. De Jager, J. T. Becker, M. W. Vernooij, D. Knopman, F. Fazekas, P. A. Wolf, A. van der Lugt, V. Gudnason, W. T. Longstreth, M. A. Brown, D. A. Bennett, C. M. van Duijn, T. H. Mosley, R. Schmidt, C. Tzourio, L. J. Launer, M. A. Ikram, and S. Seshadri. Common variants at 12q14 and 12q24 are associated with hippocampal volume. *Nature genetics*, 44(5):545–51, 2012.

[20] M. L. Bleecker, K. Bolla-Wilson, J. Agnew, and D. A. Meyers. Age-Related Sex Differences in Verbal Memory. *Journal of Clinical Psychology*, 44(3):403–411, 1988.

[21] T. Blumensath, S. Jbabdi, M. F. Glasser, D. C. Van Essen, K. Ugurbil, T. E. J. Behrens, and S. M. Smith. Spatially constrained hierarchical parcellation of the brain with resting-state fMRI. *NeuroImage*, 76:313–24, aug 2013.

[22] F. D. Bowman, L. Zhang, G. Derado, and S. Chen. Determining functional connectivity using fMRI data with diffusion-based anatomical weighting. *NeuroImage*, 62(3):1769–79, sep 2012.

[23] E. Bullmore and O. Sporns. Complex brain networks: graph theoretical analysis of structural and functional systems. *Nature Reviews Neuroscience*, 10:186–98, 2009.

[24] V. D. Calhoun, J. Liu, and T. Adali. A review of group ICA for fMRI data and ICA for joint inference of imaging, genetic, and ERP data. *NeuroImage*, 45(1 Suppl):S163–72, mar 2009.

[25] L. Cammoun, X. Gigandet, D. Meskaldji, J. P. Thiran, O. Sporns, K. Q. Do, P. Maeder, R. Meuli, and P. Hagmann. Mapping the human connectome at multiple scales with diffusion spectrum MRI. *Journal of neuroscience methods*, 203(2):386–97, jan 2012.

[26] B. J. Casey, R. M. Jones, and T. A. Hare. The adolescent brain. *Annals of the New York Academy of Sciences*, 1124:111–26, mar 2008.

[27] L. Cerliani, M. Mennes, R. M. Thomas, A. Di Martino, M. Thioux, and C. Keysers. Increased Functional Connectivity Between Subcortical and Cortical Resting-State Networks in Autism Spectrum Disorder. *JAMA psychiatry*, 72(8):767–77, aug 2015.

[28] R. W. Cox. AFNI: software for analysis and visualization of functional magnetic resonance neuroimages. *Computers and biomedical research, an international journal*, 29:162–173, 1996.

[29] R. C. Craddock, S. Jbabdi, C.-G. Yan, J. T. Vogelstein, F. X. Castellanos, A. Di Martino, C. Kelly, K. Heberlein, S. Colcombe, and M. P. Milham. Imaging human connectomes at the macroscale. *Nature methods*, 10:524–39, 2013.

[30] L. G. M. Cremers, M. de Groot, A. Hofman, G. P. Krestin, A. van der Lugt, W. J. Niessen, M. W. Vernooij, and M. A. Ikram. Altered tract-specific white matter microstructure is related to poorer cognitive performance: The Rotterdam Study. *Neurobiology of aging*, 39:108–17, mar 2016.

[31] N. A. Crossley, A. Mechelli, J. Scott, F. Carletti, P. T. Fox, P. Mcguire, and E. T. Bullmore. The hubs of the human connectome are generally implicated in the anatomy of brain disorders. *Brain*, 137(8):2382–2395, 2014.

[32] J. Cummings. Frontal-subcortical circuits and human behavior. *Archives of Neurology*, 50(8):873–880, 1993.

[33] A. Daducci, S. Gerhard, A. Griffa, A. Lemkaddem, L. Cammoun, X. Gigandet, R. Meuli, P. Hagmann, and J.-P. Thiran. The connectome mapper: an open-source processing pipeline to map connectomes with MRI. *PloS one*, 7(12):e48121, jan 2012.

[34] M. Daianu, A. Mezher, M. F. Mendez, N. Jahanshad, E. E. Jimenez, and P. M. Thompson. Disrupted rich club network in behavioral variant frontotemporal dementia and early-onset Alzheimer's disease. *Human brain mapping*, dec 2015.

[35] R. B. Dalby, J. Frandsen, M. M. Chakravarty, J. Ahdidan, L. Sørensen, R. Rosenberg,

L. Østergaard, and P. Videbech. Correlations between Stroop task performance and white matter lesion measures in late-onset major depression. *Psychiatry research*, 202(2):142–9, may 2012.

[36] J. S. Damoiseaux, S. A. R. B. Rombouts, F. Barkhof, P. Scheltens, C. J. Stam, S. M. Smith, and C. F. Beckmann. Consistent resting-state networks across healthy subjects. *Proceedings of the National Academy of Sciences of the United States of America*, 103(37):13848–53, sep 2006.

[37] R. De Boer, M. Schaap, F. Van Der Lijn, H. A. Vrooman, M. De Groot, A. Van Der Lugt, M. A. Ikram, M. W. Vernooij, M. M. B. Breteler, and W. J. Niessen. Statistical analysis of minimum cost path based structural brain connectivity. *Neuroimage*, 55:557–565, 2011.

[38] R. de Boer, H. A. Vrooman, F. van der Lijn, M. W. Vernooij, M. A. Ikram, A. van der Lugt, M. M. B. Breteler, and W. J. Niessen. White matter lesion extension to automatic brain tissue segmentation on MRI. *NeuroImage*, 2009.

[39] M. de Groot, M. A. Ikram, S. Akoudad, G. P. Krestin, A. Hofman, A. van der Lugt, W. J. Niessen, and M. W. Vernooij. Tract-specific white matter degeneration in aging: The Rotterdam Study. *Alzheimer's & Dementia*, 11(3):321–330, mar 2015.

[40] M. de Groot, B. F. J. Verhaaren, R. de Boer, S. Klein, A. Hofman, A. van der Lugt, M. A. Ikram, W. J. Niessen, and M. W. Vernooij. Changes in Normal-Appearing White Matter Precede Development of White Matter Lesions. *Stroke*, 44(4):1037–1042, apr 2013.

[41] M. de Groot, M. W. Vernooij, S. Klein, M. A. Ikram, F. M. Vos, S. M. Smith, W. J. Niessen, and J. L. R. Andersson. Improving alignment in Tract-based spatial statistics: evaluation and optimization of image registration. *NeuroImage*, 76:400–11, aug 2013.

[42] M. A. de Reus and M. P. van den Heuvel. Estimating false positives and negatives in brain networks. *NeuroImage*, 70:402–9, apr 2013.

[43] M. A. de Reus and M. P. van den Heuvel. The parcellation-based connectome: limitations and extensions. *NeuroImage*, 80:397–404, oct 2013.

[44] M. A. de Reus and M. P. van den Heuvel. Simulated rich club lesioning in brain networks: a scaffold for communication and integration? *Frontiers in Human Neuroscience*, 8(August):1–5, 2014.

[45] S. Debette and H. S. Markus. The clinical importance of white matter hyperintensities on brain magnetic resonance imaging: systematic review and meta-analysis. *BMJ*, 341(jul26 1):c3666–c3666, jul 2010.

[46] J. Desrosiers, R. Hébert, G. Bravo, and E. Dutil. The Purdue Pegboard Test: normative

data for people aged 60 and over. *Disability and Rehabilitation*, 17(5):217–224, 1995.

[47] X. Di, E. H. Kim, P. Chen, and B. B. Biswal. Lateralized resting-state functional connectivity in the task-positive and task-negative networks. *Brain connectivity*, 4(9):641–8, nov 2014.

[48] A. Di Martino, D. A. Fair, C. Kelly, T. D. Satterthwaite, F. X. Castellanos, M. E. Thomason, R. C. Craddock, B. Luna, B. L. Leventhal, X.-n. Zuo, and M. P. Milham. Unraveling the Miswired Connectome : A Developmental Perspective. *Neuron*, 83(6):1335–1353, 2014.

[49] S. Durston, M. C. Davidson, N. Tottenham, A. Galvan, J. Spicer, J. A. Fossella, and B. J. Casey. A shift from diffuse to focal cortical activity with development. *Developmental science*, 9(1):1–8, jan 2006.

[50] D. A. Fair, A. L. Cohen, N. U. F. Dosenbach, J. A. Church, F. M. Miezin, D. M. Barch, M. E. Raichle, S. E. Petersen, and B. L. Schlaggar. The maturing architecture of the brain's default network. *Proceedings of the National Academy of Sciences of the United States of America*, 105(10):1–5, 2008.

[51] D. A. Fair, A. L. Cohen, J. D. Power, N. U. F. Dosenbach, J. A. Church, F. M. Miezin, B. L. Schlaggar, and S. E. Petersen. Functional Brain Networks Develop from a "Local to Distributed" Organization. 5(5):14–23, 2009.

[52] A. J. Farrall and J. M. Wardlaw. Blood-brain barrier: ageing and microvascular disease–systematic review and meta-analysis. *Neurobiology of aging*, 30(3):337–52, mar 2009.

[53] C. Feng, H. Wang, N. Lu, T. Chen, H. He, Y. Lu, and X. M. Tu. Log-transformation and its implications for data analysis. *Shanghai archives of psychiatry*, 26(2):105–9, 2014.

[54] N. Filippini, B. J. MacIntosh, M. G. Hough, G. M. Goodwin, G. B. Frisoni, S. M. Smith, P. M. Matthews, C. F. Beckmann, and C. E. Mackay. Distinct patterns of brain activity in young carriers of the APOE-epsilon4 allele. *Proceedings of the National Academy of Sciences of the United States of America*, 106(17):7209–7214, 2009.

[55] B. Fischl. FreeSurfer, 2012.

[56] B. Fischl, M. I. Sereno, R. B. Tootell, and A. M. Dale. High-resolution intersubject averaging and a coordinate system for the cortical surface. *Human brain mapping*, 8(4):272–84, jan 1999.

[57] B. Fischl, A. Van Der Kouwe, C. Destrieux, E. Halgren, F. Ségonne, D. H. Salat, E. Busa, L. J. Seidman, J. Goldstein, D. Kennedy, V. Caviness, N. Makris, B. Rosen, and A. M. Dale. Automatically Parcellating the Human Cerebral Cortex. *Cerebral Cortex*, 14(1):11–22, 2004.

[58] M. F. Folstein, S. E. Folstein, and P. R. McHugh. "Mini-mental state". *Journal of Psychiatric Research*, 12(3):189–198, nov 1975.

[59] A. Fornito, E. T. Bullmore, and A. Zalesky. Opportunities and challenges for psychiatry in the connectomic era. *Biological Psychiatry: Cognitive Neuroscience and Neuroimaging*, 2(1):9–19, aug 2017.

[60] A. Fornito, J. Yoon, A. Zalesky, E. T. Bullmore, and C. S. Carter. General and specific functional connectivity disturbances in first-episode schizophrenia during cognitive control performance. *Biological Psychiatry*, 70(1):64–72, 2011.

[61] A. Fornito, A. Zalesky, and M. Breakspear. The connectomics of brain disorders. *Nature reviews. Neuroscience*, 16(3):159–72, mar 2015.

[62] A. Fornito, A. Zalesky, C. Pantelis, and E. T. Bullmore. Schizophrenia, neuroimaging and connectomics. *NeuroImage*, 62(4):2296–2314, 2012.

[63] C. Foulon, E. Volle, M. Urbanski, R. Lévy, M. Lunven, and M. Thiebaut de Schotten. Disconnectome maps: a new approach to assess long range disconnections induced by focal brain lesion. In *Proceedings of the 22nd Annual Meeting of the Organization for Human Brain Mapping (OHBM) Annual Meeting*, page Poster, Geneva, 2016.

[64] M. D. Fox, D. Zhang, A. Z. Snyder, and M. E. Raichle. The global signal and observed anticorrelated resting state brain networks. *Journal of neurophysiology*, 101(6):3270–83, 2009.

[65] J. Fridriksson, D. Guo, P. Fillmore, A. Holland, and C. Rorden. Damage to the anterior arcuate fasciculus predicts non-fluent speech production in aphasia. *Brain : a journal of neurology*, 136(Pt 11):3451–60, nov 2013.

[66] K. J. Friston. The disconnection hypothesis. In *Schizophrenia Research*, volume 30, pages 115–125, 1998.

[67] K. J. Friston and K. J. Friston. Schizophrenia and the disconnection hypothesis. *Acta psychiatrica Scandinavica. Supplementum*, 395:68–79, 1999.

[68] A. Galvan, T. A. Hare, C. E. Parra, J. Penn, H. Voss, G. Glover, and B. J. Casey. Earlier development of the accumbens relative to orbitofrontal cortex might underlie risk-taking behavior in adolescents. *The Journal of neuroscience : the official journal of the Society for Neuroscience*, 26(25):6885–92, jun 2006.

[69] W. Gao, J. H. Gilmore, K. S. Giovanello, J. K. Smith, D. Shen, H. Zhu, and W. Lin. Temporal and spatial evolution of brain network topology during the first two years of life. *PloS one*, 6(9):e25278, jan 2011.

[70] X. Gao, L. C. Becker, D. M. Becker, J. D. Starmer, and M. A. Province. Avoiding the high bonferroni penalty in genome-wide association studies. *Genetic Epidemiology*, 34(1):100–105, 2010.

[71] T. Ge, T. E. Nichols, P. H. Lee, A. J. Holmes, J. L. Roffman, R. L. Buckner, M. R. Sabuncu, and J. W. Smoller. Massively expedited genome-wide heritability analysis (MEGHA). *Proceedings of the National Academy of Sciences*, 112(8):2479–2484, 2015.

[72] A. Ghassabian, H. El Marroun, R. P. Peeters, V. W. Jaddoe, A. Hofman, F. C. Verhulst, H. Tiemeier, and T. White. Downstream effects of maternal hypothyroxinemia in early pregnancy: Nonverbal IQ and brain morphology in school-age children. *Journal of Clinical Endocrinology and Metabolism*, 99(7):2383–2390, 2014.

[73] G. Gibson. Hints of hidden heritability in GWAS., 2010.

[74] I. Goethals, K. Audenaert, F. Jacobs, E. Lannoo, C. Van de Wiele, H. Ham, A. Otte, K. Oostra, and R. Dierckx. Cognitive neuroactivation using SPECT and the Stroop Colored Word Test in patients with diffuse brain injury. *J Neurotrauma*, 21(8):1059–1069, 2004.

[75] C. J. Golden. Identification of Brain Disorders by the Stroop Color and Word Test. *Journal of Clinical Psychology*, 32(3):654–658, 1976.

[76] R. L. Gollub, J. M. Shoemaker, M. D. King, T. White, S. Ehrlich, S. R. Sponheim, V. P. Clark, J. A. Turner, B. A. Mueller, V. Magnotta, D. O'Leary, B. C. Ho, S. Brauns, D. S. Manoach, L. Seidman, J. R. Bustillo, J. Lauriello, J. Bockholt, K. O. Lim, B. R. Rosen, S. C. Schulz, V. D. Calhoun, and N. C. Andreasen. The MCIC collection: a shared repository of multi-modal, multi-site brain image data from a clinical investigation of schizophrenia. *Neuroinformatics*, 11:367–88, 2013.

[77] K. Gorgolewski, C. D. Burns, C. Madison, D. Clark, Y. O. Halchenko, M. L. Waskom, and S. S. Ghosh. Nipype: A Flexible, Lightweight and Extensible Neuroimaging Data Processing Framework in Python. *Frontiers in neuroinformatics*, 5:15, 2011.

[78] D. J. Greene, T. O. Laumann, J. W. Dubis, S. K. Ihnen, M. Neta, J. D. Power, J. R. Pruett Jr, K. J. Black, B. L. Schlaggar, J. R. P. Jr, K. J. Black, and B. L. Schlaggar. Developmental Changes in the Organization of Functional Connections between the Basal Ganglia and Cerebral Cortex. *Journal of Neuroscience*, 34(17):5842–5854, 2014.

[79] M. D. Greicius, K. Supekar, V. Menon, and R. F. Dougherty. Resting-state functional connectivity reflects structural connectivity in the default mode network. *Cerebral Cortex*, 19:72–8, 2009.

[80] D. N. Greve and B. Fischl. Accurate and robust brain image alignment using boundary-

based registration. *NeuroImage*, 48(1):63–72, 2009.

[81] M. Griebe, M. Amann, J. G. Hirsch, L. Achtnichts, M. G. Hennerici, A. Gass, and K. Szabo. Reduced functional reserve in patients with age-related white matter changes: A preliminary fMRI study of working memory. *PLoS ONE*, 9(8), 2014.

[82] A. Griffa, P. S. Baumann, J. P. Thiran, and P. Hagmann. Structural connectomics in brain diseases. *NeuroImage*, 80:515–526, 2013.

[83] L. Griffanti, G. Salimi-Khorshidi, C. F. Beckmann, E. J. Auerbach, G. Douaud, C. E. Sexton, E. Zsoldos, K. P. Ebmeier, N. Filippini, C. E. Mackay, S. Moeller, J. Xu, E. Yacoub, G. Baselli, K. Ugurbil, K. L. Miller, and S. M. Smith. ICA-based artefact removal and accelerated fMRI acquisition for improved resting state network imaging. *NeuroImage*, 95:232–247, 2014.

[84] M. A. Groen, A. J. O. Whitehouse, N. A. Badcock, and D. V. M. Bishop. Does cerebral lateralization develop? A study using functional transcranial Doppler ultrasound assessing lateralization for language production and visuospatial memory. *Brain and Behavior*, 2(3):256–269, 2012.

[85] S. Ha, I.-J. Sohn, N. Kim, H. J. Sim, and K.-A. Cheon. Characteristics of Brains in Autism Spectrum Disorder: Structure, Function and Connectivity across the Lifespan. *Experimental neurobiology*, 24(4):273–84, dec 2015.

[86] A. A. Hagberg, D. A. Schult, and P. J. Swart. Exploring network structure, dynamics, and function using NetworkX. In *Proceedings of the 7th Python in Science Conference (SciPy2008)*, pages 11–15, Pasadena, CA USA, aug 2008.

[87] P. Hagmann. From Diffusion MRI to Brain Connectomics. *Science*, 3230:127, 2005.

[88] P. Hagmann, L. Cammoun, X. Gigandet, S. Gerhard, P. Ellen Grant, V. Wedeen, R. Meuli, J. P. Thiran, C. J. Honey, and O. Sporns. MR connectomics: Principles and challenges. *Journal of Neuroscience Methods*, 194(1):34–45, 2010.

[89] J. Hänggi, A. Buchmann, C. R. a. Mondadori, K. Henke, L. Jäncke, and C. Hock. Sexual dimorphism in the parietal substrate associated with visuospatial cognition independent of general intelligence. *Journal of cognitive neuroscience*, 22(1):139–155, 2010.

[90] Y. He, Z. J. Chen, and A. C. Evans. Small-world anatomical networks in the human brain revealed by cortical thickness from MRI. *Cerebral Cortex*, 17(10):2407–2419, 2007.

[91] A. S. Heller, A. O. Cohen, M. F. W. Dreyfuss, and B. Casey. Changes in cortico-subcortical and subcortico-subcortical connectivity impact cognitive control to emotional cues across development. *Social Cognitive and Affective Neuroscience*, page nsw097, 2016.

[92] M. Hermesdorf, B. Sundermann, S. Feder, W. Schwindt, J. Minnerup, V. Arolt, K. Berger, B. Pfleiderer, and H. Wersching. Major depressive disorder: Findings of reduced homotopic connectivity and investigation of underlying structural mechanisms. *Human brain mapping*, 37(3):1209–17, dec 2015.

[93] A. M. Hermundstad, D. S. Bassett, K. S. Brown, E. M. Aminoff, D. Clewett, S. Freeman, A. Frithsen, A. Johnson, C. M. Tipper, M. B. Miller, S. T. Grafton, and J. M. Carlson. Structural foundations of resting-state and task-based functional connectivity in the human brain. *Proceedings of the National Academy of Sciences of the United States of America*, 110:6169–6174, 2013.

[94] D. Hibar and E. al. Novel genetic loci associated with hippocampal volume, shape, and subfields. *Nature Communications*, In Press, 2016.

[95] D. P. Hibar, J. L. Stein, and M. E. Renteria. Common genetic variants influence human subcortical brain structures. *Nature*, 520(7546):224–229, 2015.

[96] A. Hofman, G. G. O. Brusselle, S. Darwish Murad, C. M. van Duijn, O. H. Franco, A. Goedegebure, M. A. Ikram, C. C. W. Klaver, T. E. C. Nijsten, R. P. Peeters, B. H. C. Stricker, H. W. Tiemeier, A. G. Uitterlinden, and M. W. Vernooij. The Rotterdam Study: 2016 objectives and design update. *European journal of epidemiology*, 30(8):661–708, aug 2015.

[97] S. K. Holland, J. Vannest, M. Mecoli, L. M. Jacola, J.-M. Tillema, P. R. Karunanayaka, V. J. Schmithorst, W. Yuan, E. Plante, and A. W. Byars. Functional MRI of language lateralization during development in children. *International journal of audiology*, 46(9):533–51, sep 2007.

[98] A. B. Hollingshead and F. C. Redlich. Social class and mental illness: a community study. 1958. *American journal of public health*, 97(10):1756–7, oct 2007.

[99] J. L. Holtz. *Applied clinical neuropsychology: An introduction*. Springer Publishing Company, 2010.

[100] C. J. Honey, O. Sporns, L. Cammoun, X. Gigandet, J. P. Thiran, R. Meuli, and P. Hagmann. Predicting human resting-state functional connectivity from structural connectivity. *Proceedings of the National Academy of Sciences of the United States of America*, 106(6):2035–2040, 2009.

[101] C. J. Honey, J.-P. Thivierge, and O. Sporns. Can structure predict function in the human brain? *NeuroImage*, 52(3):766–76, sep 2010.

[102] Y. Y. Hoogendam, A. Hofman, J. N. Van Der Geest, A. Van Der Lugt, and M. A. Ikram. Patterns of cognitive function in aging: The Rotterdam Study. *European Journal of*

Epidemiology, 29(2):133–140, 2014.

[103] M. A. Ikram, A. van der Lugt, W. J. Niessen, P. J. Koudstaal, G. P. Krestin, A. Hofman, D. Bos, and M. W. Vernooij. The Rotterdam Scan Study: design update 2016 and main findings. *European Journal of Epidemiology*, 30(12):1299–1315, dec 2015.

[104] M. A. Ikram, A. Van Der Lugt, W. J. Niessen, G. P. Krestin, P. J. Koudstaal, A. Hofman, M. M. B. Breteler, and M. W. Vernooij. The Rotterdam Scan Study: design and update up to 2012. *European Journal of Epidemiology*, 26:811–824, 2011.

[105] M. A. Ikram, H. A. Vrooman, M. W. Vernooij, F. van der Lijn, A. Hofman, A. van der Lugt, W. J. Niessen, and M. M. Breteler. Brain tissue volumes in the general elderly population, 2008.

[106] M. Ingalhalikar, A. Smith, D. Parker, T. D. Satterthwaite, M. a. Elliott, K. Ruparel, H. Hakonarson, R. C. R. E. Gur, R. C. R. E. Gur, and R. Verma. Sex differences in the structural connectome of the human brain. *Proceedings of the National Academy of Sciences of the United States of America*, 111(2):823–8, 2014.

[107] H. I. Jacobs, P. J. Visser, M. P. Van Boxtel, G. B. Frisoni, M. Tsolaki, P. Papapostolou, F. Nobili, L.-O. Wahlund, L. Minthon, L. Frölich, H. Hampel, H. Soininen, L. van de Pol, P. Scheltens, F. E. Tan, J. Jolles, and F. R. Verhey. The association between white matter hyperintensities and executive decline in mild cognitive impairment is network dependent. *Neurobiology of Aging*, 33(1):201.e1–201.e8, 2012.

[108] V. W. V. Jaddoe, C. M. van Duijn, O. H. Franco, A. J. van der Heijden, M. H. van IIzendoorn, J. C. de Jongste, A. van der Lugt, J. P. Mackenbach, H. A. Moll, H. Raat, F. Rivadeneira, E. A. P. Steegers, H. Tiemeier, A. G. Uitterlinden, F. C. Verhulst, and A. Hofman. The Generation R Study: design and cohort update 2012. *Eur J Epidemiol*, 27(9):739–756, 2012.

[109] S. Jbabdi, P. Bellec, R. Toro, J. Daunizeau, M. Pélégrini-Issac, and H. Benali. Accurate anisotropic fast marching for diffusion-based geodesic tractography. *International journal of biomedical imaging*, 2008:320195, 2008.

[110] M. Jenkinson, P. Bannister, M. Brady, and S. Smith. Improved optimization for the robust and accurate linear registration and motion correction of brain images. *NeuroImage*, 17(2):825–841, 2002.

[111] M. Jenkinson, C. F. Beckmann, T. E. J. Behrens, M. W. Woolrich, and S. M. Smith. Fsl. *NeuroImage*, 62(2):782–790, aug 2012.

[112] J. M. Johnston, S. N. Vaishnavi, M. D. Smyth, D. Zhang, B. J. He, J. M. Zempel, J. S.

Shimony, A. Z. Snyder, and M. E. Raichle. Loss of resting interhemispheric functional connectivity after complete section of the corpus callosum. *The Journal of neuroscience : the official journal of the Society for Neuroscience*, 28(25):6453–8, jun 2008.

[113] R. E. Jorge, L. Acion, T. White, D. Tordesillas-Gutierrez, R. Pierson, B. Crespo-Facorro, and V. a. Magnotta. White matter abnormalities in veterans with mild traumatic brain injury. *The American journal of psychiatry*, 169:1284–91, 2012.

[114] M. Kaiser. A tutorial in connectome analysis: Topological and spatial features of brain networks. *NeuroImage*, 57(3):892–907, 2011.

[115] A. Krishnan, L. J. Williams, A. R. McIntosh, and H. Abdi. Partial Least Squares (PLS) methods for neuroimaging: A tutorial and review. *NeuroImage*, 56(2):455–475, may 2011.

[116] M. Kubicki, R. W. McCarley, and M. E. Shenton. Evidence for white matter abnormalities in schizophrenia. *Current opinion in psychiatry*, 18:121–134, 2005.

[117] A. Kuceyeski, J. Maruta, N. Relkin, and A. Raj. The Network Modification (NeMo) Tool: elucidating the effect of white matter integrity changes on cortical and subcortical structural connectivity. *Brain connectivity*, 3(5):451–63, 2013.

[118] A. Kuceyeski, B. B. Navi, H. Kamel, A. Raj, N. Relkin, J. Toglia, C. Iadecola, and M. O'Dell. Structural connectome disruption at baseline predicts 6-months post-stroke outcome. *Human Brain Mapping*, 37(7):2587–2601, jul 2016.

[119] C. C. D. Langen, M. W. M. Vernooij, L. G. M. L. Cremers, W. Huizinga, M. De Groot, M. A. Ikram, T. White, W. W. J. Niessen, M. D. Groot, M. A. Ikram, T. White, and W. W. J. Niessen. The structural disconnectome : a pathology-sensitive extension of the structural connectome. *Proceedings IEEE International Symposium on Biomedical Imaging*, 51:97–103, 2017.

[120] C. D. Langen, T. White, M. A. Ikram, M. W. Vernooij, and W. J. Niessen. Integrated Analysis and Visualization of Group Differences in Structural and Functional Brain Connectivity: Applications in Typical Ageing and Schizophrenia. *PloS one*, 10(9):e0137484, jan 2015.

[121] C. D. Langen, H. I. Zonneveld, T. White, W. Huizinga, L. G. Cremers, M. de Groot, M. Ikram, W. J. Niessen, and M. W. Vernooij. White matter lesions relate to tract-specific reductions in functional connectivity. *Neurobiology of Aging*, 51:97–103, mar 2017.

[122] A. J. Lawrence, A. W. Chung, R. G. Morris, H. S. Markus, and T. R. Barrick. Structural network efficiency is associated with cognitive impairment in small-vessel disease. *Neurology*, 83(4):304–11, jul 2014.

[123] A. Leemans, B. Jeurissen, J. Sijbers, and D. Jones. ExploreDTI: a graphical toolbox for

processing, analyzing, and visualizing diffusion MR data. *Proceedings 17th Scientific Meeting, International Society for Magnetic Resonance in Medicine*, 17(2):3537, 2009.

[124] R. K. Lenroot and J. N. Giedd. Brain development in children and adolescents: insights from anatomical magnetic resonance imaging. *Neuroscience and biobehavioral reviews*, 30(6):718–29, jan 2006.

[125] M.-X. Li, J. M. Y. Yeung, S. S. Cherny, and P. C. Sham. Evaluating the effective numbers of independent tests and significant p-value thresholds in commercial genotyping arrays and public imputation reference datasets. *Human genetics*, 131(5):747–56, may 2012.

[126] X. Liang, J. Wang, C. Yan, N. Shu, K. Xu, G. Gong, and Y. He. Effects of different correlation metrics and preprocessing factors on small-world brain functional networks: A resting-state functional MRI study. *PLoS ONE*, 7(3), 2012.

[127] D. J. Livy, P. M. Schalomon, M. Roy, M. C. Zacharias, J. Pimenta, R. Lent, and D. Wahlsten. Increased axon number in the anterior commissure of mice lacking a corpus callosum. *Experimental neurology*, 146(2):491–501, aug 1997.

[128] C. J. Mahoney, I. J. a. Simpson, J. M. Nicholas, P. D. Fletcher, L. E. Downey, H. L. Golden, C. N. Clark, N. Schmitz, J. D. Rohrer, J. M. Schott, H. Zhang, S. Ourselin, J. D. Warren, and N. C. Fox. Longitudinal diffusion tensor imaging in frontotemporal dementia. *Annals of Neurology*, 77(1):33–46, 2015.

[129] P. Maillard, O. Carmichael, D. Harvey, E. Fletcher, B. Reed, D. Mungas, and C. DeCarli. FLAIR and diffusion MRI signals are independent predictors of white matter hyperintensities. *AJNR. American journal of neuroradiology*, 34(1):54–61, jan 2013.

[130] D. S. Margulies, J. Böttger, A. Watanabe, and K. J. Gorgolewski. Visualizing the human connectome. *NeuroImage*, 80:445–61, oct 2013.

[131] L. Marstaller, M. Williams, a. Rich, G. Savage, and H. Burianová. Aging and large-scale functional networks: White matter integrity, gray matter volume, and functional connectivity in the resting state. *Neuroscience*, 290:369–378, 2015.

[132] K. L. Mills, A.-L. Goddings, L. S. Clasen, J. N. Giedd, and S.-J. Blakemore. The Developmental Mismatch in Structural Brain Maturation during Adolescence. *Developmental Neuroscience*, 36(3-4):147–160, 2014.

[133] D. C. Montgomery, E. A. Peck, and G. G. Vining. *Introduction to Linear Regression Analysis*, volume 49. 2001.

[134] S. E. Mous, R. L. Muetzel, H. El Marroun, T. J. C. Polderman, A. van der Lugt, V. W. Jaddoe, A. Hofman, F. C. Verhulst, H. Tiemeier, D. Posthuma, and T. White. Cortical

thickness and inattention/hyperactivity symptoms in young children: a population-based study. *Psychological medicine*, 44(15):3203–13, nov 2014.

[135] S. E. Mous, N. K. Schoemaker, L. M. E. Blanken, S. Thijssen, J. van der Ende, T. J. C. Polderman, V. W. V. Jaddoe, A. Hofman, F. C. Verhulst, H. Tiemeier, and T. White. The association of gender, age, and intelligence with neuropsychological functioning in young typically developing children: The Generation R study. *Applied neuropsychology. Child*, pages 1–19, mar 2016.

[136] R. L. Muetzel, S. E. Mous, J. van der Ende, L. M. E. Blanken, A. van der Lugt, V. W. V. Jaddoe, F. C. Verhulst, H. Tiemeier, and T. White. White matter integrity and cognitive performance in school-age children: A population-based neuroimaging study. *NeuroImage*, 119:119–128, 2015.

[137] L. T. Muftuler, E. P. Davis, C. Buss, A. Solodkin, M. Y. Su, K. M. Head, A. N. Hasso, and C. A. Sandman. Development of white matter pathways in typically developing preadolescent children. *Brain research*, 1466:33–43, jul 2012.

[138] K. Nakamura, Y. Kawasaki, T. Takahashi, A. Furuichi, K. Noguchi, H. Seto, and M. Suzuki. Reduced white matter fractional anisotropy and clinical symptoms in schizophrenia: a voxel-based diffusion tensor imaging study. *Psychiatry research*, 202:233–8, 2012.

[139] T. E. Nichols, S. Das, S. B. Eickhoff, A. C. Evans, T. Glatard, M. Hanke, N. Kriegeskorte, M. P. Milham, R. A. Poldrack, J.-B. Poline, E. Proal, B. Thirion, D. C. Van Essen, T. White, and B. T. T. Yeo. Best practices in data analysis and sharing in neuroimaging using MRI. *Nature Neuroscience*, 20(3):299–303, feb 2017.

[140] T. E. Oliphant. SciPy: Open source scientific tools for Python. *Computing in Science and Engineering*, 9:10–20, 2007.

[141] Open Science Collaboration. Estimating the reproducibility of psychological science. *Science*, 349(6251):aac4716–aac4716, aug 2015.

[142] J. X. O'Reilly, P. L. Croxson, S. Jbabdi, J. Sallet, M. P. Noonan, R. B. Mars, P. G. F. Browning, C. R. E. Wilson, A. S. Mitchell, K. L. Miller, M. F. S. Rushworth, and M. G. Baxter. Causal effect of disconnection lesions on interhemispheric functional connectivity in rhesus monkeys. *Proceedings of the National Academy of Sciences of the United States of America*, 110(34):13982–7, aug 2013.

[143] L. Pantoni. Cerebral small vessel disease: from pathogenesis and clinical characteristics to therapeutic challenges. *The Lancet. Neurology*, 9(7):689–701, jul 2010.

[144] J. D. Power, K. A. Barnes, A. Z. Snyder, B. L. Schlaggar, and S. E. Petersen. Spurious but

systematic correlations in functional connectivity MRI networks arise from subject motion. *NeuroImage*, 59(3):2142–2154, 2012.

[145] J. D. Power, K. A. Barnes, A. Z. Snyder, B. L. Schlaggar, and S. E. Petersen. Steps toward optimizing motion artifact removal in functional connectivity MRI; a reply to Carp. *NeuroImage*, 76:439–41, aug 2013.

[146] J. D. Power, A. Mitra, T. O. Laumann, A. Z. Snyder, B. L. Schlaggar, and S. E. Petersen. Methods to detect, characterize, and remove motion artifact in resting state fMRI. *NeuroImage*, 84:320–41, jan 2014.

[147] R. H. R. Pruim, M. Mennes, J. K. Buitelaar, and C. F. Beckmann. Evaluation of ICA-AROMA and alternative strategies for motion artifact removal in resting state fMRI. *NeuroImage*, 112:278–287, mar 2015.

[148] D. Renard, G. Castelnovo, C. Campello, S. Bouly, A. Le Floch, E. Thouvenot, A. Waconge, and G. Taieb. Thalamic Lesions: A Radiological Review, 2014.

[149] G. Risse, J. LeDoux, S. Springer, D. Wilson, and M. Gazzaniga. The anterior commissure in man: Functional variation in a multisensory system. *Neuropsychologia*, 16(1):23–31, jan 1978.

[150] E. C. Robinson, A. Hammers, A. Ericsson, A. D. Edwards, and D. Rueckert. Identifying population differences in whole-brain structural networks: a machine learning approach. *NeuroImage*, 50:910–919, 2010.

[151] K. Rubia. Functional brain imaging across development. *European child & adolescent psychiatry*, 22(12):719–31, dec 2013.

[152] M. Rubinov and E. Bullmore. Fledgling pathoconnectomics of psychiatric disorders. *Trends in cognitive sciences*, 17(12):641–7, dec 2013.

[153] M. Rubinov and E. Bullmore. Schizophrenia and abnormal brain network hubs. *Dialogues in clinical neuroscience*, 15(3):339–49, sep 2013.

[154] M. Rubinov and O. Sporns. Complex network measures of brain connectivity: uses and interpretations. *NeuroImage*, 52(3):1059–69, sep 2010.

[155] G. Salimi-Khorshidi, G. Douaud, C. F. Beckmann, M. F. Glasser, L. Griffanti, and S. M. Smith. Automatic denoising of functional MRI data: Combining independent component analysis and hierarchical fusion of classifiers. *NeuroImage*, 90:449–468, 2014.

[156] J. R. Sato, G. Abrahão, A. Gadelha, G. Vieira, A. Zugman, F. Almeida, P. Mario, M. Queiroz, M. Anés, L. Monteiro, M. Antonio, G. Del, N. Crossley, E. Amaro, P. Mcguire, A. L. T.

Lacerda, L. Augusto, E. Constantino, A. Parolin, and R. Affonseca. Decreased centrality of subcortical regions during the transition to adolescence : A functional connectivity study. *NeuroImage*, 104:44–51, 2015.

[157] T. D. Satterthwaite, D. H. Wolf, J. Loughead, K. Ruparel, M. A. Elliott, H. Hakonarson, R. C. Gur, and R. E. Gur. Impact of in-scanner head motion on multiple measures of functional connectivity: relevance for studies of neurodevelopment in youth. *NeuroImage*, 60(1):623–32, mar 2012.

[158] V. J. Schmithorst. Developmental sex differences in the relation of neuroanatomical connectivity to intelligence. *Intelligence*, 37(2):164–173, jan 2009.

[159] T. Schonberg, P. Pianka, T. Hendler, O. Pasternak, and Y. Assaf. Characterization of displaced white matter by brain tumors using combined DTI and fMRI. *NeuroImage*, 30(4):1100–1111, 2006.

[160] S. Seabold and J. Perktold. Statsmodels: Econometric and Statistical Modeling with Python. In *Proceedings of the 9th Python in Science Conference*, pages 57–61, 2010.

[161] M. L. Seghier, F. Lazeyras, S. Zimine, S. E. Maier, S. Hanquinet, J. Delavelle, J. J. Volpe, and P. S. Huppi. Combination of event-related fMRI and diffusion tensor imaging in an infant with perinatal stroke. *NeuroImage*, 21(1):463–472, 2004.

[162] P. C. Sham and S. M. Purcell. Statistical power and significance testing in large-scale genetic studies. *Nature reviews. Genetics*, 15(5):335–46, may 2014.

[163] X. Shen, F. Tokoglu, X. Papademetris, and R. T. Constable. Groupwise whole-brain parcellation from resting-state fMRI data for network node identification. *NeuroImage*, 82:403–15, nov 2013.

[164] D. J. Simmonds, M. N. Hallquist, M. Asato, and B. Luna. Developmental stages and sex differences of white matter and behavioral development through adolescence: a longitudinal diffusion tensor imaging (DTI) study. *NeuroImage*, 92:356–68, may 2014.

[165] S. M. Smith. Fast robust automated brain extraction. *Human Brain Mapping*, 17(3):143–155, 2002.

[166] S. M. Smith. The future of FMRI connectivity. *NeuroImage*, 62(2):1257–66, aug 2012.

[167] S. M. Smith, P. T. M. Fox, K. L. Miller, D. C. Glahn, P. T. M. Fox, C. E. Mackay, N. Filippini, K. E. Watkins, R. Toro, A. R. Laird, and C. F. Beckmann. Correspondence of the brain's functional architecture during activation and rest. *Proceedings of the National Academy of Sciences of the United States of America*, 106(31):13040–5, aug 2009.

[168] S. M. Smith, M. Jenkinson, H. Johansen-Berg, D. Rueckert, T. E. Nichols, C. E. Mackay, K. E. Watkins, O. Ciccarelli, M. Z. Cader, P. M. Matthews, and T. E. J. Behrens. Tract-based spatial statistics: Voxelwise analysis of multi-subject diffusion data. *NeuroImage*, 31(4):1487–1505, 2006.

[169] S. M. Smith, K. L. Miller, S. Moeller, J. Xu, E. J. Auerbach, M. W. Woolrich, C. F. Beckmann, M. Jenkinson, J. Andersson, M. F. Glasser, D. C. Van Essen, D. A. Feinberg, E. S. Yacoub, and K. Ugurbil. Temporally-independent functional modes of spontaneous brain activity. *Proceedings of the National Academy of Sciences of the United States of America*, 109(8):3131–6, feb 2012.

[170] S. M. Smith, D. Vidaurre, C. F. Beckmann, M. F. Glasser, M. Jenkinson, K. L. Miller, T. E. Nichols, E. C. Robinson, G. Salimi-Khorshidi, M. W. Woolrich, D. M. Barch, K. UÄ§urbil, and D. C. Van Essen. Functional connectomics from resting-state fMRI. *Trends in cognitive sciences*, 17(12):666–82, dec 2013.

[171] C. Solé-padullés, J. Castro-fornieles, E. de la Serna, R. Calvo, I. Baeza, J. Moya, L. Lázaro, M. Rosa, N. Bargalló, G. Sugranyes, E. De, R. Calvo, I. Baeza, J. Moya, L. Lázaro, M. Rosa, N. Bargalló, and G. Sugranyes. Intrinsic connectivity networks from childhood to late adolescence: Effects of age and sex. *Developmental Cognitive Neuroscience*, 17:35–44, nov 2015.

[172] J. Song, B. M. Young, Z. Nigogosyan, L. M. Walton, V. a. Nair, S. W. Grogan, M. E. Tyler, D. Farrar-Edwards, K. E. Caldera, J. a. Sattin, J. C. Williams, and V. Prabhakaran. Characterizing relationships of DTI, fMRI, and motor recovery in stroke rehabilitation utilizing brain-computer interface technology. *Frontiers in Neuroengineering*, 7(July):31, 2014.

[173] E. R. Sowell, P. M. Thompson, and A. W. Toga. Mapping Changes in the Human Cortex throughout the Span of Life. *The Neuroscientist*, 10(4):372–392, aug 2004.

[174] O. Sporns. The human connectome: a complex network. *Annals of the New York Academy of Sciences*, 1224:109–25, apr 2011.

[175] O. Sporns. Structure and function of complex brain networks. *Dialogues in clinical neuroscience*, 15(3):247–62, sep 2013.

[176] O. Sporns, G. Tononi, and R. Kötter. The human connectome: A structural description of the human brain. *PLoS computational biology*, 1(4):e42, sep 2005.

[177] C. S. Sripada, D. Kessler, and M. Angstadt. Lag in maturation of the brain's intrinsic functional architecture in attention-deficit/hyperactivity disorder. *Proceedings of the*

National Academy of Sciences of the United States of America, 111(39):14259–64, sep 2014.

[178] C. J. Stam. Modern network science of neurological disorders. *Nature Reviews Neuroscience*, 15(10):683–695, sep 2014.

[179] J. M. Starr, S. a. Leaper, a. D. Murray, H. a. Lemmon, R. T. Staff, I. J. Deary, and L. J. Whalley. Brain white matter lesions detected by magnetic resonance imaging are associated with balance and gait speed. *Journal of neurology, neurosurgery, and psychiatry*, 74(1):94–98, 2003.

[180] S. Sternberg. Memory-scanning: mental processes revealed by reaction-time experiments. *American Scientist*, 57:421–457, 1969.

[181] K. Supekar, M. Musen, and V. Menon. Development of large-scale functional brain networks in children. *PLoS Biology*, 7(7), 2009.

[182] K. Supekar, L. Q. Uddin, K. Prater, H. Amin, M. D. Greicius, and V. Menon. Development of functional and structural connectivity within the default mode network in young children. *NeuroImage*, 52(1):290–301, aug 2010.

[183] R. Tadayonnejad, S. Yang, A. Kumar, and O. Ajilore. Multimodal brain connectivity analysis in unmedicated late-life depression. *PLoS ONE*, 9(4):e96033, apr 2014.

[184] P. Tellegen, M. Winkel, B. Wijnberg-Williams, and J. Laros. Snijders- Oomen Niet-Verbale Intelligentietest: SON-R 2 1/2-7, 2005.

[185] M. E. Thomason and P. M. Thompson. Diffusion Imaging, White Matter, and Psychopathology. *Annual Review of Clinical Psychology*, 7(1):63–85, 2011.

[186] N. T. Tick, J. van der Ende, H. M. Koot, and F. C. Verhulst. 14-year changes in emotional and behavioral problems of very young Dutch children. *Journal of the American Academy of Child and Adolescent Psychiatry*, 46(10):1333–40, 2007.

[187] A. M. Tuladhar, E. van Dijk, M. P. Zwiers, A. G. van Norden, K. F. de Laat, E. Shumskaya, D. G. Norris, and F.-E. de Leeuw. Structural network connectivity and cognition in cerebral small vessel disease. *Human Brain Mapping*, 00:n/a–n/a, 2015.

[188] J. M. Tyszka, D. P. Kennedy, R. Adolphs, and L. K. Paul. Intact bilateral resting-state networks in the absence of the corpus callosum. *The Journal of neuroscience : the official journal of the Society for Neuroscience*, 31(42):15154–62, oct 2011.

[189] L. Q. Uddin, E. Mooshagian, E. Zaidel, A. Scheres, D. S. Margulies, A. M. C. Kelly, Z. Shehzad, J. S. Adelstein, F. X. Castellanos, B. B. Biswal, and M. P. Milham.

Residual functional connectivity in the split-brain revealed with resting-state functional MRI. *Neuroreport*, 19(7):703–9, may 2008.

[190] M. Ullsperger, C. Danielmeier, and G. Jocham. Neurophysiology of performance monitoring and adaptive behavior. *Physiological reviews*, 94(1):35–79, jan 2014.

[191] M. Urbanski, M.-L. Bréchemier, B. Garcin, D. Bendetowicz, M. Thiebaut de Schotten, C. Foulon, C. Rosso, F. Clarençon, S. Dupont, P. Pradat-Diehl, M.-A. Labeyrie, R. Levy, and E. Volle. Reasoning by analogy requires the left frontal pole: lesion-deficit mapping and clinical implications. *Brain*, 139(6), 2016.

[192] M. P. van den Heuvel and H. E. Hulshoff Pol. Specific somatotopic organization of functional connections of the primary motor network during resting state. *Human brain mapping*, 31(4):631–44, apr 2010.

[193] M. P. van den Heuvel and O. Sporns. Network hubs in the human brain, 2013.

[194] W. van der Elst, M. P. van Boxtel, G. J. van Breukelen, and J. Jolles. The Letter Digit Substitution Test: Normative Data for 1,858 Healthy Participants Aged 24-81 from the Maastricht Aging Study (MAAS): Influence of Age, Education, and Sex. 28(6):998–1009, sep.

[195] S. Van Der Walt, S. C. Colbert, and G. Varoquaux. The NumPy array: A structure for efficient numerical computation. *Computing in Science and Engineering*, 13(2):22–30, 2011.

[196] J. D. van Horn, A. Irimia, C. M. Torgerson, M. C. Chambers, R. Kikinis, and A. W. Toga. Mapping connectivity damage in the case of phineas gage. *PLoS ONE*, 7(5):e37454, 2012.

[197] M. P. A. van Meer, K. van der Marel, K. Wang, W. M. Otte, S. El Bouazati, T. A. P. Roeling, M. A. Viergever, J. W. Berkelbach van der Sprenkel, and R. M. Dijkhuizen. Recovery of sensorimotor function after experimental stroke correlates with restoration of resting-state interhemispheric functional connectivity. *The Journal of neuroscience : the official journal of the Society for Neuroscience*, 30(11):3964–72, mar 2010.

[198] G. Varoquaux and R. C. Craddock. Learning and comparing functional connectomes across subjects. *NeuroImage*, 80:405–415, 2013.

[199] B. F. J. Verhaaren, M. W. Vernooij, R. de Boer, A. Hofman, W. J. Niessen, A. van der Lugt, and M. A. Ikram. High blood pressure and cerebral white matter lesion progression in the general population. *Hypertension*, 61(6):1354–9, jun 2013.

[200] M. W. Vernooij, M. A. Ikram, H. A. Vrooman, P. A. Wielopolski, G. P. Krestin, A. Hofman, W. J. Niessen, A. Van der Lugt, and M. M. B. Breteler. White matter microstructural integrity

and cognitive function in a general elderly population. *Archives of general psychiatry*, 66(5):545–553, may 2009.

[201] H. A. Vrooman, C. A. Cocosco, F. van der Lijn, R. Stokking, M. A. Ikram, M. W. Vernooij, M. M. Breteler, and W. J. Niessen. Multi-spectral brain tissue segmentation using automatically trained k-Nearest-Neighbor classification. *NeuroImage*, 37(1):71–81, aug 2007.

[202] S. Wakana, H. Jiang, L. M. Nagae-Poetscher, P. C. M. van Zijl, and S. Mori. Fiber tract-based atlas of human white matter anatomy. *Radiology*, 230(1):77–87, jan 2004.

[203] R. Wang, T. Benner, A. Sorensen, and V. Wedeen. Diffusion Toolkit: A Software Package for Diffusion Imaging Data Processing and Tractography. *Proc. Intl. Soc. Mag. Reson. Med.*, 15, 2007.

[204] C.-Y. Wee, P.-T. Yap, D. Zhang, K. Denny, J. N. Browndyke, G. G. Potter, K. A. Welsh-Bohmer, L. Wang, and D. Shen. Identification of MCI individuals using structural and functional connectivity networks. *NeuroImage*, 59(3):2045–56, feb 2012.

[205] K. A. Welsh, N. Butters, R. C. Mohs, D. Beekly, S. Edland, G. Fillenbaum, and A. Heyman. The Consortium to Establish a Registry for Alzheimer's Disease (CERAD). Part V. A normative study of the neuropsychological battery. *Neurology*, 44(4):609–614, 1994.

[206] T. White, S. Ehrlich, B.-c. Ho, D. S. Manoach, A. Caprihan, S. C. Schulz, N. C. Andreasen, R. L. Gollub, V. D. Calhoun, and V. A. Magnotta. Spatial characteristics of white matter abnormalities in schizophrenia. *Schizophrenia bulletin*, 39:1077–86, 2013.

[207] T. White, H. El Marroun, I. Nijs, M. Schmidt, A. van der Lugt, P. A. Wielopolki, V. W. V. Jaddoe, A. Hofman, G. P. Krestin, H. Tiemeier, and F. C. Verhulst. Pediatric population-based neuroimaging and the Generation R Study: the intersection of developmental neuroscience and epidemiology. *European journal of epidemiology*, 28(1):99–111, jan 2013.

[208] T. White, C. Langen, M. Schmidt, M. Hough, and A. James. Comparative neuropsychiatry: white matter abnormalities in children and adolescents with schizophrenia, bipolar affective disorder, and obsessive-compulsive disorder. *European psychiatry : the journal of the Association of European Psychiatrists*, 30(2):205–213, feb 2015.

[209] T. White, R. Muetzel, M. Schmidt, S. J. E. Langeslag, V. Jaddoe, A. Hofman, V. D. Calhoun, F. C. Verhulst, and H. Tiemeier. Time of acquisition and network stability in pediatric resting-state functional magnetic resonance imaging. *Brain connectivity*, 4(6):417–27, 2014.

[210] T. White, D. O'Leary, V. Magnotta, S. Arndt, M. Flaum, and N. C. Andreasen. Anatomic

and functional variability: the effects of filter size in group fMRI data analysis. *NeuroImage*, 13:577–588, 2001.

[211] T. White, M. Schmidt, and C. Karatekin. White matter 'potholes' in early-onset schizophrenia: a new approach to evaluate white matter microstructure using diffusion tensor imaging. *Psychiatry research*, 174:110–115, 2009.

[212] R. H. Wilkins. Neurosurgical Classic-XVII. *Journal of Neurosurgery*, 21(3):240–244, mar 1964.

[213] J. Yang, B. Benyamin, B. P. McEvoy, S. Gordon, A. K. Henders, D. R. Nyholt, P. A. Madden, A. C. Heath, N. G. Martin, G. W. Montgomery, M. E. Goddard, and P. M. Visscher. Common SNPs explain a large proportion of the heritability for human height. *Nature Genetics*, 42(7):565–569, jul 2010.

[214] D. Yekutieli and Y. Benjamini. The control of the false discovery rate in multiple testing under dependency. *The Annals of Statistics*, 29(4):1165–1188, aug 2001.

[215] B. T. T. Yeo, F. M. Krienen, J. Sepulcre, M. R. Sabuncu, D. Lashkari, M. Hollinshead, J. L. Roffman, J. W. Smoller, L. Zöllei, J. R. J. R. J. R. Polimeni, B. Fischl, H. Liu, R. L. Buckner, B. T. T. Yeo, F. M. Krienen, J. Sepulcre, M. R. Sabuncu, D. Lashkari, M. Hollinshead, J. L. Roffman, J. W. Smoller, L. Zöllei, J. R. J. R. J. R. Polimeni, B. Fischl, H. Liu, R. L. Buckner, L. Zollei, B. T. Thomas Yeo, F. M. Krienen, J. Sepulcre, M. R. Sabuncu, D. Lashkari, M. Hollinshead, J. L. Roffman, J. W. Smoller, L. Zöllei, J. R. J. R. J. R. Polimeni, B. Fischl, H. Liu, and R. L. Buckner. The organization of the human cerebral cortex estimated by intrinsic functional connectivity. *Journal of neurophysiology*, 106(3):1125–1165, 2011.

[216] A. Zalesky, A. Fornito, and E. T. Bullmore. Network-based statistic: Identifying differences in brain networks. *NeuroImage*, 53(4):1197–1207, 2010.

[217] A. Zalesky, A. Fornito, I. H. Harding, L. Cocchi, M. Yücel, C. Pantelis, and E. T. Bullmore. Whole-brain anatomical networks: Does the choice of nodes matter? *NeuroImage*, 50(3):970–983, 2010.

[218] J. Zhou, E. D. Gennatas, J. H. Kramer, B. L. Miller, and W. W. Seeley. Predicting Regional Neurodegeneration from the Healthy Brain Functional Connectome. *Neuron*, 73(6):1216–1227, 2012.

[219] Y. Zhou, F. Yu, and T. Q. Duong. White matter lesion load is associated with resting state functional MRI activity and amyloid PET but not FDG in mild cognitive impairment and early Alzheimer's Disease patients. *Journal of Magnetic Resonance Imaging*, 41(1):102–109, 2015.

[220] D. Zhu, T. Zhang, X. Jiang, X. Hu, H. Chen, N. Yang, J. Lv, J. Han, L. Guo, and T. Liu. Fusing DTI and fMRI data: A survey of methods and applications. *NeuroImage*, oct 2013.

[221] Q.-H. Zou, C.-Z. Zhu, Y. Yang, X.-N. Zuo, X.-Y. Long, Q.-J. Cao, Y.-F. Wang, and Y.-F. Zang. An improved approach to detection of amplitude of low-frequency fluctuation (ALFF) for resting-state fMRI: fractional ALFF. *Journal of neuroscience methods*, 172(1):137–41, jul 2008.

Acknowledgments

As with most achievements in life, obtaining a PhD is not only the result of the hard work and perseverance of an individual, but it also requires the support of many other people. I am truly grateful for the contribution of my family, friends and colleagues to my mission to become an expert on brain connectivity. Your support not only helped me get through the last several years, but also adds meaning to this accomplishment.

To my family and friends...

... thank you for being there throughout my PhD. It is no secret that I found my PhD to be an emotionally trying experience. Without your support I would not have continued to the end.

The first words of thanks go to my husband, Michiel de Reus: In the good times of my PhD you provided inquisitive and thought-provoking conversations. In the bad times, you were there to support me as I contemplated my future. Thank you for being there for me.

To my mother and father: Thank you for providing emotional support and words of wisdom. During my upbringing you made many sacrifices to make sure that my siblings and I were well-educated and cared for, which provided a solid foundation upon which we could build future success. Even in my adult life you are there to cheer me on. Thank you for everything that you have done for me.

A great deal of other family members also supported me throughout my PhD. To my siblings (Julie, Jacquie, Sharon, Doug, Dan and Bob) and their families (Tyler, Cameron, Mike, Katie, John, Erin and Scarlett), thanks for being there when I needed you. To my in-laws, the de Reus family, (Jan, Thea, Oma, Jeroen, Robert, Marloes, Nancy, Mia, Fay and Nick), thank you for your warm welcome to the family and for your support. To my Godmother, auntie Lorainne Kalyn, thank you for a lifetime of love, support and good

humor. To my grandparents, aunts, uncles, cousins and other extended family: Thanks for your support throughout my life. You are too numerous to name individually, but you have all made a valuable contribution to who I have become.

A very special thanks goes to my dear friend, Priscilla Huber. You have been a wonderful friend since we met in the first days of our bachelor's studies. Your warmth and thoughtfulness are always appreciated. Your strength, work-ethic and life balance are inspiring. Please extend my thanks to Keith and Ava for being great hosts whenever Michiel and I are in Edmonton.

Maggie and Steve, I am always so grateful for every opportunity that we have to reconnect whenever I am in Calgary. Clarice, whenever and wherever we get together, it is still feels the same as when we worked together in Calgary ages ago. I'm looking forward to more international meetups in the future! The same goes for Amanda and Jouelle: Thank you for being great friends and I look forward to the next time we meet! To the rest of my friends from Canada, I am grateful for the great times that we shared.

Zilko and Diana, it has been so great to bond over our PhD and master's war stories. Thank you both, as well as Preethi, for being awesome travel companions. I truly value all of our journeys to far-away lands. Yas, thank you for sharing your care and passion with me. To the rest of the friends that I made during my masters studies, including Arna, Anna, Luis, Dana, Boris, Dan, Javier, and many more: it was great to get to know you in our studies at TU Delft. To all of the other friends that I made during my master's studies, I cherish all of the great memories that we share.

Veronika, Mattias and Andre I'm so happy to have made such great friends! I'd like to thank you all, as well to the rest of the Frühlingsfest / Spinaziefest crew for all of the fun we've had together, whether that be in the beer gardens, at barbecues in the park, or just hanging out. Verushka and Sjoerd, it has been a pleasure to get to know you better over the past few years.

To my colleagues...

... thank you for your positive contributions to my PhD experience. First of all, thank you to my paranymphs. Wyke and Annegreet, from the first to the last day of my time at BIGR, you have been great colleagues and even better friends. I will always remember our epic coffee / lunch breaks. Thank you both for being awesome paranymphs!

To the BIGiRls, I thoroughly enjoyed our movie / dinner / wine get togethers! Emilie, Annegreet, Wyke, Esther, Veronika, Zahra, Yao, Arna, Hortense, Nora, thanks for the great times together! To Rebecca, Pierre and Ewoud thanks for all of our *classy* get-togethers. I can't wait for the next one! I would further like to thank all of the other colleagues that shared laughs with me over drinks, including Jean-Marie, Hua, Gennady, Guillaume, Marius Gheorghe, Marius de Groot, Dirk, Adria, Valerio, Katja, Rozanna, Carolina, Olivera, Stefan, Marleen, Hazel, Lotte, Hakim, Andres, Miroslav, Gijs, Joor, Gerda, Mark, Ghassan, Marcel, Mart, Erwin, Henri, Renske.

To my KNICR colleagues, it has been a pleasure working and learning together. Ryan and Laura, my fellow ALPACA survivors, even though writing that paper became quite a tedious undertaking (to say the least), I enjoyed working with you both! Thank you for your work ethic and good humor. Akvile, I will always remember the fun we had in Hamburg! Hanan, Sabine, Andrea, Gerbrich, Koen, Marcus, Nikita, Philip, Raisa, Sandra, Ilse, Desana, Rosa and Sander, thank you all for sharing your knowledge and for all of the fun get-togethers that we had.

To my co-authors, I am grateful for all of the insights that you contributed to my work. I would especially like to thank Wiro, Meike, Arfan and Tonya for their valuable feedback. Additionally, thank you to Gennady, Ryan, Laura, Lotte, Hazel, Marius and Wyke for their hard work and insights.

Petra, I appreciate all of your work ethic, patience and kindness. BIGR would not be what it is without you! Desiree, thank you for helping me with administrational tasks throughout my PhD, and especially in the last phases as I prepared to defend.

I've met so many great people while working at Erasmus MC, whether that be in BIGR, KNICR, MI, Radiology, or otherwise. If I haven't named you personally, know that you have all made your mark on my PhD experience and I am grateful for that.

Since the end of my PhD contract I have met many more great colleagues in new work environments. To those that I worked while working at the Hyve, you are all wonderful people. I had a lot of fun at outings, DoMiBo's, potlucks, and around the office. To my new colleagues at Almende (and daughter companies), thank you for welcoming me onto the team and creating such a great work atmosphere. I have already learned a lot and look forward to what the future has in store. I am also grateful for Almende's contribution to my thesis printing costs.

To those that provided guidance and supervision...

... thank you for contributing to my development during my PhD. To my promotor, Professor Wiro Niessen, thank you for providing guidance and wisdom on matters related to my research, career choices and navigating the sometimes tricky world of academia. I will always remember your endless enthusiam and passion for science. I would also like to thank my co-promotor, Tonya White, for sharing her knowledge.

I especially want to thank Meike Vernooij, who has provided a great deal of supervision, support and guidance throughout my time at Erasmus MC. Near the beginning of my PhD, you stepped in to help when I was struggling to find a suitable dataset to work on. From that point forward, you provided immeasurable insight into my research. Not only did my knowledge about the brain grow enormously while working with you, but I also discovered how truly rewarding research can be. For that I am eternally grateful.

A very special thanks goes to Linda Everse, who is one of the PhD ombudsmen from the Department of Radiology. Your guidance and support got me through an extremely difficult period in my PhD. You went above and beyond to help me to navigate the tricky world of academia and helped to put me back on solid ground. Without you, I would most certainly would not have completed my PhD. Thank you for everything that you did, and please keep up the good work supporting other PhD's.

And last but not least...

... thank you to everyone else who contributed to my thesis. I am grateful to Greg Dunn and Brian Edwards for allowing me to use their artwork (Cortical Circuitboard, 22K reflective microetching, 2013-4) for the part dividers. I also greatly appreciate the generosity of subjects who donated data, and the efforts of all people that contributed to data collection. Without your contributions my research would not have been possible.

Summary

The brain is like a super computer: it is a collection of interconnected computational units which work together to enable both basic functions, such as regulation of breathing, as well as higher functions, such as cognition, thought and emotion. The computational units, or *regions*, are located in the grey matter (i.e. the cortical surface and in the subcortex), whereas the connections between them, or *tracts*, are found in the white matter. The development and maintenance of both grey and white matter is essential to brain function. When either tissue type becomes compromised, so too does function.

Brain connectivity can non-invasively be derived from magnetic resonance images (MRI). Structural MRI can be used to examine the three-dimensional anatomy of the brain. This combined with either diffusion weighted images (DWI) or functional MRI (fMRI) can be used to estimate *functional* or *structural* connectivity, respectively. Both types of brain connectivity can be represented by the *connectome*. The connectome is a *graph*-based data structure in which regions are represented by *nodes* and connections are represented by *edges*. Graph theory can be used to gain new insights about the connectome.

Studying brain connectivity is crucial to learning about both brain function and dysfunction. However, in the case of pathology-related dysfunction, abstractions of connectivity such as the connectome may not sufficiently represent underlying tissue damage. Pathologies, including white matter lesions, are involved in age-related neuro-degeneration as well as several neuro-psychiatric conditions. A data structure which takes pathology into account may provide additional insights into related loss of function.

The relationship between brain connectivity, disconnectivity and function is examined in this thesis. The first part focuses on the connectome, whereas the second part focuses on disconnection in the brain.

The Connectome

Connectome data is, by nature, complex and high-dimensional. This poses a challenge with regards to its analysis and visualization. This challenge is addressed in Chapter 2. It explores how group differences in both structural and functional connectivity can be analyzed both uni- and bi-modally, and how results can be visualized. It explores the *bi-modal comparison plot*, which shows the distribution of both uni- and bi-modal group differences, and uses color to show distributions of two groups withing the same plot. Distribution of group differences within groups of regions were visualized in the *worm plot*. The proposed methods and visualizations were applied in two proof-of-concept studies of aging and schizophrenia. Both studies included two types of structural and functional connectivity. In both studies, the visualizations indicated which types of connectivity were most effective in identifying group differences.

The analysis and visualization methods proposed in Chapter 2 were then applied in Chapter 3 to study brain development of six- to ten-year-old children. Age and gender differences in two methods of defining functional connectivity were investigated. In the first method, the correlation of regional mean time-series was computed. In the second method, the focal maximum of voxel-wise correlations across regions was computed. The first method is a commonly used definition which considers connectivity between regions to involve entire regions. The second method, dubbed Anatomic and Local Peak Activity Correlation Analysis (ALPACA), is a novel way of defining functional connectivity, which considers the possibility that connectivity may not be spread over entire regions, but rather that it may be more focal. The study replicated previous findings that cortico-cortical connectivity shifts from short- to long-range with age. It also found that subcortico-cortial associations with age were negative in ALPACA, but mixed in the mean time series method. Connections between subcortical regions were negative for both network types. Few associations were found with sex. This study challenged the spatial assumptions made by the traditional mean time series approach, showing that in many cases associations with age depend on whether functional connectivity is defined diffusely or focally.

Disconnection

Previous studies have established that white matter pathologies are associated with impairment in gate, depression, cognitive decline and an increased risk of stroke and dementia. The association between white matter damage and functional decline is the main motivation behind the *disconnection hypothesis*, which states that a loss of white matter connectivity will lead to a loss of communication between cortical regions, ultimately leading to a loss of function. This is the focus of Part II of this thesis, which explores disconnection within the Rotterdam Scan Study (RSS). The RSS is a population-based study which aims to uncover the determinants of cognitive decline in the elderly.

This part begins with Chapter 4, which introduces a data structure, named the *structural disconnectome*, which extends the structural connectome by estimating the degree to which each connection is affected by white matter pathologies, such as white matter lesions (WMLs). The WML-related connectome and disconnectome were estimated for each subject. Several existing graph theory measures were computed from the connectome, and new disconnection-oriented measures were derived from the disconnectome. This study found that: (1) Disconnection is not a function of streamline density; (2) Hubs are more affected by WMLs that peripheral nodes; (3) Connections between hubs are more severely and frequently affected by WMLs than other connection types; and (4) Connections between region clusters are often more severely affected than those between clusters.

The connectome, disconnectome, and the graph-theory measures derived in Chapter 4 were evaluated for their genetic underpinnings in Chapter 5. The genotype of each subject was used to derive inter-subject genetic relationship matrices for heritability analysis. The evaluated connectivity and disconnectivity measures were found to be 33 to 51% heritable, where the disconnectome was generally more frequently and intensely heritable.

The evaluation fo the connectome and disconnectome continued in Chapter 6, which studied their relationship with cognition. Lower disconnectivity and higher connectivity corresponded to better cognitive function, where the majority of significant associations were related to the disconnectome. When both the connectome and disconnectome were included in the same model, most connectome associations attenuated. WML-related disconnectivity was especially related to reduced executive functioning,

whereas increased cognitive speed corresponded to increased connectivity independent of WML presence. The combined analysis of connectivity and disconnectivity revealed that while disconnectivity explains more variance than does connectivity, efficient wiring is essential to efficient brain function regardless of WML presence.

Cognitive decline is a global expression of decreased brain function and is related to the presence of WMLs. However, little is known about the location-specific relationship between brain function and WMLs. Chapter 7 examined this relationship in anatomically defined white matter tracts. For each tract, functional connectivity and WML volume were computed. Significant associations between functional connectivity and both global and tract-specific WML volume were found in several tracts. Significant tract-specific relationships were also found in indirect connections (i.e. between functional connectivity in one tract versus WML-volume in another tract). These results suggest that not only is functional connectivity affected by WMLs in the same tract, but that functional connectivity is affected by WMLs in several tracts simultaneously.

The studies presented in this thesis made important contributions to our knowledge about how connectivity relates to brain development, age differences and schizophrenia, and how disconnectivity relates to aging, genetics and pathology. The connectome and disconnectome are complementary: Studying either connectivity or disconnectivity in isolation paints an incomplete picture. Moving forward in the field of neuroscience, it is crucial that they are considered together.

Publications

Journal papers

- **Langen, CD**; Cremers, LGM; de Groot, M; White, T; Ikram, MA; Niessen, WJ; Vernooij, MW. White matter disconnection is associated with cognitive impairment. *Alzheimer's and Dementia* **[under review]**

- **Langen, CD**; Muetzel, R; Blanken, L; van der Lugt, A; Tiemeier, H; Verhulst, F; Niessen, WJ; White, T. Differential patterns of age-related cortical and subcortical functional connectivity in 6-to-10 year old children: A connectome-wide association study. *Brain and Behavior* **[under review]**

- de Vrij, FM; Bouwkamp, CG; Gunhanlar, N; [...]; **Langen, CD**; [...] Kushner, SA. Candidate CSPG4 Mutations and Induced Pluripotent Stem Cell Modeling Implicate Oligodendrocyte Progenitor Cell Dysfunction in Familial Schizophrenia. *Molecular Psychiatry* (2018) **[Epub ahead of print]**

- Kelly, Sinead, Jahanshad N, Zalesky A, [...], **Langen, CD**, [...], Donohoe G. Widespread white matter microstructural differences in schizophrenia across 4322 individuals: results from the ENIGMA Schizophrenia DTI Working Group. *Molecular Psychiatry* (2017) **[Epub ahead of print]**

- **Langen, CD**; Zonneveld, HI; White, T; Huizinga, W; Cremers, LGM; de Groot, M; Ikram, MA; Niessen, WJ; Vernooij MW. White Matter Lesions Relate to Tract-Specific Reductions in Functional Connectivity. *Neurobiology of Aging* 51 (March): 97-103 (2017)

- **Langen, CD**; White, T; Ikram, MA; Vernooij, MW; Niessen, WJ. Integrated Analysis and Visualization of Group Differences in Structural and Functional

Brain Connectivity: Applications in Typical Ageing and Schizophrenia. *PloS One* 10 (9): e0137484 (2015)

- White, T; **Langen, CD**; Schmidt, M; Hough, M; James, A. Comparative Neuropsychiatry: White Matter Abnormalities in Children and Adolescents with Schizophrenia, Bipolar Affective Disorder, and Obsessive-Compulsive Disorder. *European Psychiatry : The Journal of the Association of European Psychiatrists* 30 (2): 205-13 (2015)

Conference papers

- **Langen, CD**; Vernooij, MW; Cremers, LGM; Huizinga, W; De Groot, M; Ikram, MA; White, T; Niessen, WJ. The Structural Disconnectome : A Pathology-Sensitive Extension of the Structural Connectome. *IEEE 14th International Symposium on Biomedical Imaging (ISBI; Melbourne; 18-21 April, 2017)* 51: 97-103. **(Finalist for best student paper)**

- **Langen, CD**; Roshchupkin, G; Adams, HH; de Groot, M; Vos, F; Vernooij, MW; Ikram, MA; Niessen; WJ. Heritability of Connectivity and Disconnectivity of the Brain in a Population-Based Study. *IEEE 14th International Symposium on Biomedical Imaging (ISBI; Melbourne; 18-21 April, 2017)* 51: 349-353. **(Finalist for best student paper)**

Conference abstracts

- **Langen, CD**; Zonneveld, H; White, J; Huizinga, W; Cremers, L; de Groot, M; Ikram, MA; Niessen, WJ; Vernooij, MW. White matter lesions cause tract-specific reductions in functional connectivity. *VasCog (Amsterdam; October 13-15, 2016*) **(Nominated for the Young Investigator award)**

- **Langen, CD**; White, T; Cremers, L; Huizinga, W; de Groot, M; Ikram, MA; Vernooij, MW; Niessen, WJ. The structural disconnectome: Characterizing connection-specific white matter abnormalities. *VasCog (Amsterdam; October 13-15, 2016*)

- **Langen, CD**; Muetzel R; Blanken L; Niessen, W; White, T. Age associations with Anatomic and Local Peak Activity Correlation Analysis (ALPACA). *Organization for Human Brain Mapping Annual Meeting (Honolulu; June 14-18, 2015)*
- **Langen, CD**; Ikram, A; Vernooij, M; White, T; Niessen, W. Integrated analysis and visualization of group differences in structural and functional connectivity of the brain. *Organization for Human Brain Mapping Annual Meeting (Honolulu; June 14-18, 2015)*
- Coutouly, M; Maiti, R; Montgomerie, S; **Langen, CD**; Wishart, DS. A method to determine protein structures with minimal information. *6th International Conference of the Canadian Proteomics Initiative (Edmonton; May 10-12, 2006)*
- Sfyrakis, K; **Langen, CD**; King, JG; Jan, A; Lassere, S; Anwar, H; Ranjan, R; Hill, SL; SchÃijrmann, F; and Markram, H. Blue Builder: Building the Neocortical Column According to Recipe. 5th Forum of European Neuroscience (Vienna; July 8-12, 2006).

Portfolio

Name PhD student:	Carolyn D. Langen
Erasmus MC departments:	Radiology & Nuclear Medicine Medical Informatics
PhD Period:	September 2012 to April 2018

	Year
Courses and workshops	
EIBIR summer school	2013
Oral presentation skills (Erasmus MC)	2013
Biostatistics (Nihes, Erasmus MC)	2013
Pattern Recognition and Classification (University of Amsterdam)	2014
Medical Imaging Summer School	2014
English Biomedical Writing and Communication (Erasmus MC)	2015
Human Neuroanatomy to Psychopathology (Maastricht University)	2015
Diffusion Imaging (OHBM)	2015
Exploring the Human Connectome (UMC Utrecht)	2015
NFBIA summer school (Radboud university)	2015
International conferences	
Organization for Human Brain Mapping (Hamburg, Germany)	2014
Organization for Human Brain Mapping (Honolulu, USA)	2015
VasCog (Amsterdam, the Netherlands)	2016
IEEE International Symposium on Biomedical Imaging (Melbourne, Australia)	2017

Presentations at international conferences	
OHBM (poster)	2014
OHBM (poster)	2015
VasCog 1 (oral, nominated for Young Investigator award)	2016
VasCog 2 (poster)	2016
VasCog 3 (poster)	2016
ISBI 1 (oral, finalist for best student paper)	2017
Meetings	
KNICR	2012-2016
MISERE	2012-2016
Medical Informatics research lunch meetings	2012-2016
Present at Medical Informatics research lunch meetings	2012-2016
Teaching	
Assisted in MeVisLab practicums	2013-2015
Introduction to image analysis for medical students	2014-2015

About the author

Carolyn Langen was born in Calgary, Canada on March 6, 1985. Her academic inclinations lead her to pursue the International Baccalaureate program in her high school years. Her first experience with academic research was in the Heritage Youth Research Summer Program in the summer of 2002, where she used immunohistochemistry to localize genetic markers in chick embryos in the lab of Dr. Cairine Logan. Prior to beginning her bachelor's studies in the summer of 2003, she worked for Dr. Valerie Kirk in a clinic that studied juvenile obstructive sleep apnea.

From 2003 to 2007 she pursued a Bachelor of Health Sciences with a major in bioinformatics at the University of Calgary. Her bachelor's studies focused on computer science and biology. She gained research experience in several subjects including medical imaging (summer of 2004 with Prof.dr. Ross Mitchell), immunohistochemistry (independent study, 2004-2005 with Dr. Cairine Logan), protemics (summer of 2005 with Prof.dr. David Wishart), the Blue Brain Project (summer of 2006 with Dr. Felix Shürmann), agent-based swarm simulations (honor's thesis project, 2006-2007 with Prof.dr. Christian Jacob). She graduated from her bachelor's with first-class honors.

After her bachelor's studies, she became a software developer for Telvent Canada (now named Schneider Electric). At Telvent she customized the software and databases behind pipeline control systems.

In 2010 she moved to Europe to pursue an Erasmus Mundus dual degree program in Computer Simulation for Science and Engineering (COSSE), with a specialization in bio-simulations. In her first year she studied at the Delft University of Technology in the Netherlands. Her second year was completed at KTH Royal Institute of Technology in Stockholm, Sweden. She received masters degrees in applied math from both universities. In her master's thesis project she built a patient-specific poroelastic model of subdural hematoma growth in the brain under the supervision of Dr. Johnson Ho.

After her master's studies, she started working towards her PhD in NeuroImaging via the Biomedical Imaging Group, Rotterdam under the supervision of Prof.dr. Wiro

Niessen and Dr. Tonya White. Her topic was the extraction and analysis of brain connectivity data from MR images, the results of which are presented in this thesis.

Upon completion of her PhD contract she began working as a software developer and data scientist at the Hyve BV. She is now a research engineer at Almende BV, where she uses agent-based models to study self-organization in a variety of applications.